FINAL REPORT

FHWA-WY-2203F

State of Wyoming

EVALUATION OF MITIGATION MEASURES AND DEVELOPMENT OF AN ULTRA-ACCELERATED TEST TO EVALUATE ALKALI SILICA REACTION POTENTIAL IN CONCRETE

By:
Department of Civil and Architectural Engineering
University of Wyoming
1000 East University Avenue, Dept. 3295
Laramie, WY 82071

August 2022

Notice

This document is disseminated under the sponsorship of the Wyoming Department of Transportation (WYDOT) in the interest of information exchange. WYDOT assumes no liability for the use of the information contained in this document. WYDOT does not endorse products or manufacturers. Trademarks or manufacturers' names appear in this report only because they are considered essential to the objective of the document.

Quality Assurance Statement

WYDOT provides high-quality information to serve Government, industry, and the public in a manner that promotes public understanding. Standards and policies are used to ensure and maximize the quality, objectivity, utility, and integrity of its information. WYDOT periodically reviews quality issues and adjusts its programs and processes to ensure continuous quality improvement. Further, if the report contains either confidential information or, if any information in the report is subject to copyright, patent, or trademark requirements, the report must contain additional disclaimers that may be obtained through the Research Center.

Creative Commons

Copyright

• Caveat for Unpublished Work —Some material may be protected under common law or equity even though no copyright notice is displayed on the material. Credit will be given, and permission will be obtained as appropriate.
• Proprietary Information — To avoid restrictions on the availability of reports, proprietary information will not be included in reports, unless it is critical to the understanding of a report and prior approval is received from WYDOT. Reports containing such proprietary information will contain a statement on the Technical Report Documentation Page restricting the availability of the report.

TECHNICAL REPORT DOCUMENTATION PAGE

1. Report No. WY-22/03F	**2. Government Accession No.**	**3. Recipient's Catalog No.**
4. Title and Subtitle Evaluation of Mitigation Measures and Development of an Ultra-Accelerated Test to Evaluate ASR Potential in Concrete		**5. Report Date** July 2022 **6. Performing Organization Code:**
7. Author(s) Md Tarik Hossain (0000-0002-4514-5620), Caleb Pachel (0000-0003-4151-1993), Jennifer Eisenhauer Tanner (0000-0002-8279-6289)		**8. Performing Organization Report No.**
9. Performing Organization Name and Address University of Wyoming Department of Civil and Architectural Engineering University of Wyoming, Dept 3295 Laramie, WY 82071-3295		**10. Work Unit No.** **11. Contract or Grant No.** 1804F
12. Sponsoring Agency Name and Address Wyoming Department of Transportation 5300 Bishop Blvd Cheyenne, WY 82009-3340 WYDOT Research Center (307) 777-4182		**13. Type of Report and Period** Final Report **14. Sponsoring Agency Code** WYDOT
15. Supplementary Notes WYDOT Project Manager: Wesley Bybee , Assistant State Materials Engineer		

16. Abstract

Abstract: A comprehensive study was performed to evaluate mitigation options to reduce premature expansion due to alkali-silica reaction (ASR) for selected Wyoming aggregates. State-of-the-art and standardized test methods were performed, and results were used to compare expansion levels. Two different fly-ash sources were tested using the Concrete Prism Test (CPT). All the fly ash sources mitigated the moderately reactive aggregates; the most highly expansive aggregate was mitigated by only one of the fly ash sources.

An ultrarapid test, the Autoclave Concrete Prism Test (ACPT) was comprehensively evaluated by a robust testing program exceeding 150 specimens and compared results with those in the literature. For separated coarse and fine aggregate fractions, test data confirms that a limit of 0.09 percent expansion produces a 97.2 percent accuracy for 36 tested concrete mixtures. Miniature Concrete Prism Test (Min-CPT) and outdoor exposure block (OEB) results are also presented for selected aggregates.

The ultrarapid test method was applied to another group specimens cast using recycled concrete aggregate (RCA) as the coarse aggregate source. An interlaboratory study was conducted to evaluate the effect of different operators on the measuring process. Results fell within the coefficient of variation for the CPT. Another study evaluated results of seven laboratories conducting ACPTs. Again, those results are within the CPT standard indicating that those limits could also be applied for RCA.

17. Key Words Wyoming, Alkali silica reaction, expansion, aggregate, concrete, durability	**18. Distribution Statement** This document is available through the National Transportation Library and the Wyoming State Library.		
19. Security Classif. (of this report) Unclassified	**20. Security Classif. (of this page)** Unclassified	**21. No. of Pages** 110	**22. Price**

Form DOT F 1700.7 (8-72) Reproduction of completed page authorized.

SI* (MODERN METRIC) CONVERSION FACTORS

APPROXIMATE CONVERSIONS TO SI UNITS

Symbol	When You Know	Multiply By	To Find	Symbol
		LENGTH		
in	inches	25.4	millimeters	mm
ft	feet	0.305	meters	m
yd	yards	0.914	meters	m
mi	miles	1.61	kilometers	km
		AREA		
in^2	square inches	645.2	square millimeters	mm^2
ft^2	square feet	0.093	square meters	m^2
yd^2	square yard	0.836	square meters	m^2
ac	acres	0.405	hectares	ha
mi^2	square miles	2.59	square kilometers	km^2
		VOLUME		
fl oz	fluid ounces	29.57	milliliters	mL
gal	gallons	3.785	liters	L
ft^3	cubic feet	0.028	cubic meters	m^3
yd^3	cubic yards	0.765	cubic meters	m^3
		NOTE: volumes greater than 1000 L shall be shown in m^3		
		MASS		
oz	ounces	28.35	grams	g
lb	pounds	0.454	kilograms	kg
T	short tons (2000 lb)	0.907	megagrams (or "metric ton")	Mg (or "t")
		TEMPERATURE (exact degrees)		
°F	Fahrenheit	5 (F-32)/9 or (F-32)/1.8	Celsius	°C
		ILLUMINATION		
fc	foot-candles	10.76	lux	lx
fl	foot-Lamberts	3.426	$candela/m^2$	cd/m^2
		FORCE and PRESSURE or STRESS		
lbf	poundforce	4.45	newtons	N
lbf/in^2	poundforce per square inch	6.89	kilopascals	kPa

APPROXIMATE CONVERSIONS FROM SI UNITS

Symbol	When You Know	Multiply By	To Find	Symbol
		LENGTH		
mm	millimeters	0.039	inches	in
m	meters	3.28	feet	ft
m	meters	1.09	yards	yd
km	kilometers	0.621	miles	mi
		AREA		
mm^2	square millimeters	0.0016	square inches	in^2
m^2	square meters	10.764	square feet	ft^2
m^2	square meters	1.195	square yards	yd^2
ha	hectares	2.47	acres	ac
km^2	square kilometers	0.386	square miles	mi^2
		VOLUME		
mL	milliliters	0.034	fluid ounces	fl oz
L	liters	0.264	gallons	gal
m^3	cubic meters	35.314	cubic feet	ft^3
m^3	cubic meters	1.307	cubic yards	yd^3
		MASS		
g	grams	0.035	ounces	oz
kg	kilograms	2.202	pounds	lb
Mg (or "t")	megagrams (or "metric ton")	1.103	short tons (2000 lb)	T
		TEMPERATURE (exact degrees)		
°C	Celsius	1.8C+32	Fahrenheit	°F
		ILLUMINATION		
lx	lux	0.0929	foot-candles	fc
cd/m^2	$candela/m^2$	0.2919	foot-Lamberts	fl
		FORCE and PRESSURE or STRESS		
N	newtons	0.225	poundforce	lbf
kPa	kilopascals	0.145	poundforce per square inch	lbf/in^2

TABLE OF CONTENTS

LIST OF FIGURES

LIST OF TABLES

LIST OF ACRONYMS

AASHTO – American Association of State Highway and Transportation Officials
ACPT – Autoclaved Concrete Prism Test
AMBT – Accelerated Mortar Bar Test
ASR – Alkali-silica reaction
ASTM – American Society of Testing Materials
HR - highly reactive
Min-CPT - miniature concrete prism test,
MR - moderately reactive, or very-highly reactive (VHR)
NR - non-reactive
PR - potentially reactive
OEB - outdoor exposure block
RCA - recycled concrete aggregate
SCM - supplementary cementitious material
T/C - tension-to-compression ratio
UW - University of Wyoming
WYDOT - Wyoming Department of Transportation

EXECUTIVE SUMMARY

Alkali-silica reaction (ASR) is a global concrete durability problem, and aggregate reactivity has plagued concrete worldwide. The gel produced in ASR readily absorbs water and expands; this can lead to cracking and premature deterioration in concrete. ASR is a significant problem in Wyoming because of the presence of reactive aggregates. This research project evaluated locally available fly ashes as mitigation measures that will improve sustainability and make concrete construction even more cost-effective.

Concrete Prism Test (CPT), the most widely accepted test for evaluating ASR potential, takes one year for Portland cement concrete mixes and two years for mixes with supplementary cementitious material (SCM), such as fly ash. Mitigating concrete mixtures were evaluated for a suite of fly ashes. All the fly ash sources mitigated the moderately reactive aggregates; the most highly expansive aggregate was mitigated by one of the two fly-ash sources. Beyond mitigation efforts, Miniature Concrete Prism Test (Min-CPT) and outdoor exposure block (OEB) results after 12 years are also presented for selected aggregates.

To test concrete mixes within a short time, the development of an ultra-accelerated test method would reduce uncertainty and delays in construction. An autoclave test was explored in this research and compared to CPT data. Based on a suite of 36 concrete mixtures, this test correctly identified an aggregate's reactivity with a 97.2 percent accuracy for coarse and fine aggregate fractions tested separately. Additional work is recommended for combining coarse and fine aggregates from the same source.

The ultrarapid test method was subsequently applied to another group specimens cast using recycled concrete aggregate (RCA) as the coarse aggregate source. An interlaboratory study was conducted to evaluate the effect of different operators on the measuring process. Results fell within the coefficient of variation for the CPT. Another study evaluated results of seven laboratories conducting ACPTs. Again, those results are within the CPT standard indicating that those limits could also be applied for RCA.

Accelerated Mortar Bar Testing (AMBT) with companion strength testing was completed at several stages of exposure to consider the rate of reduction. Based on a total of 1,872 physical tests and regression analyses, both the splitting tensile and compression strengths of the exposed mortar bars showed marked decreases when compared to the control mortar bars. The splitting tensile strength was affected more adversely than the compressive strength.

1 INTRODUCTION

Concrete is the most widely used construction material in the world. There are numerous reasons for the popularity of concrete as a primary building material, such as durability, low relative cost, low maintenance, and high fire resistance. However, exposure to an aggressive environmental condition for an extended period can cause premature deterioration of concrete. The lifespan of concrete can be reduced by various factors, such as reinforcement corrosion, alkali-silica reaction (ASR), carbonation, and leaching. Among all the concrete damage mechanisms, ASR is one of the most severe durability-related issues for concrete that may cause extensive damage to concrete structures. Repair works of structures affected by ASR can be very complicated, expensive, and time-consuming (Saha, Khan et al. 2018). In 1940, Stanton pointed out that concrete can suffer deleterious expansion due to the use of reactive aggregates. He further observed the effectiveness of using pozzolans as a partial replacement for cement to reduce ASR (Stanton 1950). Since then, researchers reported ASR expansion in concrete structures in different parts of the world (Saha, Khan et al. 2018). In 1980, Cole investigated dams in Australia suffering from deleterious cracking due to a similar phenomenon (Cole, Lancucki et al. 1981). Likewise, Ono observed concrete structures in Japan exhibiting significant cracking due to deleterious expansion by ASR (Ono 1988). Failure of airfield pavements in New Zealand due to ASR expansions was reported by Swamy (Swamy 1990). Recently, structural damages due to ASR have been identified in Seabrook nuclear power in the USA (Saouma and Hariri-Ardebili 2014) and Mactaquac Dam in Canada (Hayman, Thomas et al. 2010). Though the fundamental concept of ASR in structural concrete has been acknowledged by the scientific community for decades, modern structures still suffer from severe damage due to this deleterious expansion which proves the complexity of the ASR mechanism (Saha, Khan et al. 2018). ASR continues to plague current construction.

The Wyoming Department of Transportation (WYDOT) has traditionally handled the problem by replacing 20–25 percent of cement with fly ash. While the mitigated ASR potential of the mixture can be confirmed by testing, this testing process takes two years. During this time, changes in coal sources and burning methods may unexpectedly impact the mitigation capabilities of any fly ash. To effectively mitigate the effects of ASR, experimental identification of several fly ash sources is imperative. While time and reliability are the most important testing factors, experimental work will never be eliminated. Therefore, establishing quicker and more effective test methods is crucial (Fiore, Hossain et al. 2018).

1.1 Research objectives

The objectives of this research are:

- To determine the effectiveness of fly ashes to mitigate the ASR problem in locally sourced aggregates.

- To determine aggregate reactivity using miniature concrete prisms test.
- To evaluate if an autoclave concrete prism test to determine aggregate reactivity within a shorter period.
- To evaluate the ASR reactivity of aggregates from long-term outdoor exposure blocks.

1.2 Report overview

Chapter 1 introduces the research.
Chapter 2 provides detailed relevant literature on alkali-silica reaction, fly ash, and the mitigation potential of aggregates.
Chapter 3 addresses the materials used throughout the study, their makeup, and physical and chemical properties, as they apply.
Chapter 4 describes the test methods and equipment used in this research.
Chapter 5 demonstrates the results of the experiments on outdoor exposure blocks, mitigated, and unmitigated concrete prism tests, miniature concrete prism tests, and the autoclave test.
Chapter 6 presents the conclusions of this research and the recommendations for future work.

2 LITERATURE REVIEW

2.1 Alkali-silica reaction

ASR is a chemical reaction between the reactive silica of aggregates and the alkaline solutions in micro-pores of concrete. The silica structure is dissolved by the nucleophilic attack of OH- ions, and the highly degraded silica structure behaves as a hygroscopic silica gel. Alternatively, the dissolved silica can cross-link (in presence of Ca ions), coagulate, and form ASR gel. Swelling of this gel leads to stress development and potentially, cracking of concrete (Figueira, Sousa et al. 2019). Any poorly crystalline silica has an affinity to react with water and generate amorphous hydrous silica. Some examples of poorly crystallized silica are opal, chert, chalcedony, and glasses, Portlandite ($Ca(OH)_2$), and calcium silicate hydrate (C-S-H) produced by the reaction of cement with water in the hydration process. This ($Ca(OH)_2$) contributes hydroxyl ions (OH^-) into the pore solution (Glasser 1991, Saha, Khan et al. 2018).

From the available information, ASR only takes place in certain conditions. The four requirements that must be simultaneously satisfied for the development of ASR in concrete are;

- the existence of reactive aggregates with concentrations within a critical range i.e., the source of reactive silica.
- high-alkali concentration, or more precisely high OH^- ions concentration in interstitial concrete pore solution (for silica attack).
- a source of soluble calcium, such as portlandite, to react with dissolved silica and form the deleterious gel.
- High-humidity conditions as the access to moisture allow the gel expansion

(Bérubé, Duchesne et al. 2002, Rajabipour, Giannini et al. 2015, Figueira, Sousa et al. 2019).

If any of the mentioned factors do not exist, then the ASR does not occur (Lindgård, Andiç-Çakır et al. 2012, Gautam and Panesar 2017). Therefore, all the specifications recommended and mitigation methods to prevent depreciation by ASR seek to exclude at least one of these (Figueira, Sousa et al. 2019).

2.1.1 Mechanism of Reaction and Expansion

ASR damage is a result of several sequential reactions, including 1) dissolution of metastable silica, 2) formation of nano-colloidal silica sol, 3) gelation of the sol, and 4) swelling of the gel, as shown in Equation 1. Alternatively, a highly degraded $(SiO_2)_{solid}$ may transform directly into $(SiO_2)_{gel}$, as long as sufficient but not excessive cross-linking is maintained between silica chains (Rajabipour, Giannini et al. 2015). Among these reactions, silica dissolution is often the slowest (Brantley, Kubicki et al. 2008), and as such, primarily controls the rate of ASR in concrete. Factors that accelerate silica dissolution

(e.g., higher alkalinity and temperature) are often used to speed up ASR in concrete, which is used in accelerated ASR tests. In addition to silica dissolution, swelling of the gel depends on the availability of moisture and mass transport properties of concrete and could limit the rate of ASR damage in dry and dense concrete (Rajabipour, Giannini et al. 2015).

$$(SiO_2)_{solid} \xrightarrow{1} (SiO_2)_{aqueous} \xrightarrow{2} (SiO_2)_{sol} \xrightarrow{3} (SiO_2)_{gel} \xrightarrow{4} \text{swelling of gel.}$$

Equation 1. Sequential ASR reactions. Source: (Rajabipour, Giannini et al. 2015)

The ASR mechanism consists of three major stages of chemical reaction equations, as shown in Equation 2. At the initial stage of ASR, the hydroxyl ions undergo a reaction with Si-O-Si bonds of amorphous silica to produce silicic acid (OH-) and alkali silicate (Si-O-R), where (R^+) represents the alkali metal ions (Saha, Khan et al. 2018). Dissolution products formed include mono-silicic $Si(OH)_4$ and $Si_nO_a(OH)_b$ oligomers, where 2a+b=4n (Iler and Iler 1979, Golmakani 2017). Those oligomers can easily convert to monomers ($H_2SiO_4^{--}$) and $H_3SiO_4^-$), di-, tri-, tetra-, and other polymeric silicate ions (Sjöberg 1996). Then the silicic acid reacts with the hydroxyl ions (OH^-) and metal alkali that forms alkali silicate hydrate by liberating water and precipitating as C-S-H, C-K-S-H, and C-N-S-H of varying compositions (Bulteel, Garcia-Diaz et al. 2002, Saha, Khan et al. 2018). The products are hygroscopic, and thus, absorb free water. The less viscous gels may dissipate from the generation site, flow along cracks, and fill pores and voids in the cement paste (Thomas, Nixon et al. 1991). Finally, the expansion occurs due to hydration of the alkali silicate gel (Glasser 1991, Swamy 1992, Ichikawa and Miura 2007). Excessive expansion can cause cracking of aggregate and cement paste to initiate degradation of concrete (Saha, Khan et al. 2018). Thus, ASR manifests as map cracking, pop-outs, and misalignment of structural elements. Examples prevalent around the state are presented in Figure 1.

$$\equiv Si\text{-}O\text{-}Si \equiv + OH^- + R^+ \rightarrow \equiv Si\text{-}O\text{-}R + H\text{-}O\text{-}Si\equiv$$

$$\equiv Si\text{-}O\text{-}H + OH^- + R^+ \rightarrow \equiv Si\text{-}O\text{-}R + H_2O$$

$$\equiv Si\text{-}O\text{-}R + nH_2O \rightarrow \equiv Si\text{-}O^- - (H_2O)_n + R^+$$

Equation 2. Sequential ASR reactions. Source: (Saha, Khan et al. 2018).

a) Map cracking-Federal Street in Riverton b) pop-outs and map cracking-Cheyenne

Figure 1. Photo. ASR damage in Wyoming. Source: UW Tanner Research Group.

2.1.2 Effect of Aggregate Characteristics

Aggregates play a significant role in ASR expansion. Depending on the reactivity of aggregates, it can be classified into two categories. Aggregates mostly containing amorphous silica are classified as reactive (e.g. opal, tridymite, cristobalite, and acid volcanic glass) and those containing crystalline silica are classified as non-reactive (e.g. chalcedony, cryptocrystalline quartz, and strained quartz). The reactive aggregates may also consist of meta-stable crystals, microcrystalline silica, and other crystalline forms containing many lattice defects, residual strains, or internal micro-cracks (Vayghan, Rajabipour et al. 2016). The reactive aggregates can be found from natural sources, as well as from by-products of industrial processes. Furthermore, aggregates from the same rock may show different potential reactivity (Figueira, Sousa et al. 2019).

The reactivity of an aggregate also depends on its size. Smaller particles have a greater surface area, which increases exposure to chemicals and ultimately increases ASR expansion (Suwito, Jin et al. 2002). However, Poyet et al. found that very small size reactive aggregates could also reduce ASR expansion. This is because very finely ground particles of reactive aggregate may take part in the pozzolanic reaction and reduce the alkalinity of the pore solution (Poyet, Sellier et al. 2007). In another case, the maximum pressure was observed for particles with the size of 2-3 mm suggesting that the swelling pressure of ASR gel depends on particle diameter. (Bažant and Steffens 2000). However, Maraghechi et al. argued that ASR expansion increases with the increase of particle size because larger particles consist of a greater amount of reactive micro-cracks (Maraghechi, Fischer et al. 2012). Aggregate containing amorphous silica may contribute to concrete strength by pozzolanic reaction at early ages or may cause ASR expansion at matured ages depending on the size (Saha, Khan et al. 2018).

2.1.3 Pessimum Effect

In the last two decades, selected manuscripts have focused on the pessimum effect, which is generally described as the balance between the alkali hydroxide concentration of a pore solution and the aggregates reactivity. For the first time, it has been shown by Stanton that a definite proportion of certain reactive siliceous aggregates induced the highest concrete expansion (Figueira, Sousa et al. 2019). Ichikawa confirmed the effectiveness of reactive aggregate proportions that exceed the pessimum proportion can reduce ASR expansion (Ichikawa 2009). There were two primary reasons to explain this phenomenon. Firstly, calcium hydroxide was consumed by the alkali silicates with the increase of reactive aggregates. As a result, the formation of the reaction rims was reduced. Secondly, the reduction of alkali hydroxides for individual aggregate particles reduced the reaction. Despite this fact, the pessimum proportion for a different type of aggregate can be very hard to predict (Saha, Khan et al. 2018).

A linear relationship between the potential reactive components in the concrete and the expansion does not exist. The pessimum behavior graph can be divided into four regions, as shown in Figure 2 and described in Table 1. The proportion of the reactive components that provides the highest expansion is called the "pessimum rate". As the ratio of the reactive components is higher or lower than this, the expansion decreases. The pessimum rate is also for the alkaline content of the concrete as in the reactive material in the aggregate (Hafçı 2019). Other parameters also exhibit this behavior: volume fraction, type and size of reactive aggregate, composition of the cement, and mixture proportion of the concrete such as water-cement ratio (Suwito, Jin et al. 2002).

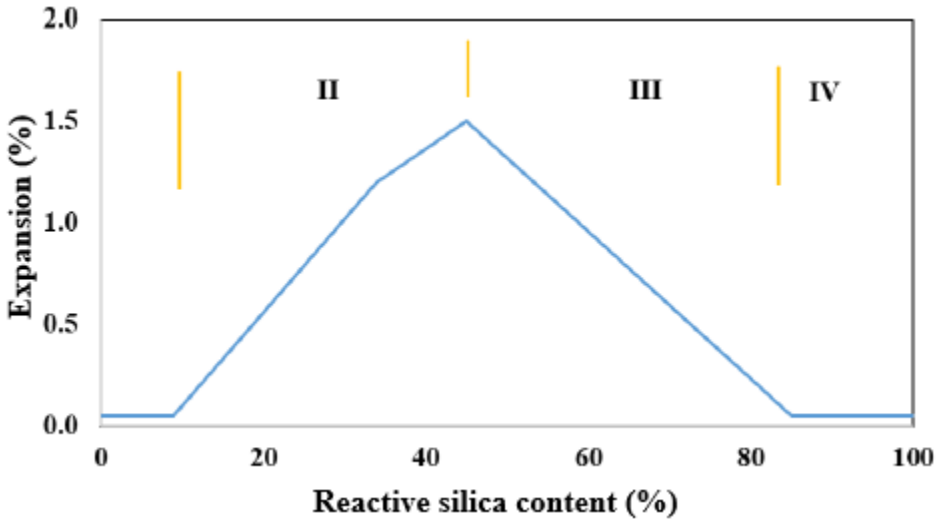

Figure 2. Pessimum effect divided into four regions. Source: (Hafçı 2019).

Table 1. Explanation of pessimum effect regions**.**

Region	Activity	Clarification
I	Reaction starts but cracking does not appear.	Sufficient gel has not been produced to initiate structure damage.
II	Reaction continues, with sufficient reactive silica, cracking may start.	Expansion is the maximum percent if reactive silica is entirely used up. Alkali/silica ratio may not affect gel composition.
III	Reaction continues, if sufficient alkali is available, cracking may start.	Expansion does not continue if alkali level is not enough to keep up the reaction. As silica content increase, process of gel expansion starts to decelerate.
IV	Reaction continues slowly but cracking comes to the end.	Although reactive silica content is very high and speed of reaction is very fast, gel formation starts to stop due to the completion of concrete hardening.

Source: (Hafçı 2019).

2.1.4 Role of alkali in ASR

Portland cement (PC) is the main source of alkalinity in concrete and its hydration contributes to a highly alkaline pore solution. Therefore, reducing the alkalinity of any pore solution is complicated. In addition, a less alkaline pore solution can cause carbonation and corrosion of the reinforcement (Saha, Khan et al. 2018). Concrete with a high alkali content will have a pH ranging between 13.5 and 13.9, while concrete with low alkali content will have a pH between 12.7 and 13.1. The high concentration of alkalis optimizes the appearance of ASR due to the increase of OH^- concentration, and therefore, the increase of pH (Figueira, Sousa et al. 2019). The risk assessment of ASR linked to alkali content, considering the contribution of sodium and potassium, in PC can be expressed in terms of equivalents of sodium oxide (Na_2O_{eq}) using the equation given in Equation 3. Bérubé et al. considered that the main cause for the development of ASR was the use of cement with high alkalis content, higher than 0.60 percent Na_2O_{eq} (Bérubé, Tremblay et al. 2004). However, some studies showed alkali contents between 0.45 percent and 0.60 percent of Na_2O_{eq} may react while others showed that contents of 0.40 percent or less rarely did (Figueira, Sousa et al. 2019).

$$Na_2O_{eq} = Na_2O + 0.658K_2O$$

where 0.658 is the ratio between the molecular weight Na_2O & K_2O

Equation 3. Equation for equivalent sodium oxide. Source: (ASTM-C1293 2009)

Alkalis can also be found in both reactive and non-reactive aggregates. Reactive aggregates are those that contain a metastable silica structure that is attacked and dissolved by OH^- ions, leading to the formation and swelling of ASR gel and ultimately cracking of concrete. Furthermore, even some alkali-containing aggregates that are classified as non-reactive have been shown to contribute to the alkalinity of concrete pore solution (Rajabipour, Giannini et al. 2015). It is reported that reactive aggregates, such as volcanic aggregates, glass aggregates, and non-reactive aggregates such as granite, mica, zeolites, clay minerals, and feldspars, can release alkali and increase the pH of pore solution (Lu, Zhou et al. 2006, Maraghechi, Fischer et al. 2012, Saha, Khan et al. 2018). Grattan-Bellew pointed out that the alkali released from aggregates can be a significant reason behind the ASR expansion of concrete (Grattan-Bellew 1995). The amount of alkali released from an aggregate depends on its mineral structure. The mechanism of alkali dissolution from the aggregates was attributed to the cation exchange with the calcium hydroxide of pore solution (Saha, Khan et al. 2018).

It has been observed that there are different types of supplementary cementing materials (SCMs) that contain a significant amount, often more than 6 percent by mass which is the allowable limit for OPC, of alkali. Nevertheless, SCMs can reduce the alkalinity of pore solution by alkali binding (Saha, Khan et al. 2018). External alkalis may increase expansion due to ASR, especially when concrete is cracked or is highly permeable. Common sources of external alkalis are deicing salts, seawater, groundwater, and water from industrial processes. In particular, the use of pavement deicers can contribute significantly to alkalis. Sodium chloride deicing salt solutions or seawater can provide virtually unlimited amounts of alkali. Certain non-chloride anti-icers and deicers, such as potassium acetate or sodium, are currently being investigated regarding their effect on ASR. In addition to proper handling, placing, and curing of concrete, the use of supplementary cementitious materials and a low water-cementitious materials ratio will reduce concrete permeability, slow the entrance of external alkalis, and reduce potential ASR expansion. Protective coatings and sealers provide a barrier to seawater, deicing salts, and other alkali sources (James and Kerkhoff 2007).

2.1.5 Role of calcium

The amount of $Ca(OH)_2$ has an important role in ASR as the calcium ions (Ca^{2+}) reacts with dissolved silica forming the deleterious calcium-rich ASR gel rim around aggregate particles. Formed by the reactions of cement hydration the Ca^{2+}, whose main source is portlandite, leads to the formation of calcium, sodium, and potassium silicate gels of

variable composition around the aggregates. These gels absorb water molecules and expand. The swelling caused by this absorption will generate expansive forces and tensile stress causing micro cracking near the reaction site and subsequent expansion and cracking of the concrete (Figueira, Sousa et al. 2019). A schematic representation of the mechanism of ASR in concrete is presented in Figure 3.

Figure 3. Diagram. Schematic representation of ASR mechanism. Source: (Figueira, Sousa et al. 2019).

The chemical composition of ASR products can be different depending on the location of the gel. For instance, a gel located in pores and cracks contains a higher amount of calcium as compared to the gel in the reactive aggregates. Therefore, it is difficult to correlate the chemical composition and the expansion of ASR products (Fernandes 2009, Saha, Khan et al. 2018). Vayghan et al. found significant expansion for a sufficient concentration of calcium in a binder matrix (Vayghan, Rajabipour et al. 2016). The authors explained that the viscosity and yield strength of ASR gel increased due to the presence of calcium. As a result, greater stress was caused by the gel expansion. However, Lehmann et al. demonstrated that the water binding capacity of ASR gel not only depends on calcium content but also on calcium to silicon ratio (Ca/Si) (Leemann, Le Saout et al. 2011). According to their study, ASR gel would bound water both physically and chemically. The amount of physically bound water is considerably higher than the amount of chemically bound water. Figure 4 shows that both the physically and chemically bound water gradually decreased with the increment of the Ca/Si ratio.

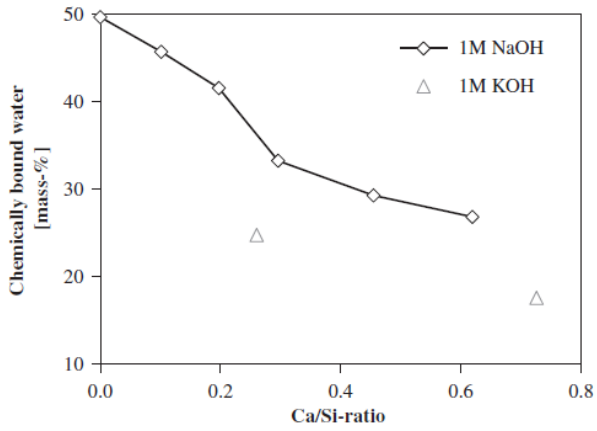

a) Chemically bound water

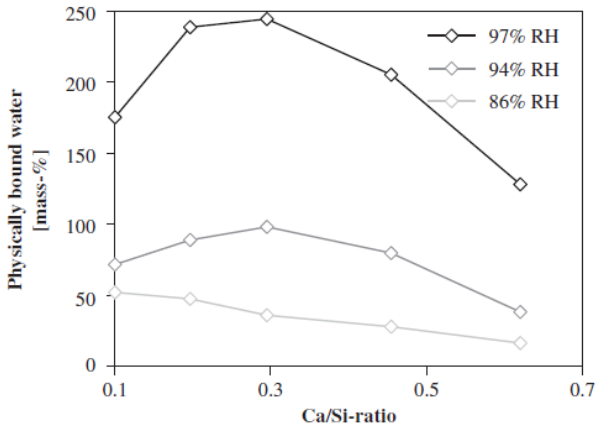

b) Physically bound water

Figure 4. Graphs. Water binding capacity by ASR gel with respect to molar Ca/Si ratio. Source: (Leemann, Le Saout et al. 2011).

2.1.6 Effect of moisture

Water appears to have a double effect on ASR; first, as a reactive agent because it influences the rate of expansion at the time of formation of the reaction product and as a transport agent of different reactive species. Second, reducing the exposure to water may constrain or halt the reaction and expansion. However, the expansion will re-develop at a rapid pace when the concrete has retained the necessary relative humidity (Oberholster and Davies 1986). For ASR development concrete must be exposed to high humidity, over 80–85 percent RH, and the ASR should not occur when the concrete is exposed to low humid conditions, even with highly reactive aggregates. The ASR expansion is not entirely dependent on water ingress. Instead, the expansion due to ASR may occur as a result of the moisture inside the concrete. This idea is supported by the appearance of cracking in dry areas compared to permanently immersed areas. However, once the reaction has occurred and enough gel has formed, any increase in the humidity may lead to quick expansion and then to cracking, that is why wetting-drying cycles can endanger a structure (Hobbs 1988, Bérubé and Fournier 1993, Larive, Laplaud et al. 2000, Figueira, Sousa et al. 2019).
All concrete structures are susceptible to ASR except for the ones where the concrete, by itself, can control the internal humidity to values lower than 80 percent and that is permanently protected from atmospheric conditions and other sources of moisture (Figueira, Sousa et al. 2019).

2.1.7 Preventive measures of ASR

As mentioned earlier, in the section Mechanism of Reaction and Expansion, the preventive measures of ASR seek to exclude at least one of the four requisites (source of reactive silica, high alkalis concentration, a source of soluble calcium, and high humidity). The following sections will discuss in detail the main achievements on how to control each requirement:

- <u>*Limiting the alkali content of concrete:*</u> The control of the alkali content assumes that the manufacturers and/or suppliers of cement certify the average alkali content and its variability. This measure is already used in several countries as part of the concrete control and standardization process. In addition to cement, other sources of alkalis for concrete, such as pozzolan additions, aggregates, kneading water, and additives should be considered. The reduction of the alkali content of the interstitial concrete pore solution can be performed by: (i) controlling the alkali content in concrete by limiting the content of concrete soluble alkalis or using suitable binders; (ii) using a total alkali content < 0.60 percent Na_2O_{eq}; and (iii) mineral addition to the concrete (Lindgård, Andiç-Çakır et al. 2012, Figueira, Sousa et al. 2019). According to the ASTM C150, 0.60 percent Na_2O_{eq} is accepted as the maximum limit for cement to be used with

reactive aggregates and is an optional limit when concrete contains deleteriously reactive aggregate (ASTM-C150 2001, Figueira, Sousa et al. 2019).

- *Use of non-reactive aggregate:* Not all aggregates are susceptible to ASR. So, non-reactive aggregates (those producing less than 0.04 percent expansion in ASTM C1293 (ASTM-C1293 2009) test or less than 0.01 percent expansion in ASTM C1260 (ASTM-C1260 2014)) can be used to avoid severe ASR problem (Rajabipour, Giannini et al. 2015).
- *Concrete moisture control:* As mentioned previously, a certain content of RH (above 80 percent) is necessary to initiate ASR in concrete. Multon and Toutlemonde have shown that if the water is supplied, regardless of the age of an ASR damaged structure, it swells if the ASR gel is already produced (Multon and Toutlemonde 2010). The authors also proposed that the ASR reaction could stop by removing water in certain areas of the structure. Therefore, any methodology that restrains water access to the concrete with reactive aggregates mitigates the risk of ASR development. These include equipment or project solutions that avoid the accumulation of water. Allowing water to drain away from the concrete structure should be a first defense (Figueira, Sousa et al. 2019). Bérubé et al. tested the behavior of different sealant materials in ASR mitigation, namely silane, oligosiloxane, polysiloxane, linseed oil, or epoxy resin on specimens prepared with a w/c = 0.50 exposed to different conditions (Bérubé, Chouinard et al. 2002). The authors showed that all the specimens sealed early with silane, oligosilixane, or polysiloxane did not expand considerably nor showed a map-cracking pattern. The epoxy resin was not effective and samples sealed with linseed oil showed poorer results compared to silane-based sealers. Therefore, a good sealer may provide an improved aesthetic appearance and stop the ASR expansion of the concrete specimens (Figueira, Sousa et al. 2019).
- *Use of lithium compounds:* The use of lithium salts to prevent ASR was reported for the first time by McCoy and Caldwell in 1951 (McCoy and Caldwell 1951). The authors tested over 100 different compounds, including organic products, metallic salts, acids and adjuvants, and reported that the lithium compounds were the most effective. Three main lithium compounds emerged as candidates for controlling ASR: LiOH, LiCO3 and LiNO3 (Rajabipour, Giannini et al. 2015). The mechanisms proposed to explain the effectiveness of lithium compounds against ASR are not fully understood (Figueira, Sousa et al. 2019). Several mechanisms were postulated by which lithium compounds may control ASR; a) lithium may reduce the dissolution rate of silica, b) lithium may impede the formation of alkali-silica gel, c) lithium may reduce repulsive forces between the colloidal gel particles of ASR, thus reducing swelling, and d) lithium may

incorporate into the alkali-silica gel, altering its properties and expansion (Rajabipour, Giannini et al. 2015).

- *Use of supplementary cementitious material (SCM):* SCMs primarily reduce the alkalinity (pH) of pore solution by OH^- consumption and alkali binding, consume portlandite, and reduce permeability and mass transport of concrete, all due to the pozzolanic reaction. Using a sufficient quantity of SCMs is the most common method of ASR mitigation for new structures. SCMs with low CaO and low alkali contents are the most effective (Rajabipour, Giannini et al. 2015). Numerous studies have shown that SCMs have a significant impact on the concentration of alkalis in the pore solution. Figure 5 illustrates the OH^- concentration at 2 years as a function of the level of SCM. Silica fume is the most efficacious SCM in this role, at least initially, followed by metakaolin, low-calcium fly ash, and slag. High-calcium or high-alkali fly ashes are less effective and have to be used at relatively high levels of replacement to produce a significant reduction in the pore solution alkalinity (Thomas 2011). It has been suggested that a minimum of 15 percent class F fly ash, 30 percent class C ash, 25 percent slag, and 5 percent silica fume cement replacement or lithium admixtures will be effective in mitigating ASR problems (James and Kerkhoff 2007).

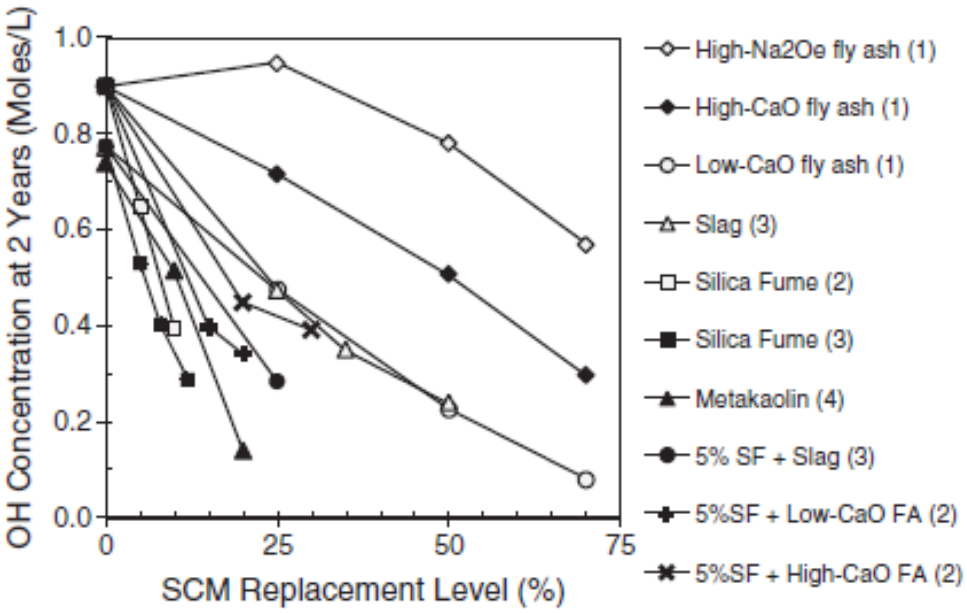

Figure 5. Graph. Effect of SCM type and replacement level on the pore solution OH^- concentration at 2 years. Source: (Thomas 2011).

2.2 Fly ash and ASR mitigation

Fly ash, a widely known SCM, is a fine powder in the form of small spherical particles with pozzolanic and binding properties. Figure 6 shows the fly ash powder along with a micrograph with spherical fly ash particles (Thomas 2007). Although the use of fly ash has

been studied extensively as an ASR mitigation technique, contradictory opinions on its effect can be observed among researchers (Saha, Khan et al. 2018). Therefore, the mechanisms associated with fly ash to mitigate ASR expansion are presented and discussed in the following sections.

a) Fine powder b) micrograph showing spherical particles

Figure 6. Fly ash particles. Source: (Thomas 2007).

2.2.1 Effect of chemical composition of fly ash

Both cement and fly ash comprise several chemical constituents, which are typically measured as oxides. The oxides include SiO_2, Al_2O_3, Fe_2O_3, CaO, MgO, SO_3, sodium oxide (Na_2O), potassium oxide (K_2O), and other minor oxides. Chemical constituents can be divided into two groups; (CaO, MgO, SO_3, Na_2O, K_2O, etc.), which promote the development of ASR, and those, (SiO_2, Al_2O_3, Fe_2O_3, etc.), which inhibit ASR (Deschenes, Jones et al. 2019). The influence of each chemical constituent originating from cement or fly ash is summarized in Table 2.

Table 2. The influence of each chemical constituent originating from cement or fly ash on ASR.

Oxide	Cement	Fly Ash
SiO_2	Inhibits ASR; promotes C-S-H formation	Inhibits ASR; promotes C-S-H, C-A-S-H formation
Al_2O_3	May inhibit ASR; most alumina goes to form Af_t and AF_m phases	Inhibits ASR; mostly present in soluble glassy phases
Fe_2O_3	Inhibits ASR; mostly present in glassy/very slowly soluble phases	Similar to alumina if present in glassy phases; crystalline forms may be inert
CaO	Promotes ASR	Promotes ASR
MgO	Promotes expansion – similar behavior to CaO if free MgO, but most is periclase. Could be magnesium-hydroxide formation, not ASR.	Free MgO promotes expansion (possible ASR); periclase phase is inert in ASR (and more common if MgO >2 %)
Na_2O	Promotes ASR	May promote ASR, but not as severely as cement alkalis.
K_2O	Promotes ASR, but not as strongly as Na_2O	Similar to Na_2O
SO_3	Weak correlation to ASR	Promotes ASR; however, could also be an expansion from ettringite formation

Source: (Deschenes, Jones et al. 2019).

The chemical composition of fly ash plays a vital role in its ASR mitigation mechanism. According to ASTM C618, fly ash containing low alkali and low calcium is classified as class F, and those with high alkali and high calcium content belong to class C (ASTM-C618 2008). Several studies conclude that class F fly ash showed better performance in ASR mitigation when compared to class C fly ash. Figure 7 shows class C and class F require different doses to reach similar expansion levels due to ASR (Shehata and Thomas

2000). Class F fly ash is very efficient in controlling expansion with 20 percent fly ash replacement reducing expansion to just 0.043 percent; a replacement of 25 percent would have undoubtedly reduced expansion to less than 0.04 percent. On the other hand, class C fly ash on the other hand is far less effective in this role and a replacement of 45– 60 percent would be required to limit expansion to less than 0.04 percent with this material. The other class C fly ashes exhibited similar behavior.

Class F fly ash contains a high amount of amorphous silica and a significantly low amount of lime. As a result, the presence of high amorphous silica consumes the portlandite from the pore solution and reduces its alkalinity. On the other hand, in the case of class C fly ash, the higher amount of calcium oxide eventually contributes to the generation of portlandite. Furthermore, the amorphous silica of class F fly ash reduces porosity by the product of the pozzolanic reaction. As a result, fewer voids are available in class F fly ash mixed concrete to accumulate the viscous ASR gels (Saha, Khan et al. 2018).

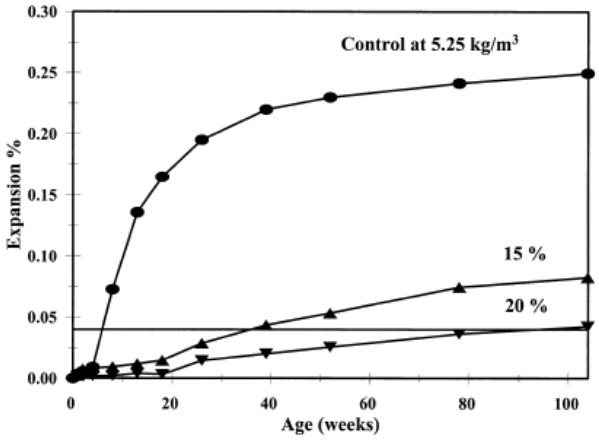

a) low-calcium fly ash, class F

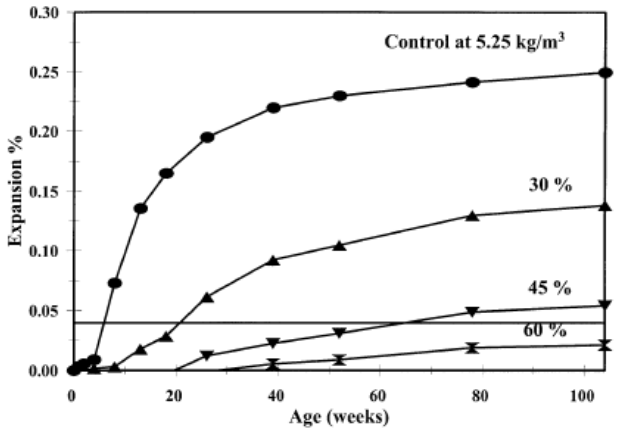

b) high-calcium fly ash, class C

Figure 7. Graph. Effect of fly ash on ASR expansion. Source: (Shehata and Thomas 2000).

2.2.2 Reduction of aggregate dissolution

ASR is initiated with the aggregate dissolution process. At first, the alkali from the pore solution attacks the amorphous silica bonds of the aggregate. Then, this generates alkali-silica gel, which absorbs moisture and expands which may cause cracking and reduction of strength. Therefore, the aggregate dissolution process was mainly responsible for ASR. Fly ash reduced the alkali concentration at the aggregate surface by providing available silicate surface area that reacted with the available alkali in pore solution. As a result, the aggregate dissolution rate decreased significantly. Figure 8 shows the mass loss of glass aggregates at 7 and 14 days (Saha, Khan et al. 2018). It can be seen that the mass loss of glass aggregates significantly decreased when 10 g and 20 g of fly ash were added to a 1 M NaOH solution. Therefore, the mass loss of the aggregates significantly decreased with the addition of fly ash.

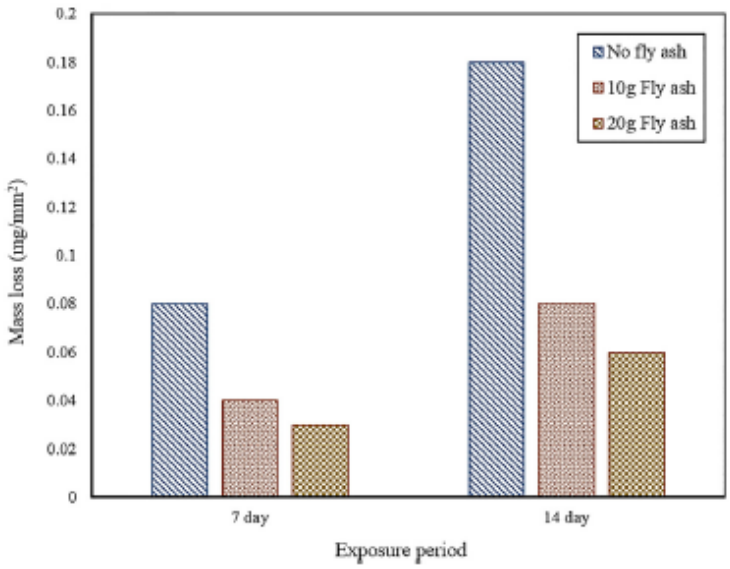

Figure 8. Aggregate dissolution by NaOH exposure. Source: (Saha, Khan et al. 2018).

2.2.3 Pore solution chemistry

Pore solution chemistry undoubtedly plays the most significant role to initiate ASR expansion. Fly ash mitigates ASR because of its effect on the pore solution. First, fly ash reduces the alkalinity of pore solution by alkali binding. The inclusion of fly ash engaged the alkali ion from the pore solution by providing a free silicate surface that reduced the concentration of alkali ion. Second, fly ash consumes alkali from the pore solution by the pozzolanic reaction. Pozzolanic C-S-H gel confined the alkali from the pore solution, thus minimizing the alkalinity of the pore solution (Saha, Khan et al. 2018). Furthermore, Hong and Glasser stated that the alkali binding capacity primarily depends on the calcium to silica (C/S) ratio of the C-S-H gel (Hong and Glasser 1999). Figure 9 illustrates the relationship between the C/S ratio of C-S-H gel and the related alkali (Na and K) binding capacity (Hong and Glasser 1999). It can be seen that low C/S has higher alkali binding

capacity as compared to a high C/S ratio. The authors concluded that C-S-H gel with low C/S leads to form acidic silanol (Si-OH) groups, which are neutralized by the reaction of the alkalis (NaOH or KOH). Finally, fly ash reduces the calcium (Ca) concentration, portlandite, in pore solution. Portlandite has been suggested to be a necessary component of the reaction and is reduced due to pozzolanic action. Additionally, portlandite contributes to the overall pH of the pore solution, which can help maintain the solution's alkalinity even when free hydroxyl ions are consumed (Shafaatian, Akhavan et al. 2013).

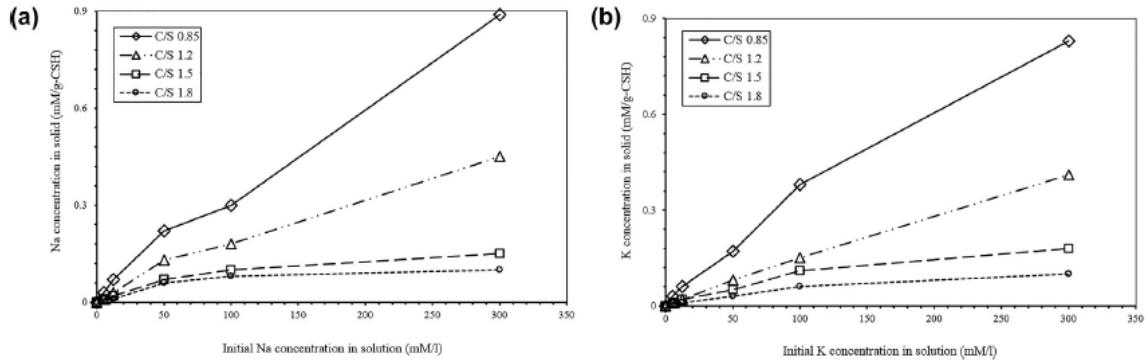

a) sodium b) potassium ion in C-S-H with respect to C/S

Figure 9. Graphs. The concentration of pore solution. Source: (Saha, Khan et al. 2018).

2.2.4 Reduction of porosity

The porosity of concrete plays a vital role in expansion due to ASR. Usually, the high porosity of concrete allows moisture from the surroundings to penetrate and trigger ASR. Haha et al. reported that highly porous aggregates suffered from greater expansion when compared to the aggregates with lower porosity (Haha, Gallucci et al. 2007). Lowering porosity increases the ASR resistance of concrete structures (Steffens, Li et al. 2003). Concrete with fly ash has lower permeability due to two main reasons; first, reduction of the transition zone thickness between surrounding aggregates and cement matrix; and second, fly ash reduces the pore size of the binder matrix by pozzolanic reaction product and filling effect of the fine unreacted particles. Thus, the low permeability of fly ash samples reduces alkali diffusion from the surroundings. Furthermore, the presence of fewer pores in cement paste mitigates the alkali-silica reaction as well as the accumulation of alkali-silica gel. As a result, fly ash specimens exhibit less expansion (Saha, Khan et al. 2018). In contrast, Pandey & Sharma found that the use of fly ash as a partial replacement of cement increased the porosity of the mortar samples at the initial stages of curing (Pandey and Sharma 2000). Although the use of fly ash may show higher porosity at the early age of curing, it can reduce the internal pores and prevent the ASR gel accumulation around the aggregates at the later ages. Furthermore, fly ash reduces permeability by pozzolanic reaction and filler effect that can eventually reduce the alkali attack from the surrounding environment.

2.2.5 Alteration of ASR gel

Some research indicates that ASR gel is produced in mortar and concrete containing fly ash without considerable expansion. This is because fly ash can change the ASR gel properties by reducing the viscosity, swelling capacity, and swelling pressure (Ichikawa 2009, Saha, Khan et al. 2018). Bonakdar et al. suggested that fly ash specimens contained fibrous platelets of Ca-Na-Si-O groups and it formed a non-expansive dense network of scattered distribution (Bonakdar, Mobasher et al. 2010). Therefore, the presence of fly ash modifies the alkali-silica gel properties, which leads to the reduction of expansion. However, contradictory opinions are found about the chemical composition of ASR gel and its swelling pressure (Saha, Khan et al. 2018).

2.3 Mechanical Properties

The pertinent mechanical properties of concrete include the tensile strength, compressive strength, shear strength, ductility, stiffness, and Poisson's ratio. In addition to the direct effect on strength and elastic modulus, cracking due to ASR also functions as a gateway for other degradation processes (Mehta and Monteiro 2014).

2.3.1 Tensile Strength

The most common way for the tensile strength of concrete to be measured is indirectly by using the splitting tensile test. The splitting tensile test involves adding a concentrated compressive line load on opposite sides along the length of the test specimen. The maximum horizontal stress as a result of the vertical line loads can then be calculated (Parker, Tanner et al. 2007, C496 2017). Generally, the strength of concrete decreases with an increase in size (Suchorzewski and Tejchman 2018, Zhong, Pan et al. 2021). However, the splitting tensile test was determined not to be sensitive to the length of the specimen and the most deterministic factor was the size of the aggregate used in the concrete mix (Słowik and Akram 2022). Another crucial factor of testing concrete in splitting tension is the strain rate. It is well understood that the strength of concrete increases with higher strain rates (Zhong, Pan et al. 2021). In addition to the size effect and strain rates, the moisture content is a crucial factor in the splitting tensile strength of concrete. The higher the moisture content, the lower the splitting tensile strength (Chen, Huang et al. 2012). Other pertinent factors include the loading strip material, or lack thereof. Although the loading strip is chiefly used to align and prevent slippage of the specimen in the splitting tensile apparatus, it was found to have a noticeable effect on the measured strength (Suchorzewski and Tejchman 2018). These factors must be addressed when developing tensile strength testing methods for concrete, and the cumulative effect of all these factors results in inherent variation in the splitting tensile strength.

Research on the relationship between tensile strength and ASR is limited. Splitting tension tests were performed on 1 in. (25.4 mm) sections of mortar bars that were part of an AMBT and it was found that there was a decrease in the splitting tensile strength when comparing

the mortar bars that experienced ASR to the ones that did not (Pathirage, Bousikhane et al. 2019). Another study has had the same conclusion (Gautam, Panesar et al. 2017). One study, that examined direct tensile strength, found that both the indirect and direct tensile strengths were negatively affected by ASR (Mohammadi, Ghiasvand et al. 2020).

2.3.2 Compressive Strength

Direct compressive strength is the most common way to compare the strength of concrete specimens. ASTM C39 and ASTM C109 provide information on the processes of direction compressive strength testing (C39 2021, C109 2021). These standards can be used as a point of reference for developing compressive strength tests under slightly different conditions. Like the splitting tensile strength testing, the direct compressive strength tests are influenced by the size of the specimen and the strain rate used to break it. An aspect ratio of 2:1 is ideal in order to avoid aspect ratio correction factors and limit the effect of crushing (del Viso, Carmona et al. 2008, Sudin and Ramli 2014). Saint-Venant's principle states that the measured stress is uniform as long as the location measured is far enough away from the loaded region, so an aspect ratio of at least 2:1 is necessary.

Like tensile strength, the relationship between compressive strength and ASR is limited. In conjunction with AMBTs, uniaxial, unconfined compression tests have been performed on mortar bars cut into 2 in. (50.8 mm) sections (Pathirage, Bousikhane et al. 2019). In general, compressive strength is affected less than the tensile strength, but the total strength gain of mortar with reactive aggregates is noticeably less when compared to control groups (Gautam, Panesar et al. 2017, Pathirage, Bousikhane et al. 2019).

2.3.3 Other Mechanical Properties

Researchers have studied the effect of ASR on other mechanical properties, such as ductility, stiffness, and Poisson's ratio. It was determined that ASR has adverse effects on both the strength and the ductility of the RC beams (Hajighasemali, Ramezanianpour et al. 2014). Additionally, it was found that mortar with reactive aggregates had a larger decrease in both stiffness and Poisson's ratio than mortar containing non-reactive aggregates (Yurtdas, Chen et al. 2013).

3 MATERIALS

3.1 Aggregates

Aggregates from different locations throughout Wyoming were evaluated and used for ASR testing in this research. The aggregates come directly from a natural source, The physical properties of washed aggregates were determined following ASTM C29, C127, and C128 standards (ASTM-C127 2015, ASTM-C128 2015, ASTM-C29 2016). The summary of the physical properties of aggregates is presented in Table 3. After receiving the aggregates, sieving of aggregates is completed using a mechanical screen shaker to get the required gradation for all ASR tests. As delivered fine aggregates were used with a gradation that meets ASTM C33 limits (ASTM-C33 2018). All the aggregates for the ASR investigations tests were washed after the completion of sieving. After washing, the aggregates were dried at 230 degrees F (110 degrees C) for 24 hours. Then the oven-dried aggregates were stored in selves till casting.

Table 3. Physical properties of aggregates.

Properties	**BT-C**	**JP-C**	**VR-C**	**2M-C**	**KR-C**	**BK-C**	**BT-F**	**JP-F**	**VR-F**	**2M-F**	**KR-F**	**BK-F**
Apparent Specific Gravity	2.61	2.62	2.70	2.68	2.56	2.58	2.70	2.79	2.73	2.76	2.65	2.78
Bulk Specific Gravity (Dry)	2.57	2.56	2.65	2.62	2.52	2.43	2.64	2.73	2.67	2.65	2.61	2.59
Bulk Specific Gravity (SSD)	2.59	2.58	2.66	2.64	2.54	2.49	2.66	2.75	2.69	2.69	2.63	2.66
Absorption (%)	0.62	0.95	0.70	0.83	0.67	2.33	0.76	0.89	0.92	1.54	0.57	2.64
Dry-rodded Unit Weight, lb/ft^3 (kN/m^3)	104 (16.3)	102 (16.0)	101 (15.9)	104 (16.3)	101 (15.9)	100 (15.7)	107 (16.8)	107 (16.8)	112 (17.6)	106 (16.7)	108 (17.0)	109 (17.1)

Source: UW Tanner Research Group.

For the AMBT and strength testing, the aggregates used were natural aggregates (NAs); no recycled aggregates (RCAs) were used. Out of the 12 aggregates used, 10 are sourced from Wyoming: 2M, DF, GP, HP, JP, KR, LBG, LX, VR, and WOR. One of the aggregates, BK, is sourced from Texas, and one, BT, is sourced from Colorado.

The specific gravity (SG) and absorption of each of the 12 aggregates were determined in accordance with ASTM C128 (C128 2015). Only fine aggregates are required for the AMBT, so the physical properties of the coarse aggregates are not provided. The summary of the relevant physical properties of the fine aggregates is shown in Table 4.

Table 4. Physical properties of fine aggregates used in the AMBT.

Aggregate	SG (SSD)	Absorption (%)
2M	2.69	1.54
BK	2.66	2.64
BT	2.66	0.76
DF	2.61	1.56
GP	2.63	1.01
HP	2.62	2.25
JP	2.75	0.89
KR	2.63	0.57
LBG	2.62	1.05
LX	2.60	1.81
VR	2.69	0.92
WOR	2.61	1.56

Source: UW Tanner Research Group.

Each aggregate was graded using a mechanical screen shaker. The trays were organized from top to bottom as follows: #4, #8, #16, #30, #50, #100, and, finally, the dust tray. After the gradation, the individual sizes of aggregates were washed. This was achieved by propping up a #200 sieve tray in the laboratory sink at a shallow angle. While providing agitation, water was sprayed over the aggregate until the water ran relatively clear. Following the washing, the aggregate was placed into a 230 °F (110 °C) oven until it was dry. This process typically took 24 hours. The aggregate was then placed into airtight containers and stored until casting. The graded and washed aggregates are shown in Figure 10.

Figure 10. Graded and washed aggregates. Source: UW Tanner Research Group.

3.2 Cement

High alkali cement came from Mississauga, Ontario, Canada, and was used in this research. Two shipments of the high alkali cement were received, one in 2017 and another in 2019. The chemical composition of each shipment is indicated in Table 5. The bolded section Na_2O_{eq} is the governing factor when determining the total alkalis available in the cement paste matrix. The value is determined by percent Na2O + 0.658 times percent K_2O.

Table 5. Chemical composition of high alkali cements.

Chemical	**Shipment 1**	**Shipment 2**
Silica Oxide (SiO_2) (%)	19.2	20.5
Alumina Oxide (Al_2O_3) (%)	5.3	5.5
Iron Oxide (Fe_2O_3) (%)	2.7	2.3
Calcium Oxide (CaO) (%)	61.8	61.6
Magnesium Oxide (MgO) (%)	2.4	2.4
Sulphur Trioxide (SO_3) (%)	4.0	4.0
Total Alkali (Na_2O_{eq}) (%)	0.90	0.98
C_3S (Adjusted) (%)	51	40
C_2S (Adjusted) (%)	15	25
C_3A (Adjusted) (%)	9	11
C_4AF (Adjusted) (%)	8	7

Source: UW Tanner Research Group.

Only one type of cement was used for the AMBT and strength testing, a type I/II cement from a 2019 shipment to the University of Wyoming. The chemical analysis of the cement is shown in Table 6. Na_2O_{eq} is referred to as the alkali equivalent and it is a measure of the total alkali available in the cement paste matrix. It is calculated by multiplying the percent concentration of K_2O by 0.658 and adding it to the percent concentration of Na_2O. The alkali equivalent is useful for gauging the total alkalinity of cement and determining if it is adequate for use. After the cement bag was opened, the cement was placed into sealed buckets to keep it from absorbing excess moisture from the environment.

Table 6. Type I/II cement chemical analysis.

Chemical	Weight (%)
Silicon Dioxide (SiO_2)	19.97
Aluminum Oxide (Al_2O_3)	5.32
Iron Oxide (Fe_2O_3)	2.38
Calcium Oxide (CaO)	60.91
Magnesium Oxide (MgO)	2.40
Sodium Oxide (Na_2O)	0.101
Potassium Oxide (K_2O)	1.04
Total Alkalies (Na_2O_{eq})	0.79
Titanium Dioxide (TiO_2)	0.28
Manganic Oxide (Mn_2O_3)	0.065
Phosphorus Pentoxide (P_2O_5)	0.126
Strontium Oxide (SrO)	0.08
Barium Oxide (BaO)	0.11
Sulfur Trioxide (SO_3)	4.02
Tricalcium Silicate (C_3S)	45.57
Dicalcium Silicate (C_2S)	22.89
Tricalcium Aluminate (C_3A)	10.08
Tetracalcium Aluminoferrite (C_4AF)	7.23

Source: UW Tanner Research Group.

3.3 Fly ash

Two locally available class F fly ashes were used to evaluate the mitigation of ASR for aggregates from different sources. Twenty-five percent of cement weight was replaced with fly ashes for various non- and moderately-reactive aggregates. For highly reactive aggregates, an additional 30 and 40 percent replacement was investigated to mitigate ASR. The physical and chemical properties of these fly ashes are presented in Table 7.

Table 7. Physical and chemical properties of fly ashes.

Physical Properties	**FA1**	**FA2**	**FA3**	**FA4**	**FA5**	**FA6**
Specific gravity	2.33	2.39	2.52	2.45	2.34	2.43
Chemical Properties						
Silica Oxide (SiO_2) (%)	55.48	60.63	52.42	52.86	60.66	55.75
Alumina Oxide (Al_2O_3) (%)	23.32	18.08	16.30	19.62	21.24	18.26
Iron Oxide (Fe_2O_3) (%)	4.58	4.68	6.10	5.68	5.02	10.79
Calcium Oxide (CaO) (%)	8.08	6.02	13.03	13.66	5.24	5.88
Magnesium Oxide (MgO) (%)	2.08	2.14	4.53	3.04	1.39	1.49
Sulphur Trioxide (SO_3) (%)	0.38	0.80	0.69	0.56	0.42	1.03
Sodium Oxide (Na_2O) (%)	1.50	3.07	1.85	0.52	1.92	1.23
Potassium Oxide (K_2O) (%)	1.09	1.18	2.45	1.05	1.42	2.72
Titanium dioxide (TiO_2) (%)	0.90	1.01	0.66	1.27	1.12	0.91
Phosphorus pentoxide (P_2O_5) (%)	1.23	0.54	0.24	0.26	0.19	0.52
Total Alkali (Na_2O_{eq}) (%)	2.22	3.85	3.46	1.21	2.86	3.02

Source: UW Tanner Research Group.

3.4 Additional materials

Technical grade NaOH pellets were purchased from the chemical stockroom and used to boost the alkalinity of field specimens and to meet the alkalinity requirements of CPT, ACPT prisms, and field exposure blocks. A polycarboxylate-based superplasticizer was also added to improve workability for field specimens. Leeman et al. studied the effect of superplasticizers on ASR expansion and concluded that polycarboxylate superplasticizers had a negligible effect on concrete expansion due to ASR (Leemann, Lothenbach et al. 2011).

4 TEST METHODS

Ever since Stanton (1940) reported his discovery of alkali-silica reaction in California, there has been keen interest in laboratory tests to predict whether a given aggregate will cause expansion and cracking in concrete and to evaluate preventive measures to allow for safe use of those aggregates found to be potentially reactive. The method developed by Stanton, which is essentially the same as the current ASTM C 227 test method, is still in use today by some researchers and practitioners, but a wide variety of test methods have been developed and implemented since the time of Stanton's pivotal research on ASR. Some of these test methods have been successful, some have proven to be complete failures, and others fall somewhere in the middle. Through research and development, as well as trial and error, test methods have evolved over the years, and there has been a general convergence in terms of the tests that are generally used (Thomas, Fournier et al. 2013).

Some test methods are based on the direct analysis of aggregates, such as chemical methods, and petrographic examination, and other test methods are based on the expansive behavior of cement–aggregate combinations, such as the mortar bar expansion test or concrete prism expansion test (Bavasso, Costa et al. 2020). The development of a reliable ASR test that can be completed in a reasonable time frame remains elusive. Field structures can be exposed to variable and fluctuating conditions with different temperature cycles, moisture ingress, loading, loads of restraint, and external ionic sources.

Thomas et al summarized the attributes for an ideal test as follows (Thomas, Fournier et al. 2006):

- The test should be reliable in terms of predicting how the combination of materials will behave under field conditions.
- The test should use the reactive aggregate (or the combination of aggregates) under consideration rather than a standard reactive aggregate.
- The test should not involve excessive processing of the aggregate (such as crushing a coarse aggregate to allow it to be tested in mortar).
- The test should be capable of evaluating the contribution of the cement alkalis rather than requiring an increase in the level of alkali.
- The test should be rapid, providing results in weeks or months rather than years.
- The test should be capable of assessing all types of SCM, lithium compounds and combinations of SCM and lithium (with cements of different alkali levels).

In terms of reliability, the concrete prism test offers the best prediction of field performance when SCMs or lithium compounds are used with high-alkali cement and reactive aggregates. Its main shortcoming is the length of time required to run the test (Thomas,

Fournier et al. 2006). An ideal test method would fulfill all of the aforementioned conditions, have a low inter-laboratory coefficient of variation, and provide information on long-term field performance. With that being said, current test methods could still be improved to more rapidly and reliably identify more aggregate or aggregate-cement combinations (Golmakani 2017), in particular the timing.

The following sections will cover the test methods used in this study with a discussion on the procedures, advantages, and limitations of each.

4.1 Concrete prism test (CPT)

There are a number of different concrete prism tests used to identify reactive aggregates or evaluate preventive measures, but most of them are similar to the extent that elevated temperature and augmented cement alkalis are used to accelerate the reaction (Thomas, Fournier et al. 2006). The CPT was first standardized in Canada in the 1950s and is now designated as CSA A23.2-14A. The test method was originally published in the United States as ASTM C1293 in 1995 and has been revised and reapproved most recently in 2015. In RILEM AAR-3, the CPT uses slightly different test parameters and a different recommended expansion limit (Wood 2017).

Two types of CPTs are explored in this project: standard aggregate analysis and mitigation with various fly ashes. This test, as defined by ASTM C1293, is carried out over one year for normal concrete specimens and two years for concrete specimens containing SCMs. The test requires three 3 x 3 x 11.25 inch (75 x 75 x 285 mm) prisms, this project used a fourth specimen for redundancy. The fresh concrete was prepared to cast four CPT prisms along with three 4 x 8 inch (100 x 200 mm) cylinders according to the ASTM C192 and C1293 (ASTM-C1293 2009, ASTM-C192 2016). The prisms within the molds were kept covered with wet towels and wrapped with a non-absorbent plastic sheet to prevent any moisture loss before demolding. The CPT molds with prisms and prevention of moisture loss are illustrated in Figure 11 and Figure 12, respectively.

Figure 11. Photo. CPT molds with prisms. Source: UW Tanner Research Group.

a) Prisms covered with wet towels b) Wrapped the molds with plastic sheet

Figure 12. Photo. Prevention of moisture loss before demolding. Source: UW Tanner Research Group.

After 24 hours of casting, the prisms were demolded and initial readings were measured using a length change comparator, as shown in Figure 13. Then the prisms were placed into 5-gallon buckets over approximately 1 inch (25 mm) of water using the bottom rack to achieve more than 95 percent relative humidity. A top mold was also used to secure and separate the specimens. A wicking fabric lined the inside of the bucket to help maintain the desired humidity constant. A screw top lid was used to seal the bucket and trap the moisture. A storage container with the supporting racks can be seen in Figure 14.

a) Comparator with reference bar

b) Comparator with prisms

Figure 13. Photo. CPT measurement. Source: UW Tanner Research Group.

Figure 14. Photo. Storage container with supporting racks. Source: UW Tanner Research Group.

The prisms inside the buckets were stored in the oven at 100 ± 3 degrees F (38 ± 2 degrees C), as displayed in Figure 15. A temperature-controlled heater was used to maintain a constant temperature, and two fans were used to circulate the air within the room. To measure CPT expansion after specified times the prisms were brought out of the buckets and wrapped with wet towels and placed into the curing chamber for 16 ± 4 hours, as shown in Figure 16. The expansion limit for the CPT is 0.04 percent at one year to classify the aggregate as potentially deleteriously reactive aggregate. If supplementary cementitious materials (SCMs) are used, the limit is 0.04 percent after two years.

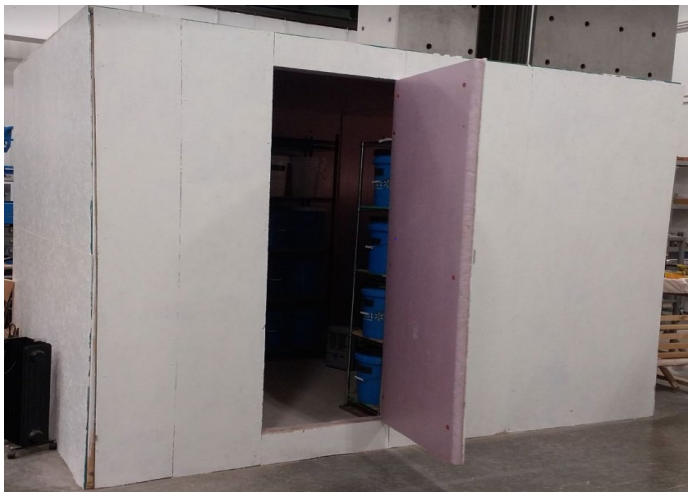

a) Outside

b) inside oven

Figure 15. Photo. CPT prism storage oven. Source: UW Tanner Research Group.

Figure 16. Photo. CPT prisms in curing chamber. Source: UW Tanner Research Group.

4.2 Miniature concrete prism test (MIN-CPT)

Existing test methods to assess alkali-silica reactivity of aggregates, such as the AMBT, have been shown to be less than satisfactory due to excessive false-positive and false-negative test results. While the CPT test is considered to be a more reliable alternative, the unusually long test duration (1 or 2 years, depending on the purpose) renders it unsuitable for routine evaluation of materials. A new test method, the miniature concrete prism test (Min-CPT), was developed that addresses the shortcomings of both the AMBT and the CPT test methods. Results from this investigation indicate that the Min-CPT test method can reliably identify aggregate reactivity within 56 days for the majority of aggregates, whereas it may take up to 84 days for some slowly reactive aggregates (Latifee and Rangaraju 2015). The Min-CPT has performed well enough that it is a provisional standard of the American Association of State Highway and Transportation Officials (AASHTO), as AASHTO TP 110 (AASHTO-TP110-14 2014, Wood 2017).

In the Min-CPT method, 2 x 2 x 11.25 inch (50 x 50 x 285 mm) concrete prisms containing aggregates with a maximum size of 1/2 inch (12.5 mm) are used. Similar to the CPT test, the total alkali content of the cement used in this test method should have a Na_2O_{eq} content of 0.90 ± 0.10 percent. Additional alkalis (NaOH) then are added to the mixing water to obtain a total alkali content of 1.25 percent (by mass of cement). Mixture proportions of ingredients used in preparing the Min-CPT specimens based on AASHTO TP 110 are summarized in Table 8 (AASHTO-TP110-14 2014). The fresh concrete is prepared and cast into three Min-CPT prisms molds, as illustrated in Figure 17 according to the ASTM C192 (ASTM-C192 2016). Then the molds are placed in the moist cabinet immediately after molds have been filled.

Table 8. Mixture Proportions for the Min-CPT Specimens.

Item	**Mix proportion**
Cement content of the mix	708 lb/yd^3 (420 kg/m^3)
Water-to-cement ratio	0.45
Coarse aggregate volume fraction (dry)	0.65
Fine aggregate	Determined based on Absolute Volume Method
Coarse aggregate gradation (by weight)	
12.5–9.5 mm	57.5 %
9.5–4.75 mm	42.5 %

Source: Prepared from (AASHTO-TP110-14 2014).

Figure 17. Photo. Min-CPT prisms inside molds. Source: UW Tanner Research Group.

After 24 ± 2 hrs of casting, the specimens are demolded, and an initial reading is taken. The specimens are then placed in a container with sufficient water inside an oven at 140 ± 3 degrees F (60 degrees C ± 1.7 degrees C) for 24 hrs. The prisms are then measured as day zero with a comparator and placed in a 1 N NaOH solution that has been preheated to 140 ± 3 degrees F (60 degrees C ± 1.7 degrees C), as shown in Figure 18. Subsequent comparator readings of the specimens were taken periodically. With slowly reacting

aggregates, additional measurements may be needed at 70 and 84 days. The proposed expansion limit is 0.04 percent at 56 days. Proposed criteria for characterizing the aggregate reactivity and effectiveness of ASR mitigation measures in Min-CPT method are presented in Source: UW Tanner Research Group.

Table 9 and Table 10.

a) specimens in soak solution b) specimens stored inside an oven

Figure 18. Photo. Min-CPT prisms curing. Source: UW Tanner Research Group.

Table 9. Proposed Criteria for Characterizing the Aggregate Reactivity in the Min-CPT Protocol.

Degree of Reactivity	**Expansion at 56 Days, % (8 Weeks)**	**Average 2-Week Rate of Expansion from 8 to 12 Weeks**
Nonreactive	≤0.030	N/A
Nonreactive	0.031–0.040	≤0.010% per 2 weeks
Low/slow reactive	0.031–0.040	>0.010% per 2 weeks
Moderate reactive	0.041–0.120	N/A
Highly reactive	0.121–0.240	N/A
Very highly reactive	>0.240	N/A

Source: (AASHTO-TP110-14 2014).

Table 10. Proposed Criteria for Characterizing Effectiveness of ASR Mitigation Measures in Min-CPT Method.

Efficiency of Mitigation	**Expansion at 56 Days, % (8 Weeks)**
Effective	<0.020
Uncertain	0.020%–0.025
Not effective	>0.025

Source: (AASHTO-TP110-14 2014).

4.4 Autoclaved concrete prism test (ACPT)

An autoclave is a pressure vessel used to create a pressurized, high-temperature environment in excess of ambient temperatures and pressures. Steam autoclaves are used to raise the internal temperature of the concrete or mortar specimens in order to accelerate the alkali-silica reaction. Additionally, an alkali hydroxide is commonly added to the mixing water in ASR testing to facilitate the reaction by ensuring a sufficient supply of both alkalis and hydroxides. This is also done in the CPT, usually to a lesser degree (Wood 2017). A number of autoclave test methods have been developed for ASR testing, most notably those by Ming-Shu et al., Tamura, Nishibayashi et al., Fournier et al., Nishibayashi et al., and Giannini & Folliard (Ming-Shu, Su-Fen et al. 1983, Nishibayashi, Yamura et al. 1987, Tamura 1987, Fournier, Bérubé et al. 1991, Nishibayashi, Kuroda et al. 1996, Giannini and Folliard 2013). Some of those methods demonstrated promise, but none have come into wider use or been standardized (Wood 2017). The test parameters of each of these methods are summarized and compared in Table 11.

Table 11. Comparison of autoclave test methods for ASR.

Test Parameter	**Ming-Shu et al. (1983)**	**Tamura (1987)**	**Nishibayashi et al. (1987)**	**Fournier et al. (1991)**	**Nishibayashi et al. (1996)**	**Giannini &Folliard (2013)**
Initial curing after mixing	3 days	3 days	2 days	2 days	NM*	4 days
Duration of conditioning	6 hours	2 hours	4 to 5 hours	5 hours	4 hours	24 hours
Specimen type	Mortar	Mortar	Mortar	Mortar	Concrete	Concrete
Specimen Size, inch (mm)	0.4 x 0.4 x 1.6 (10 x 10 x 40)	1.6 x 1.6 x 6.4 (40 x 40 x 160)	1.6 x 1.6 x 6.4 (40 x 40 x 160)	1 x 1 x 11.4 (25 x 25 x 285)	3 x 3 x 16 (75 x 75 x 400)	3 x 3 x 11.4 (75 x 75 x 285)
w/cm	0.30	NM*	0.45	0.50	0.54	0.42
Na2Oeq, by mass of cement	1.5%	2.5%	1.5%	3.5%	3.0%	3.0%
Temperature	302 °F (150 °C)	232 °F (111 °C)	262 °F (128 °C)	266 °F (130 °C)	271°F (133 °C)	271 °F (133 °C)
Conditioning	10% KOH solution inside autoclave	boiling water inside pressure vessel	Inside autoclave	Inside autoclave	Inside autoclave	Inside autoclave
Proposed Limit	-	-	-	0.15%	-	0.08%

NM*-Not mentioned.

Source: (Wood 2017).

Although not a new concept, the use of autoclaving to quickly determine aggregate alkali-silica reactivity has been mostly limited to testing fine aggregates in mortar specimens rather than using concrete. One of the limitations of using only fine aggregate in mortar is some coarse aggregates perform differently when crushed into fine aggregates (Lu, Fournier et al. 2006, Wood 2017). The autoclaved concrete prism test (ACPT), has the goal of expediting ASR testing in concrete specimens while providing reliable results compared to CPT results (Wood 2017). The autoclave is shown in Figure 19.

a) exterior

b) interior with prisms

Figure 19. Photo. Autoclave. Source: UW Tanner Research Group.

This test follows the same procedure as the standard CPT with the following exceptions:

- Total alkalis are raised to 3.0 percent.
- Specimens cure another 24 hours after demolding.
- Initial measurement is made at this point.
- Prepare the autoclave with deionized water to create steam environment.
- The specimens are placed in an autoclave for 24 hours at 29 psi (0.2 MPa) with the temperature set at 271.4 degrees F (133 degrees C).
- After the specimens are autoclaved, the specimens are cooled from 194 degrees F (90 degrees C) to 73.4 degrees F (23 degrees C) for 40 ± 5 minutes by submerging them in 194 degrees F (90 degrees C) water and running cool water through the tank. This was achieved by placing a five-gallon bucket full of water into the oven at 194 degrees F (90 degrees C) to have hot water of 194 degrees F (90 degrees C) ready before the autoclave is opened.
- The final measurement is taken once the prisms are cool.

4.5 Field specimens

Although less common, large-scale field testing of ASR has been a priority at the University of Wyoming (UW) because these specimens represent field performance more

closely. The original outdoor exposure blocks (OEBs) were cast in 2008. Aggregate gradations for each specimen were the same as the gradation of the aggregate as it was received from each source. In addition, the aggregate used for both coarse and fine came from the same source. Each field specimen was cast using the same amounts, by weight, of coarse aggregate, fine aggregate, cement, and air entrainment admixture. Quantities of additional materials for each specimen are displayed in Appendix B. To represent an upper-bound estimate of an aggregate's reactive potential, at least one field specimen from each aggregate source was boosted to 1.25 percent Na_2O equivalent by the addition of NaOH to the mixing water. This also serves to keep the alkalis in the same condition for comparison to CPT and other blocks. The amount of water added to each mixture varied by a small amount depending on the workability of the concrete. Superplasticizer was added to many of the mixtures in order to improve workability and to further represent field mixtures. Each specimen was 15 x 15 x 26 inches (380 x 380 x 660 mm) and kept to the site for outdoor exposure as shown in Figure 20. The blocks rest on 3/4 inch (19.5 mm) angular gravel atop a bed of 4 inches (101.6 mm) rock to ensure a level surface and a properly drained foundation.

Figure 20. Photo. Outdoor exposure site. Source: UW Tanner Research Group.

Threaded steel inserts were utilized to create 12 measurement locations for each block. The measurement locations are illustrated in Figure 21. Four longitudinal and two transverse measurements are on the top, two longitudinal measurements are along each side, and one vertical measurement is on the ends.

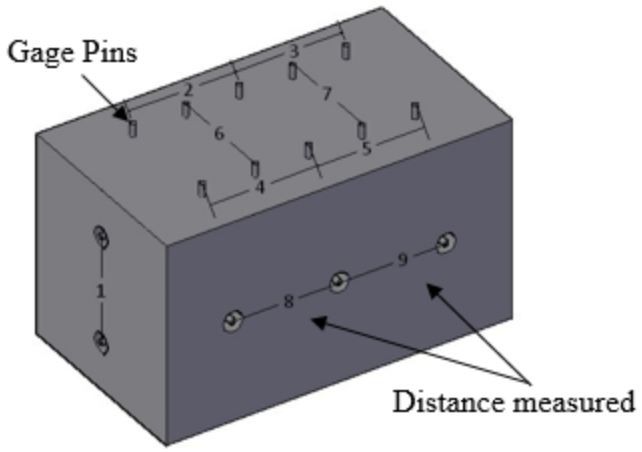

Figure 21. Diagram. Field block measurement locations. Source: UW Tanner Research Group.

Measurements are taken utilizing a mechanical strain gauge and are recorded to the nearest 3.9 x 10^{-5} inches (0.001 mm). As each measurement was recorded the effect of variations in exposure conditions during the time of measurement was significant. Initially, the effects of thermal gradients were minimized by shading the block with a 10 x 10 ft (3 x 3 m) shade for at least 1 hour prior to measuring, as shown in Figure 22, to reduce temperature differences on different block faces. To reduce thermal expansion effects, the surface temperature was taken at the time of measurement, and the recorded measurements were then scaled to obtain an equivalent value at 70 °F (21 °C). For preliminary results, 5.5 x 10^{-6} /°F (11.7 x 10^{-6} /°C), a generally accepted coefficient of thermal expansion for concrete (Darwin, Dolan et al. 2016) was used to scale the measurements. Suggestions for measuring consistently with this device are outlined in Kimble et al (Kimble, Fertig et al. 2015):

1. Expose the instrument, thermostat, and the reference bar to field conditions to avoid discrepancies due to thermal changes in the measurement equipment. If it is sunny, shade the equipment and the block for at least twenty minutes prior to measuring to reduce thermal gradients.
2. After the instrument and reference bar have been normalized to the outdoor temperature, turn on the instrument and measure the reference bar to obtain the reference measurement.
3. On the block, measure each distance between studs at least three times, and confirm that the difference in measurements is less than 0.2 x 10^{-3} inches (0.005 mm) each time.
4. Record the average of these three measurements.
5. Repeat steps 2 through 4. The second series of measurements should be completely independent of the first measurement series.

6. If the difference between related measurements in the two series is more than 0.59 x 10^{-3} inch (0.015 mm which is equivalent to 0.0075 percent expansion) then that location on the specimen should be measured again.

Figure 22. Photo. Exposure blocks shading prior to measurement. Source: UW Tanner Research Group.

4.6 Accelerated Mortar Bar Tests (AMBTs) and Strength Testing

The AMBT, as defined by ASTM C1260, is used to test potential alkali reactivity of aggregates by measuring expansions of mortar bars that have been exposed to sodium hydroxide (C1260 2021). This standardized test, however, does not provide methodology for determining the tensile and compressive strengths of the mortar bars. By referring to testing standards and other literature, a method of determining the relative strength of the mortar bars was developed. The test will still be referred to as the AMBT, and the deviations from the standardized AMBT will be explained and justified.

4.6.1 Casting and Curing

Before casting, the aggregate was first sorted into airtight bags following specific grading requirements from ASTM C1260. For a standard three-bar mix containing an aggregate with a relative density above 2.45, the total quantity of aggregate is 34.92 oz. (990 g) (C1260 2021). The graded aggregate quantities are shown in Table 12.

Table 12. Aggregate grading requirements.

Passing Sieve	Retained on Sieve	Quantity (%)	Quantity (oz.)	Quantity (grams)
No. 4	No. 8	10	3.49	99.0
No. 8	No. 16	25	8.73	247.5
No. 16	No. 30	25	8.73	247.5
No. 30	No. 50	25	8.73	247.5
No. 50	No. 100	15	5.24	148.5
Total		**100**	**34.92**	**990**

Source: UW Tanner Research Group.

The required proportion of the cement to aggregate is 1:2.25. For a standard three-bar mix, with 34.92 oz. (990 g) of graded aggregate, 15.52 oz. (440 g) of cement is needed. Additionally, the required water-cement ratio of 0.47 means 7.29 oz. (206.8 g) of free water is necessary (C1260 2021). The AMBT molds were prepared by spraying a coat of mold release onto the interior surfaces and twisting the gauge pins into the ends of each mold. The mixing and casting procedures were in accordance with ASTM C305 and ASTM C1260 respectively (C305 2020, C1260 2021). Following the casting, the mortar bars were placed into a fog cabinet that was maintained at 73 °F (23 °C) and above 95 percent relative humidity. The mortar bars were left in the cabinet for approximately 24 hours.

4.6.2 Comparator Readings and Initial Storage

After removal from the fog cabinet, the mortar bars were demolded and labeled. The labeling convention used in this investigation is the aggregate symbol, followed by the batch number (1–13), and then the bar number (A–C). Initial comparator readings of each of the bars were taken using a length comparator. The batches of mortar bars were sorted into groups of two according to the total amount of curing required. For example, the batches 2M7 and VR7 were grouped together because they were both control mortar bars that required 28 days of curing after the zero reading. The grouping was primarily done to save space in the oven and avoid using more sodium hydroxide than necessary. A prepared box, with 2M7 and VR7, is shown in Figure 23. Each box was filled with 8.82 lb (4 kg) of water to completely submerge the mortar bars. The mortar bars were then placed into an oven maintained at 176 °F (80 °C) for 24 hours. This was all done in accordance with ASTM C1260 (C1260 2021).

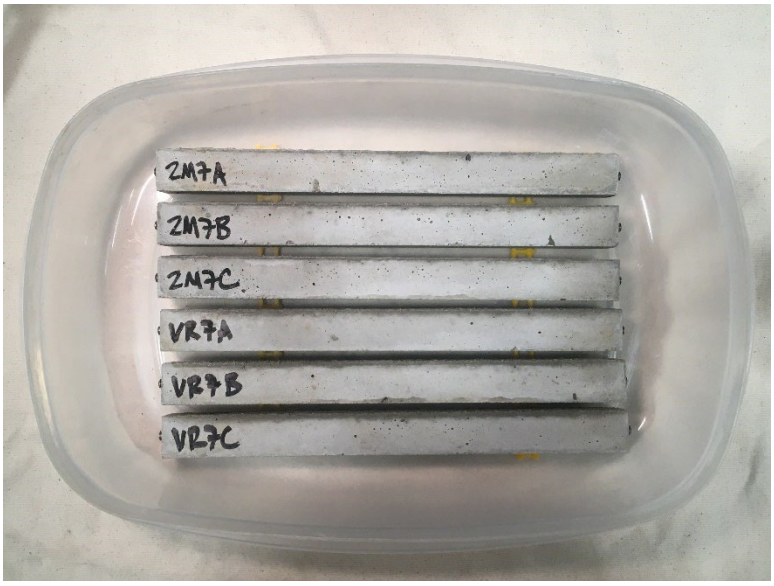

Figure 23. Prepared box of two batches of mortar bars. Source: UW Tanner Research Group.

4.6.3 Zero Readings and Long-Term Storage

After the initial storage, the mortar bars were removed from the oven, and zero readings were performed using a length comparator. This AMBT deviates from the standardized AMBT due to the use of control mortar bars. The differences in methodology for the control mortar bars and the conventional exposed mortar bars will be explained. Following the reading, the boxes of control mortar bars were filled with 8.82 lb (4 kg) of new, preheated water, and placed back into the 176 °F (80 °C) oven for the designated amount of time. Although the use of control mortar bars is not specified by ASTM C1260, it was necessary to completely evaluate the differences between the control mortar bars and the exposed mortar bars. For the exposed mortar bars, the boxes were filled with 8.82 lb (4 kg) of sodium hydroxide and placed back into the 176 °F (80 °C) oven for the designated amount of time. This is identical to the procedure in ASTM C1260 (C1260 2021). The batch numbers, mentioned in the previous section, are used to differentiate the mortar bars. Batch numbers 1–7 refer to the control mortar bars and 8–13 refer to the exposed mortar bars. The batch number is also used to indicate the total time that the mortar bars were stored in their respective conditions. A summary of the conditions is shown in Table 13. The expansions and strengths for the 0-day mortar bars were used in both the control mortar bar analysis and exposed mortar bar analysis, so the condition is not specified in the table.

Table 13. Mortar bar condition summary.

Bar ID	Condition	Time (days)
1	None	0
2	C	3
3	C	7
4	C	10
5	C	14
6	C	21
7	C	28
8	E	3
9	E	7
10	E	10
11	E	14
12	E	21
13	E	28

Source: UW Tanner Research Group.

4.6.4 Final Readings and Strength Testing

After the mortar bars were kept in their respective conditions for the designated amount of time, they were removed, and final readings were performed using a length comparator. The mortar bars were then set aside for approximately 10 minutes while they cooled down and the surface of the mortar bars dried. Although the control mortar bars dried more quickly than their exposed counterparts, the same amount of time elapsed before cutting both groups to produce the most consistent results for the relative analysis. Additionally, waiting a small amount of time before continuing with strength testing is similar to what is specified in ASTM C109 (C109 2021). Using a miter saw outfitted with a concrete blade, the mortar bars were cut into 1.5 in. (38.1 mm) and 2 in. (50.8 mm) sections. Some of the more expansive exposed mortar bars had irregular expansion, so extra care was taken to ensure plane and parallel faces. The specimens were checked for squareness and the faces were checked to make sure that there were no protruding bumps or rough edges. Each three-bar batch produced six specimens of each size. All specimens that were cut from a single batch are shown in Figure 24.

Figure 24. Mortar bars cut into sections. Source: UW Tanner Research Group.

The shorter specimens were subsequently tested in splitting tension and the longer specimens were tested in direct compression. The test equipment and procedures for the splitting tension tests and the direct compression tests will be explained. Both procedures use the same general test apparatus, which is shown in Figure 25. This test setup does not restrict the necessary movement to accommodate for slight variations in the placement of the specimens. The individual plates can rotate back and forth slightly in both horizontal planes. Additionally, the platen that presses on the upper plate can pivot through about five degrees where it connects to the rod that is attached to the frame. This would accommodate any potential cuts that were not exactly square.

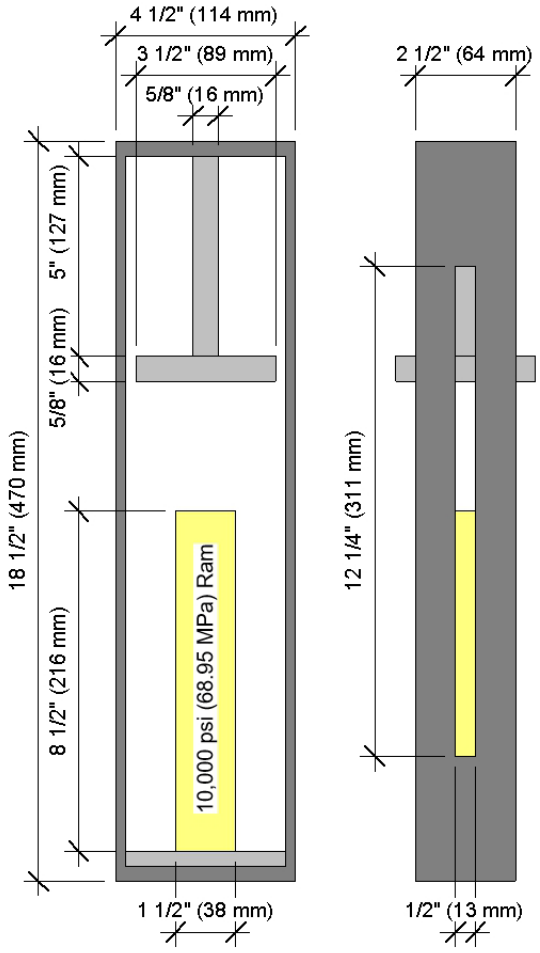

Figure 25. General apparatus. Source: UW Tanner Research Group.

For the splitting tension test, the plates shown in Figure 26 were slotted into the general test apparatus shown in Figure 25. ASTM 496 was used as a reference for conducting splitting tension tests (C496 2017).

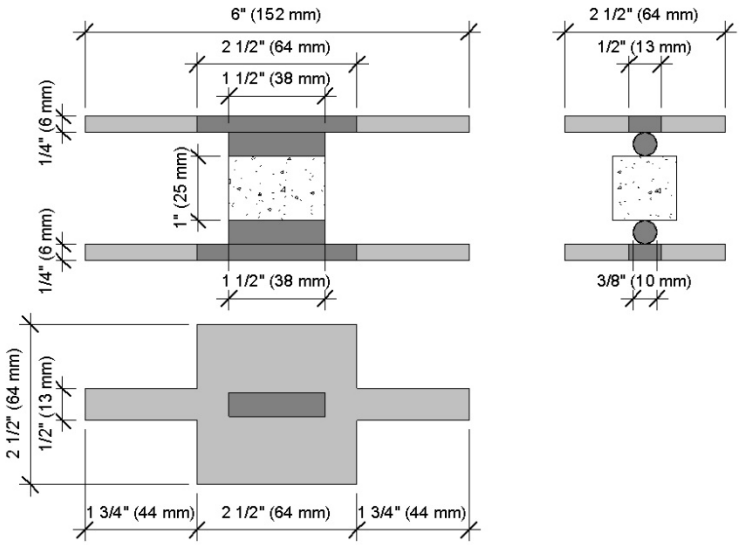

Figure 26. Splitting tension plates and setup. Source: UW Tanner Research Group.

The splitting tension test was conducted by holding the 1.5 in. (38.1 mm) specimen between the plates and adding pressure to the ram until the specimen was secured. After ensuring the specimen was correctly positioned between the round bars, a cover was placed over the apparatus. The 1.5 in. (38.1 mm) length for the splitting tension test was chosen to fit with the plates shown in Figure 26, but some studies have used 1 in. (25.4 mm) sections for the splitting tension test (Pathirage, Bousikhane et al. 2019). However, the actual length of the specimen was documented to have an insignificant effect on the splitting tensile strength (Słowik and Akram 2022). Using a 10,000 psi (68.95 MPa) single acting pump, the pressure in the ram was increased at a rate of about 50 psi/s (0.345 MPa/s). Although further research into the stress-strain relationship of mortar that has undergone ASR is needed, a reasonable range of the modulus of elasticity of mortar is from 3,200 ksi (22.06 GPa) to 3,500 ksi (24.13 GPa) (Marques, Morais et al. 2020). Based on this modulus of elasticity, the approximate strain rate range was calculated to be about 14 με/sec to 16 με/sec that is low enough to assume that the dynamic size effect is about equal to the static size effect (Zhong, Pan et al. 2021). The apparatus used for the direct compression test is almost identical to the one used for splitting tension. The only difference is that the plates shown in Figure 27 were used instead. ASTM C39 and ASTM C109 were used as a

references for conducting direct compression tests (C39 2021, C109 2021). The test was conducted by holding the 2 in. (50.8 mm) specimen vertically between the plates and adding pressure to the ram until the specimen was secured. After ensuring the specimen was positioned in the center of the plates, and there was no unexpected rotation of the plates, a cover was placed over the apparatus. No capping was required on the specimens because they were ground flat with the concrete blade and cut at a right angle. The 2 in. (50.8 mm) length for the direct compression test was chosen to achieve an aspect ratio of 2:1 and avoid aspect ratio correction factors (Sudin and Ramli 2014). Additionally, previous direct compression tests used 2 in. (50.8 mm) lengths of mortar bars (Pathirage, Bousikhane et al. 2019). The pressure in the ram was increased at a rate of approximately 100 psi/s (0.69 MPa/s). Again, by using an approximate range of the modulus of elasticity of 3,200 ksi (22.06 GPa) to 3,500 ksi (24.13 GPa), the range of approximate strain rate was calculated to be 28 με/sec to 31 με/sec.

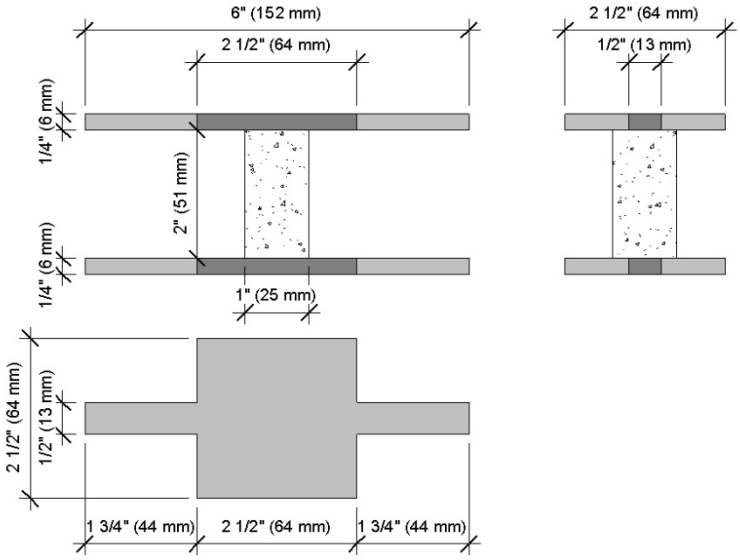

Figure 27. Direct compression plates and setup. Source: UW Tanner research group.

5 RESULTS AND DISCUSSIONS

5.1 Concrete prism tests (CPT)

To classify an aggregate's reactivity level for alkali-silica reaction, the CPT test results are presented for selected aggregates. Separated coarse and fine aggregates, as well as combinations from the same source were tested. To test coarse aggregates, nonreactive fine aggregates were used and the opposite combination was used to test fine aggregates. Results of this work are provided in Figure 28 for JP, VR, 2M, and KR aggregates. The legend is organized by decreasing expansion, with the top label having the most expansion. Circular, triangular, and diamond markers indicate separated coarse, separated fine, and combined coarse and fine aggregates, respectively. The same line style is used for all combinations from the same pit.

CPT results indicate JP and VR pit aggregates as moderately reactive (percent expansion greater than 0.04 percent) aggregate. In addition, CPT results classify 2M aggregate as very highly reactive (percentage expansion greater than 0.24 percent and KR aggregate as highly reactive (percentage expansion greater than 0.12 percent (Thomas, Fournier et al. 2012). For all four aggregates, the CPT expansion is higher for fine aggregates than coarse aggregates because of the higher surface area of the fine aggregate compared to the corresponding coarse aggregate (Suwito, Jin et al. 2002). This indicates that fine aggregates are more susceptible to ASR problems.

An additional comparison between the combined and separated aggregate sources is given in Figure 29. For three (JP, VR, and KR) out of four aggregates, the measured expansion increases when we combine both the fine and the coarse aggregate. This is attributed to the increase of reactive silica content with the addition of both fine and coarse aggregate, as shown in zone II of Figure 2 in chapter 2. On the other hand, for 2M aggregate, the combined coarse and fine CPT expansions have a lower observed reactivity. This could be the result of a pessimum effect which is explained in section 2.1.3.

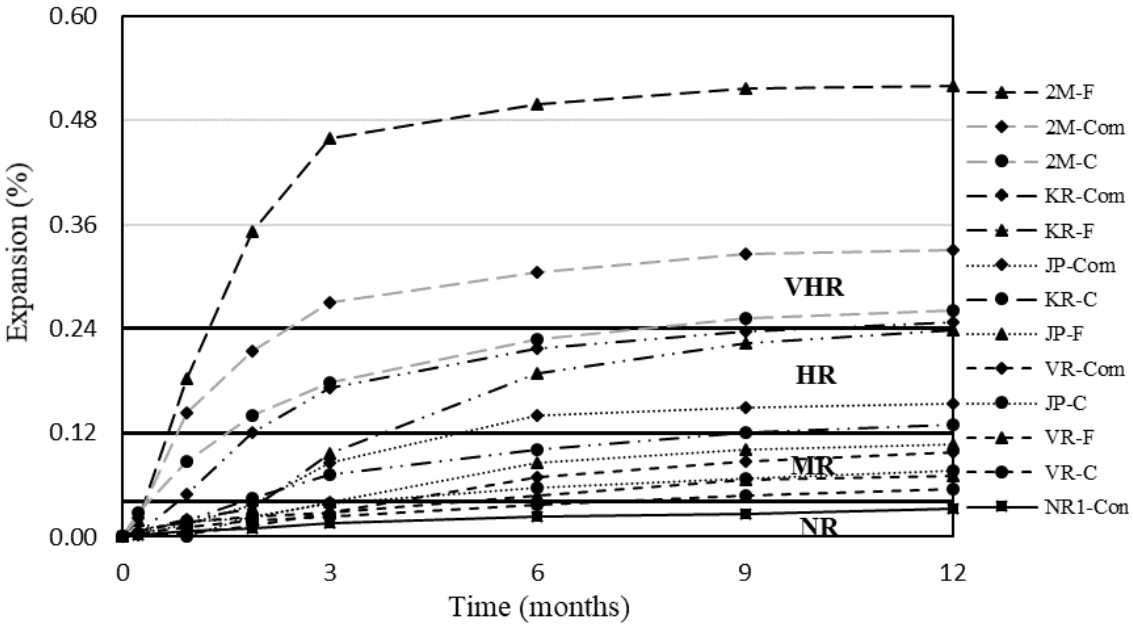

C=coarse, F=fine, Com=combined, Con=control

Figure 28. Graph. One-year CPT results for different aggregate combinations using NR1. Source: UW Tanner Research Group.

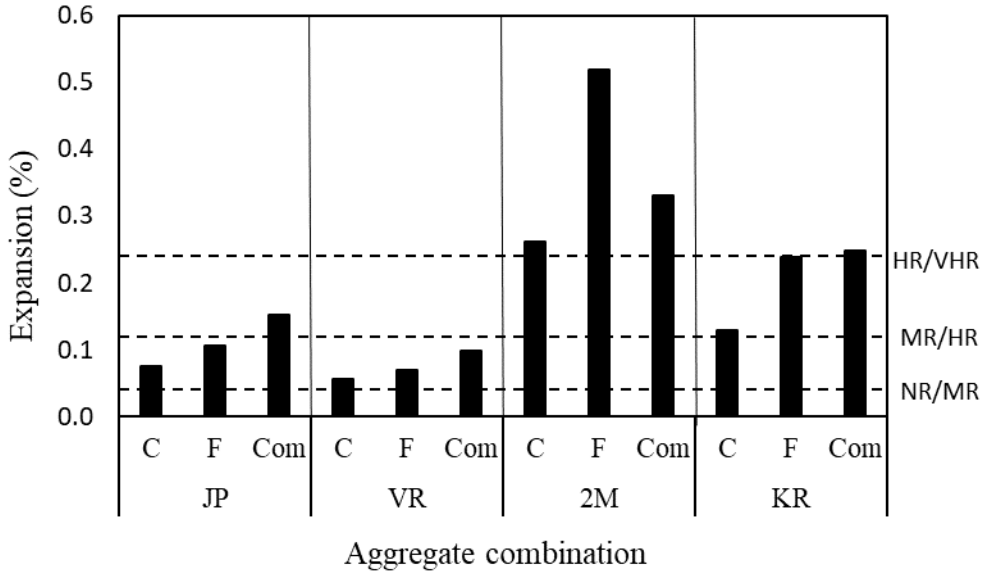

Figure 29. Graph. Comparison of separated CPT and combined CPT using NR1. Source: UW Tanner Research Group.

5.1.1 CPT with second non-reactive aggregates

The aforementioned CPT tests were performed using non-reactive BT (NR1) aggregates incorporating four different natural aggregate sources. NR1 aggregates have expansions that are roughly 75 percent of those permitted in the CPT test. In addition, a second non-

reactive aggregate, BK (NR2), was considered as an alternative source. A suite of CPT testing is underway using the same four natural aggregates and NR1 aggregates paring with NR2 aggregates. One year CPT results of this work are depicted in

Figure 30 for all five aggregates. For comparison purposes, one-year CPT data are compared for both non-reactive aggregates in Table 14. The one-year data shows a slightly lower CPT expansion (0.030 percent) for NR2 aggregates compared to NR1 aggregates (0.033 percent) and seven out of eight aggregate combinations show higher CPT expansion when paired with NR1.

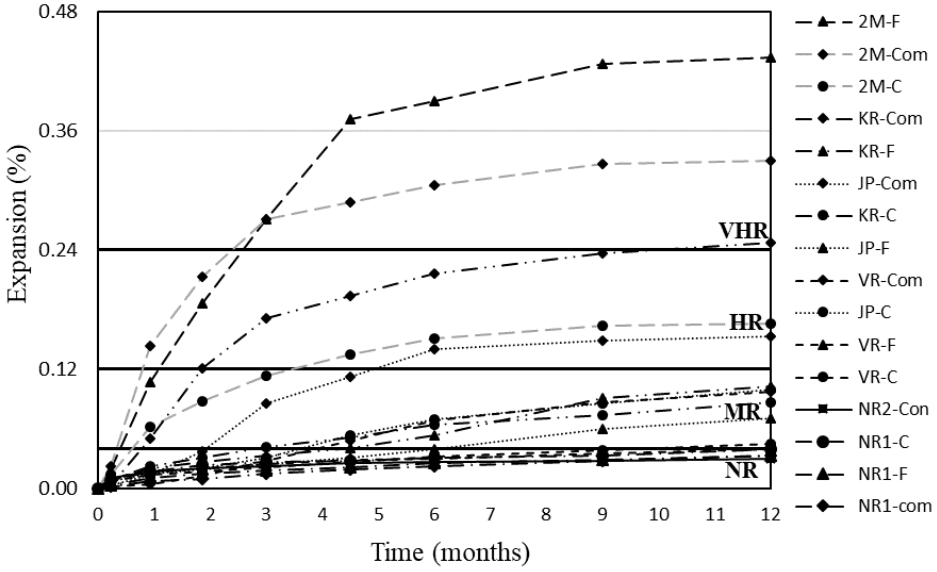

Figure 30. Graph. CPT results for different aggregate combinations with NR2 aggregate. Source: UW Tanner Research Group.

Table 14. One-year CPT expansion comparison for two non-reactive aggregates.

Batch	Paired with NR1 aggregate	Paired with NR2 aggregate
JP-C	0.076	0.100
JP-F	0.107	0.071
VR-C	0.056	0.045
VR-F	0.070	0.039
2M-C	0.262	0.167
2M-F	0.519	0.0434
KR-C	0.129	0.087
KR-F	0.239	0.103
NR1-Control	0.033	-
NR2-Control	-	0.030

Source: UW Tanner Research Group.

5.1.2 Mitigated CPT with fly ash

The mitigated CPT experiments (Mit-CPT) contain a 25-percent fly ash replacement with a 2-year exposure period. These experiments provide data on how well ASR can be mitigated using two sources of fly ash – FA1 and FA6. FA2 through FA5 has been previously tested in CPT (Fiore, Hossain et al. 2018) and a summary of those tests is presented in Figure 66 and Figure 67 of Appendix C. Two-year Mit-CPT expansions along with one-year CPT results are illustrated in Figure 31 to Figure 34 for all four aggregates and the data are presented in Table 20 to Table 23 in APPENDIX D. In these figures, blue lines indicate unmitigated specimens, while orange and grey lines illustrate results for mitigated specimens using FA1 and FA6, respectively. Figure 35 and Figure 36 separate the data in terms of the type of fly ash being utilized. The graphs are intended to illustrate the relationship between aggregate sources and their individual expansions when using the specified fly ash treatment. Figure 37 displays how effective each fly ash treatment is for each aggregate combination from different sources. For reference, CPT values are included, and the data is sorted by fly ash type. Expansion values are the most current measurement for each specimen set. The horizontal lines show the average expansion of each aggregate source for each fly ash to illustrate the overall behavior of each fly ash. At the end of two years, a 25 percent fly ash replacement for both types, successfully mitigates ASR below the 0.04 percent limit.

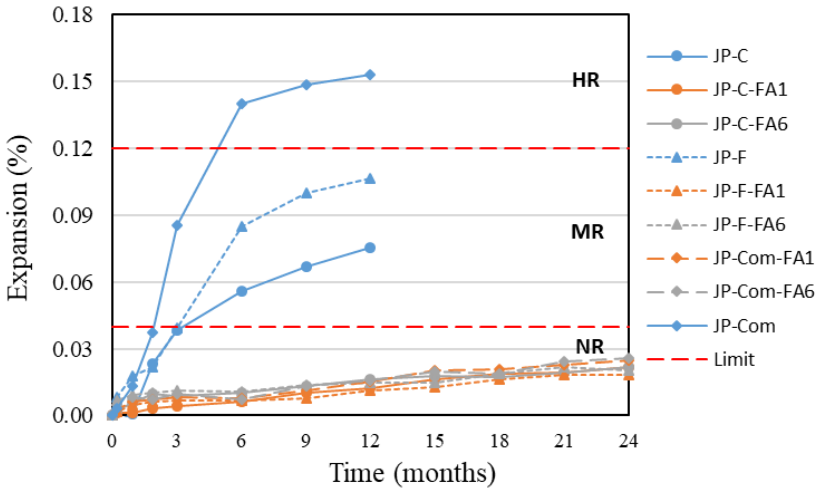

C=coarse, F=fine, Com=combined and FA=fly ash

Figure 31. Graph. CPT and Mit-CPT results for JP aggregate. Source: UW Tanner Research Group.

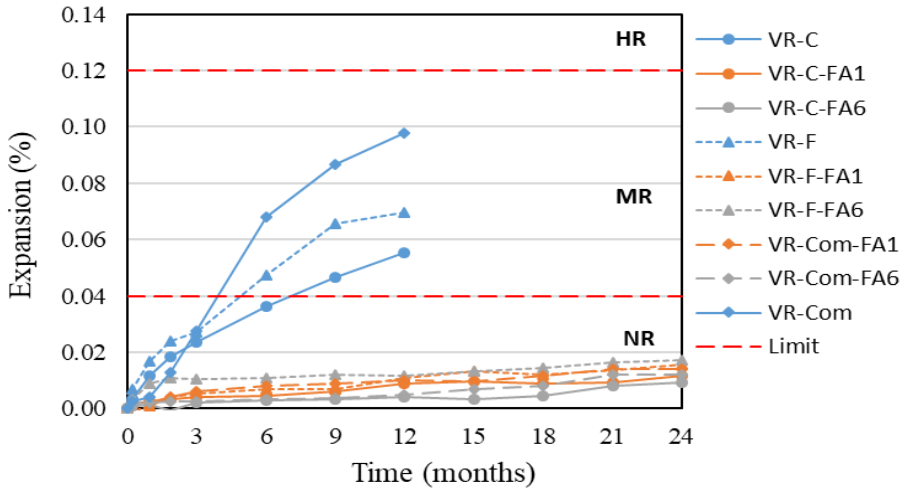

Figure 32. Graph. CPT and Mit-CPT results for VR aggregate. Source: UW Tanner Research Group.

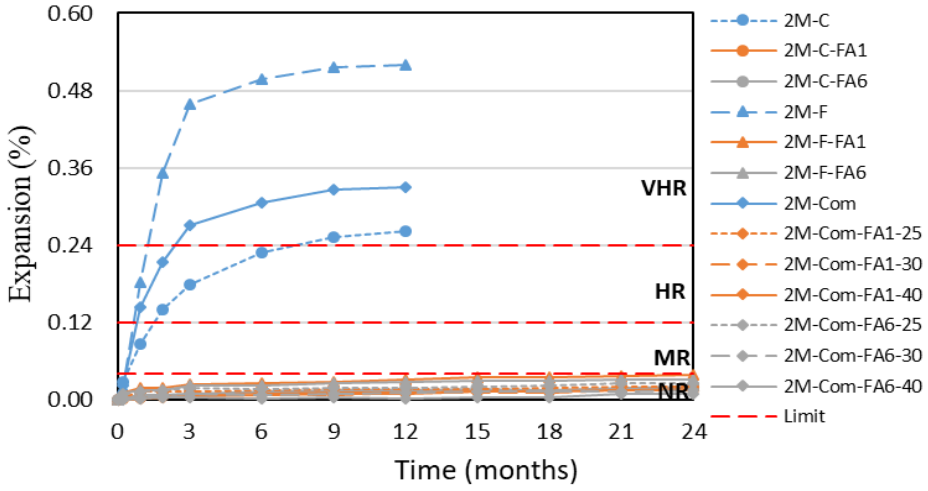

Figure 33. Graph. CPT and Mit-CPT results for 2M aggregate. Source: UW Tanner Research Group.

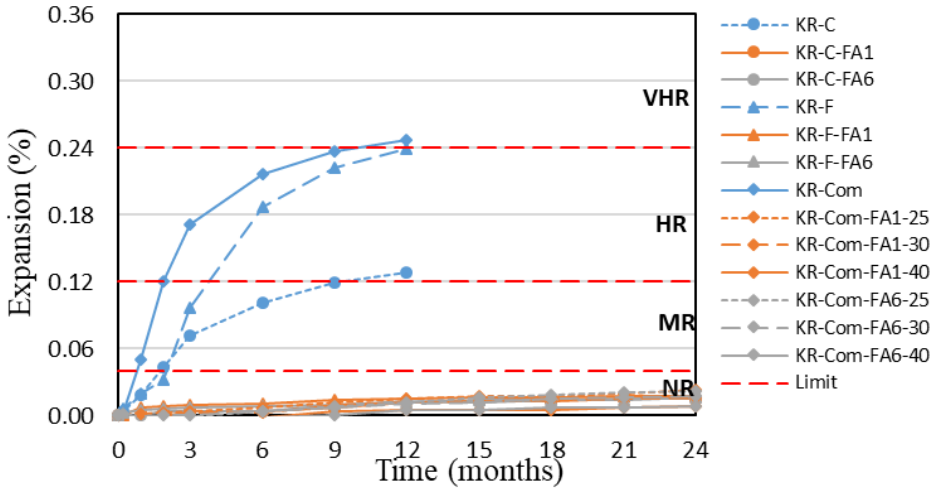

Figure 34. Graph. CPT and Mit-CPT results for KR aggregate. Source: UW Tanner Research Group.

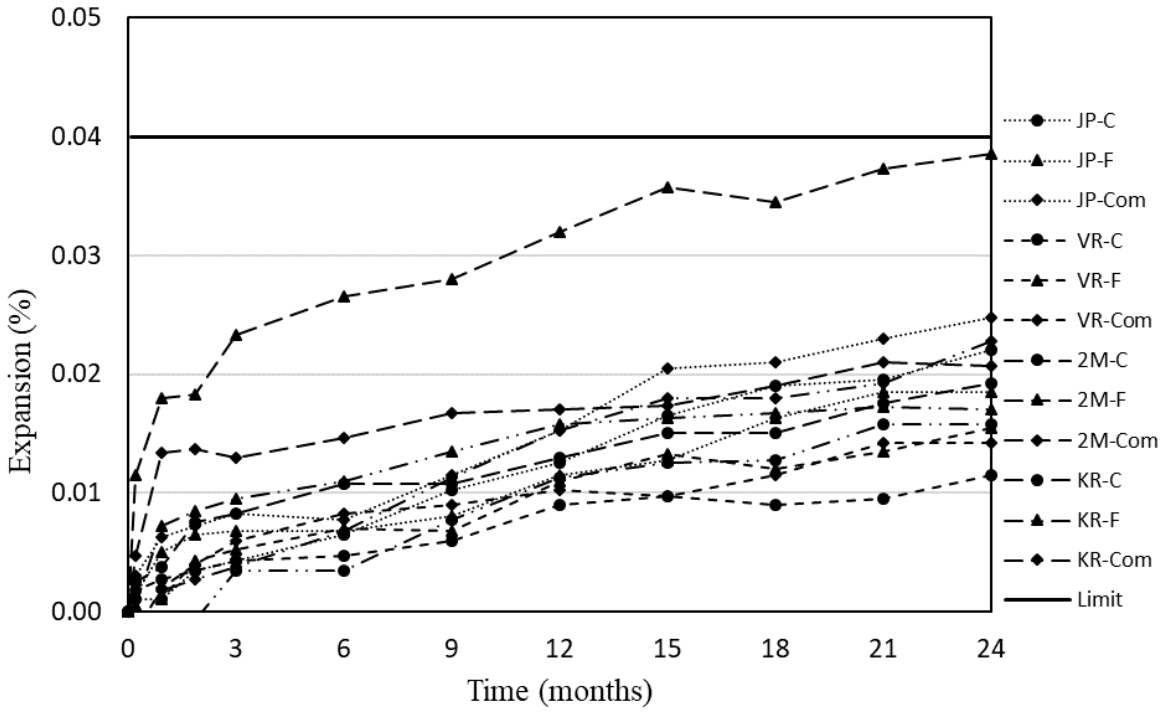

Figure 35. Graph. Mit-CPT results for FA1 fly ash. Source: UW Tanner Research Group.

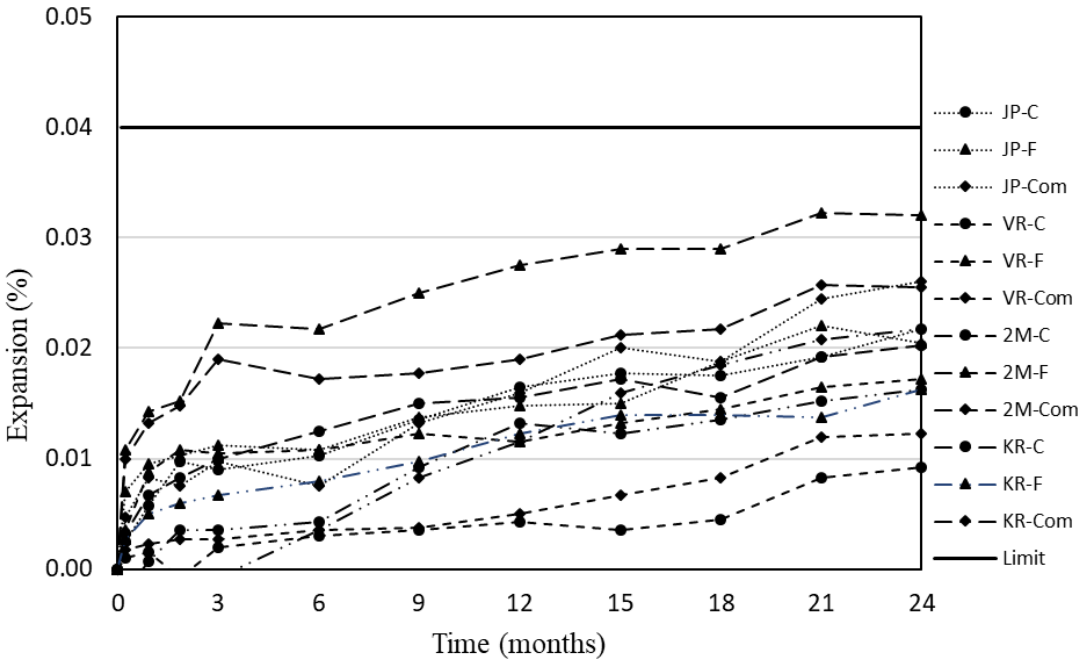

Figure 36. Graph. Mit-CPT results for FA6 fly ash. Source: UW Tanner Research Group.

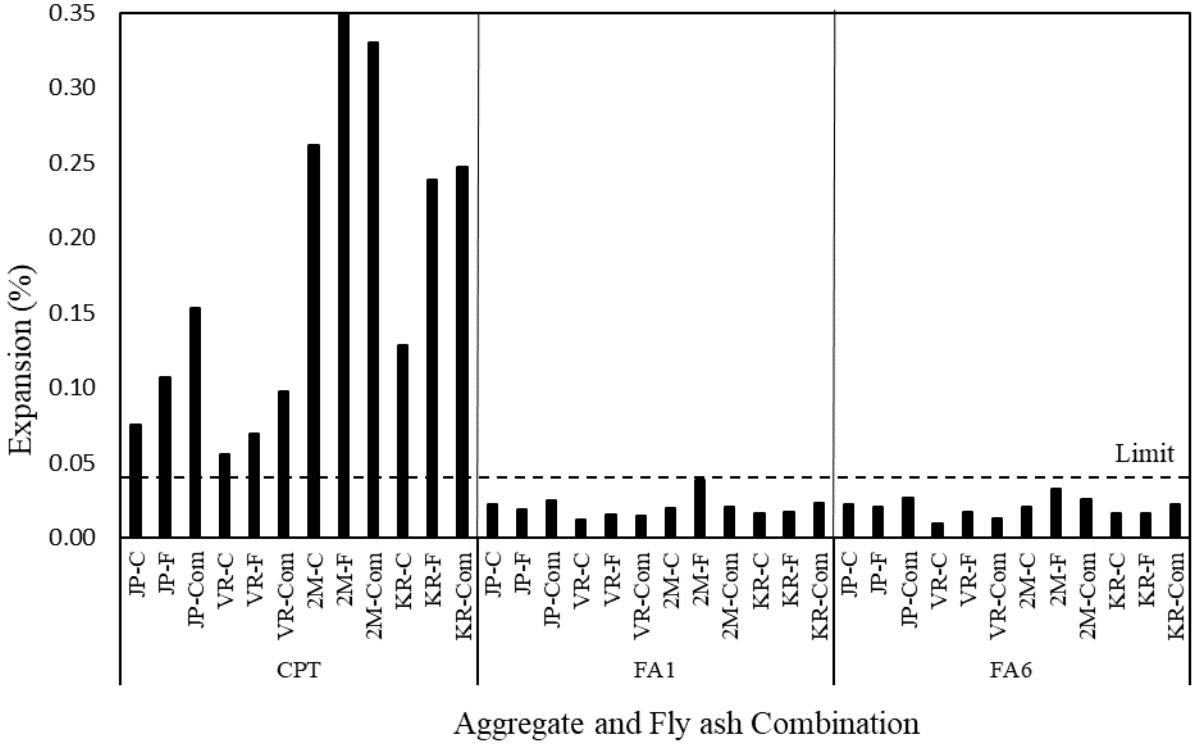

Figure 37. Graph. Fly ash effectiveness with each aggregate combination. Source: UW Tanner Research Group.

From the CPT test results, it was found that 2M and KR expansions indicate very high reactivity when used as a combination of both fine and coarse aggregate, as illustrated in

Figure 33 and Figure 34. Because WYDOT uses concrete mixtures in combination with the same source, additional testing using a 30 and 40 percent fly ash replacement for a combined 2M and KR is completed. The two-year data is available as depicted in Figure 38; it indicates that ASR mitigation increases with the increase of dosages for both fly ashes. This provides an opportunity for designers who wish to reduce the total expansion.

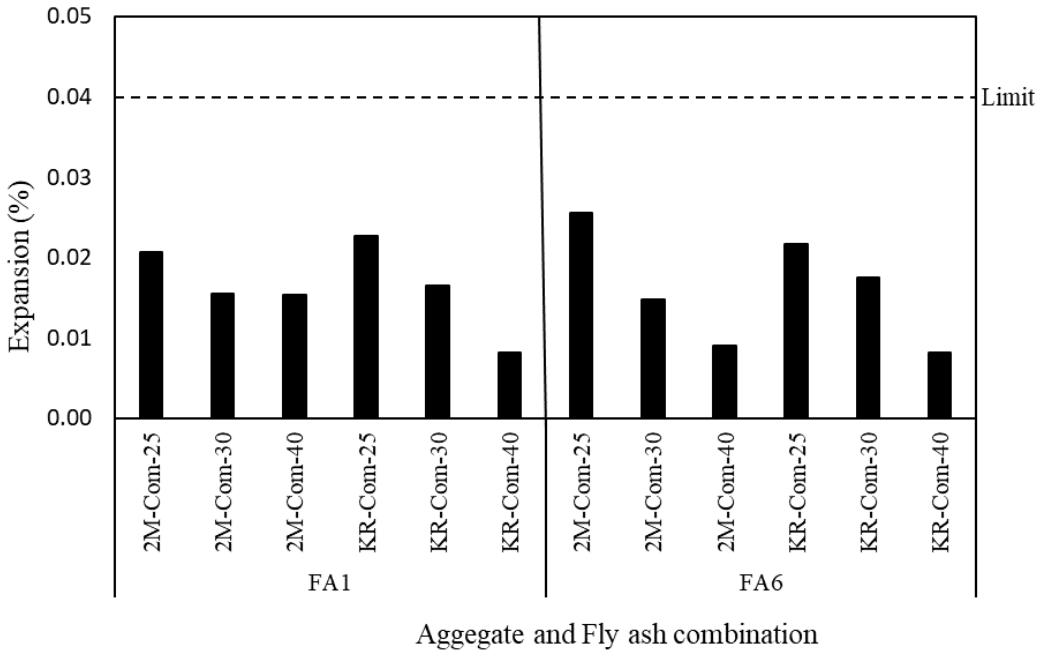

Figure 38.Graph. ASR mitigation with different fly ash dosages for combined 2M and KR aggregates. Source: UW Tanner Research Group.

5.1.3 Compressive strength

To ensure quality control, three cylinders were cast from each concrete mixture. Measured compressive strengths of each CPT and Mit-CPT are illustrated in Figure 39 for comparison. The horizontal lines show the average compressive strength of each aggregate source for each fly ash to illustrate the overall behavior of each fly ash. When 25 percent of the cement is replaced with FA1 and FA6, results in 7 and 14 percent compressive strength reductions, respectively. Additional testing was performed using a 30 and 40 percent fly ash replacement for the most highly reactive aggregates, 2M and KR. This testing quantifies the effect of fly ash dosages on compressive strength. Figure 40 shows that the compressive strength decreases with the increase of dosages for both fly ashes. For reference, without fly ash values are included and the data is sorted by fly ash type.

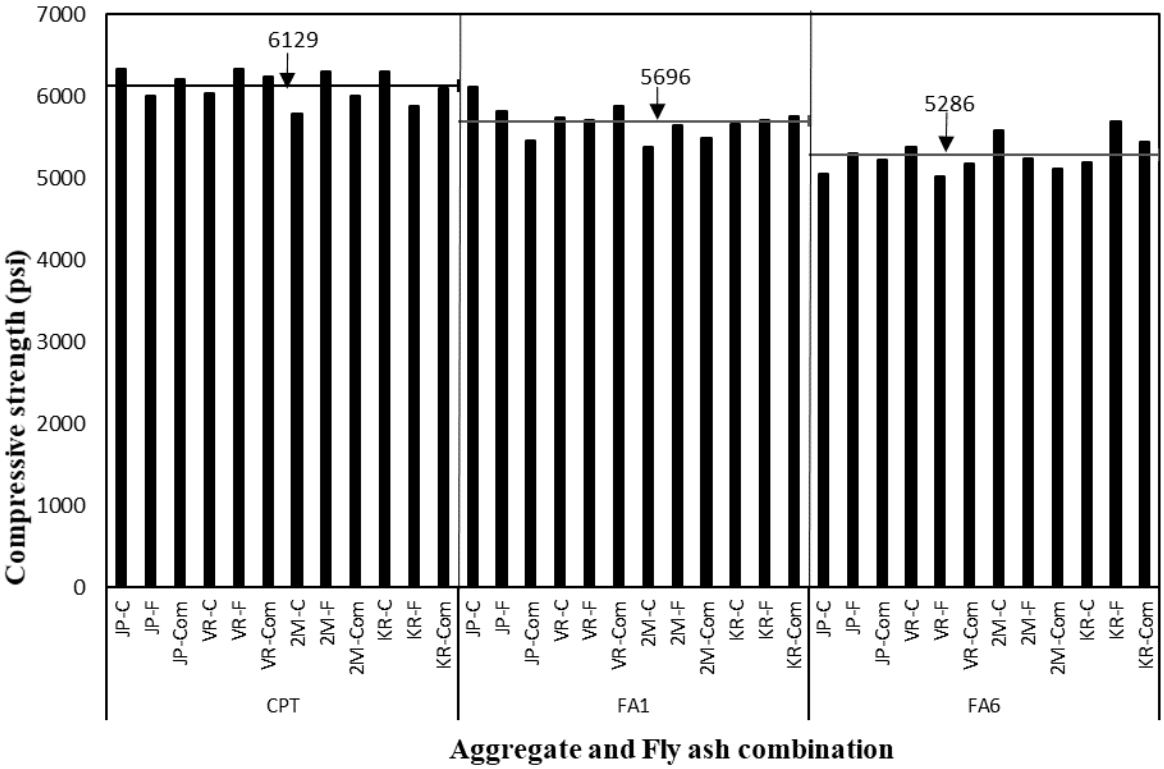

Figure 39. Graph. Comparison of 28-day compressive strength. Source: UW Tanner Research Group.

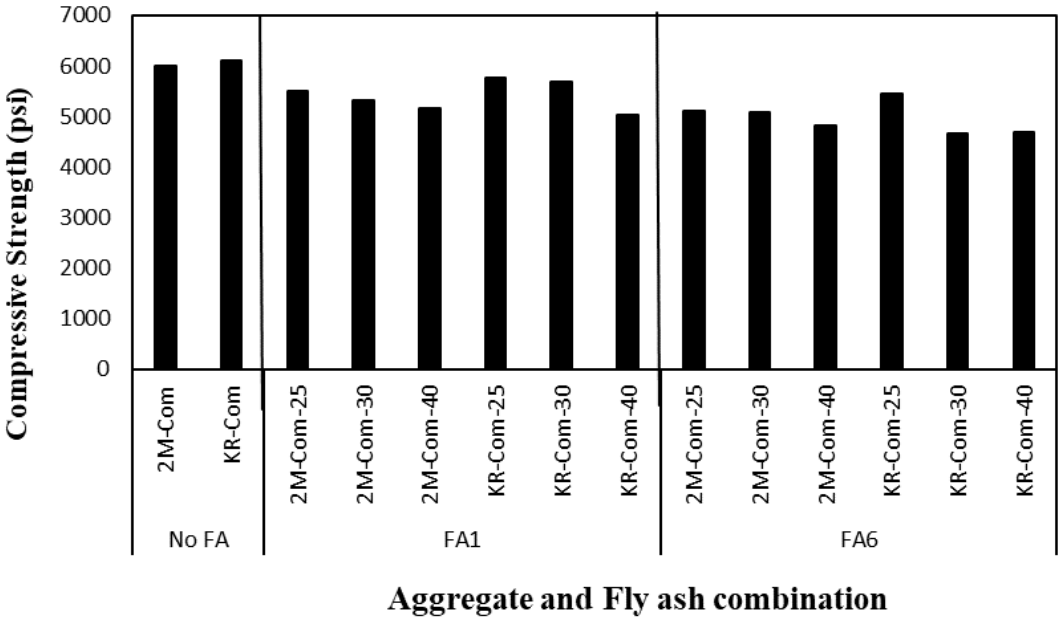

Figure 40. Graph. Effect of fly ash dosages on the 28-day compressive strength of concrete. Source: UW Tanner Research Group.

5.2 Miniature concrete prism test (MIN-CPT)

A suite of 13 sets of specimens, was evaluated according to TP-110 (AASHTO 2014), referred to as Min-CPT in this document. Results of this work are provided in Figure 41 where the legend is organized by decreasing expansion. Circular, triangular, and diamond markers indicate separated coarse, separated fine, and combined coarse and fine respectively for all aggregates. The same line style is used for all combinations from the same pit.

The Min-CPT results are compared to the one-year CPT data as shown in Figure 42, using consistent notation. Reactivity classification, whether aggregates are reactive or nonreactive, an agreement is identified by the grey shaded regions. Detailed reactivity classification, such as moderately reactive, highly reactive, and very highly reactive, is also compared. Eleven out of the 13 test results show one level of higher reactivity for Min-CPT expansion compared to CPT expansion. For example, one aggregate was found highly reactive in the Min-CPT test but moderately reactive in the CPT test. This indicates that the Min-CPT is not an exact fit when compared to the CPT test to evaluate aggregate reactivity. For this set of data, higher limits for the Min-CPT test might also bring a good agreement.

A linear regression ($y = 1.466x + 0.049$) of the Min-CPT and CPT expansion data was obtained in this study as presented in Figure 42. The slope of the trend line relates the Min-CPT expansions to those obtained from the CPT. The regression with a y-intercept has the best correlation ($R^2=0.86$) which interprets 86 percent of the mean variation of Min-CPT results are explained by CPT results. The intercept may indicate the potential for inherent expansions in the test method for a nonreactive aggregate of 0.049 percent when CPT expansions are 0 percent. This inherent expansion is attributed to the elevated temperature in Min-CPT.

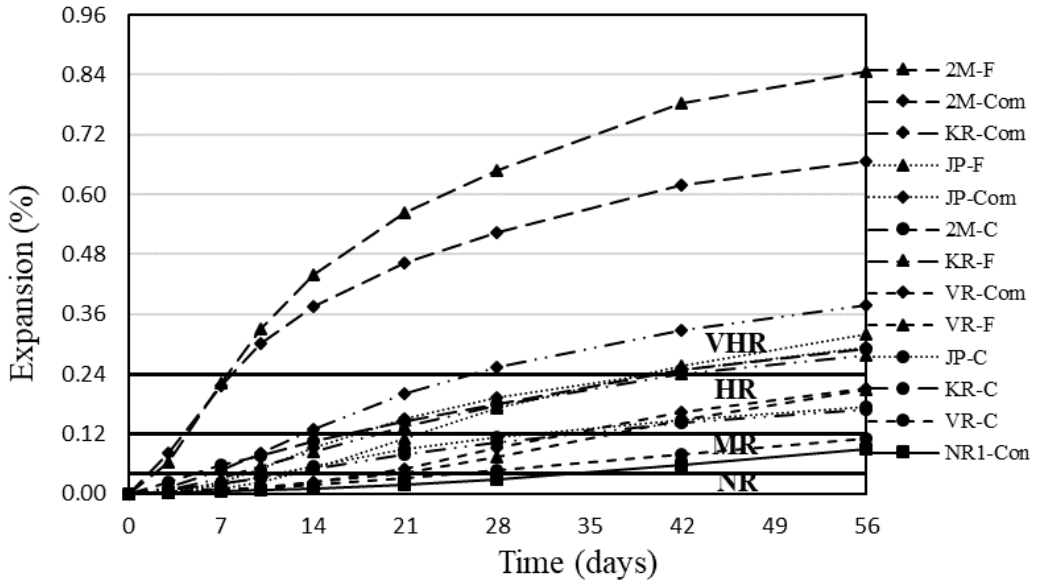

Figure 41. Graph. Min-CPT results for different aggregate combinations. Source: UW Tanner Research Group.

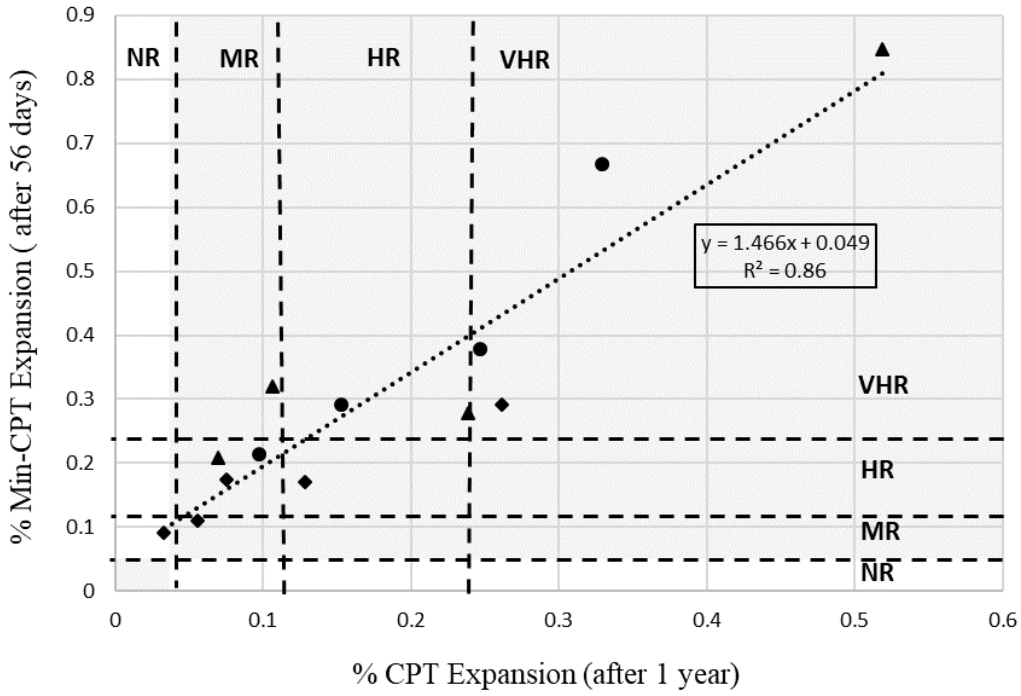

Figure 42. Graph. Comparison of ACPT results with one-year CPT results. Source: UW Tanner Research Group.

A statistical model was created to evaluate the validity conditions for the best-fit model using RStudio software. For the sample size of 13, the residual versus fitted plot in Figure

43. Since the residuals vary consistently (in a band) around 0 (other than 2 potential outliers in points 7 and 11), linearity is met. Because the residuals do not increase or decrease as fitted values increase and vary consistently about 0, constancy is met. The normal Q-Q plot in Figure 43 illustrates that the normality is met because the majority of the standardized residuals agree with the theoretical values under normality. However, the Shapiro-Wilk normality test yields a p-value of 0.87 (>0.05) which confirms a normal distribution at a 95 percent significance level.

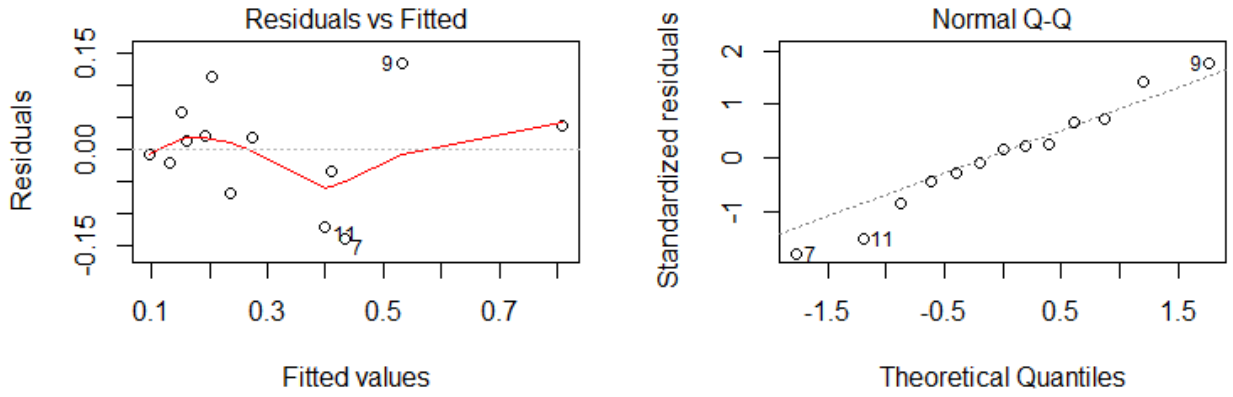

Figure 43. Graph. Regression assumptions check for the linear model for Min-CPT and CPT. Source: UW Tanner Research Group.

5.3 Autoclave tests

Unmitigated autoclave tests are completed for all JP, VR, 2M and KR aggregates considering separated coarse, fine, and combined aggregates. The casting and measurement procedure followed CPT using an accelerated exposure duration. Unmitigated ACPT test results are presented in Figure 44. As expected, the separated coarse aggregate fractions are lower than the fines or combined results.

The ACPT results are compared to the one-year CPT data as shown in Figure 45. Circular, triangular, and rectangular markers represent separated coarse, separated fine, and combined coarse and fine aggregates, respectively. Typically, the fine and combined aggregate fractions have larger expansions than coarse fractions alone. There is a trend that shows a pattern of increase for the ACPT results with the increase in CPT results.

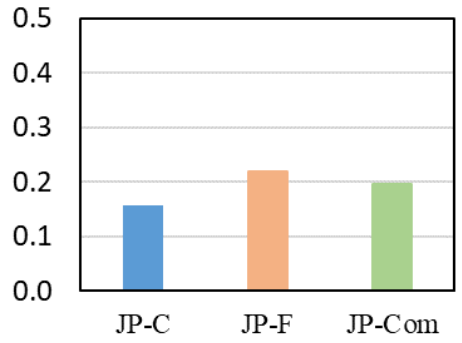

a) JP aggregate

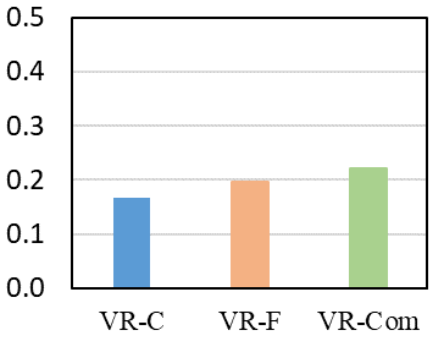

b) VR aggregate

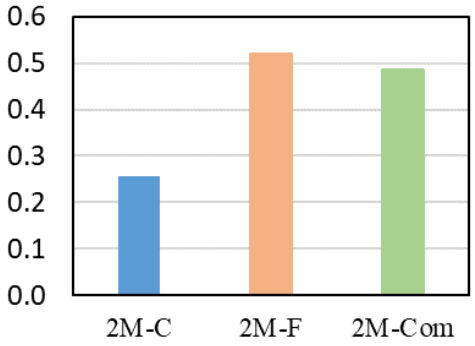

c) 2M aggregate

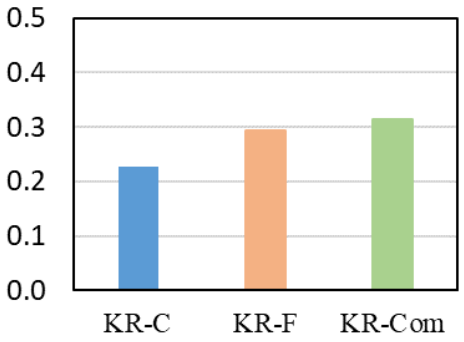

d) KR aggregate

Figure 44. Graph. Unmitigated ACPT expansion results for all four aggregates. Source: UW Tanner Research Group.

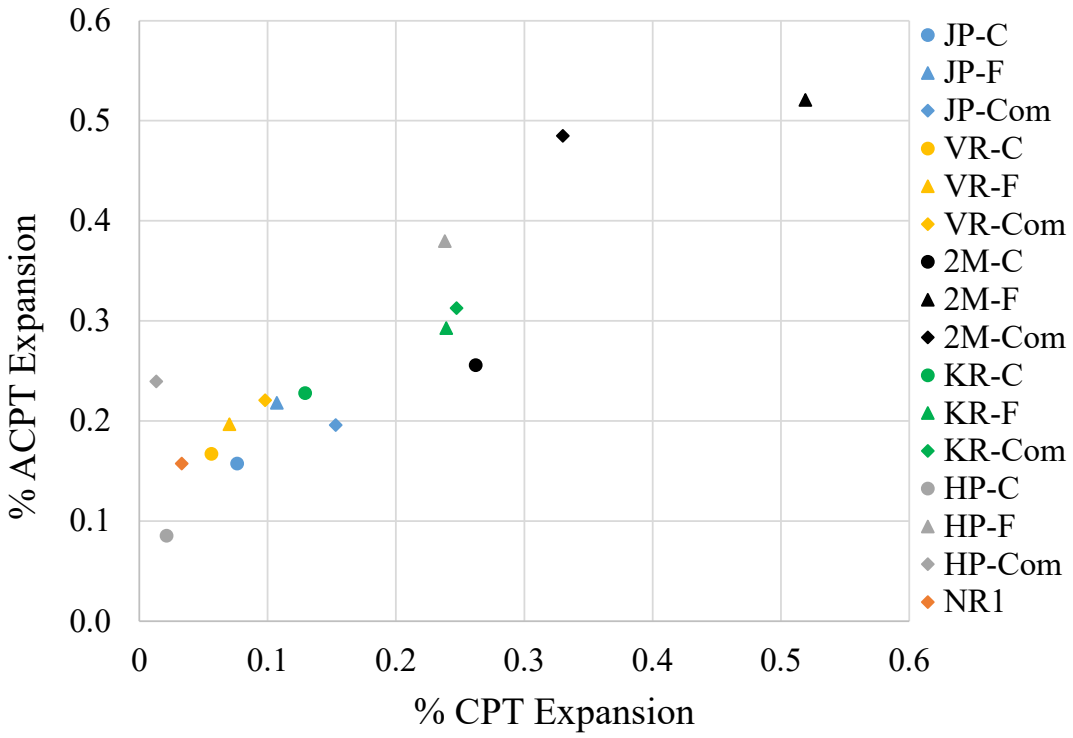

Figure 45. ACPT results compared with one-year CPT results. Source: UW Tanner Research Group.

Figure 46 evaluates the relationship between ACPT with CPT results for coarse, fine, and combined aggregate fractions. Each set of data includes a linear regression that has a y-intercept. Fine and combined aggregates have the largest y-intercept and the lowest y-intercept occurs in coarse aggregates. Although the data is limited to five points for each type of testing, different limits could exist for combined aggregate fractions. This warrants further investigation.

In Figure 47, an additional nine test results, tested in the same laboratory by another operator, are added to increase the data points. A clear trend exists between the two tests; in general, ACPT expansions increase with increasing CPT expansions.

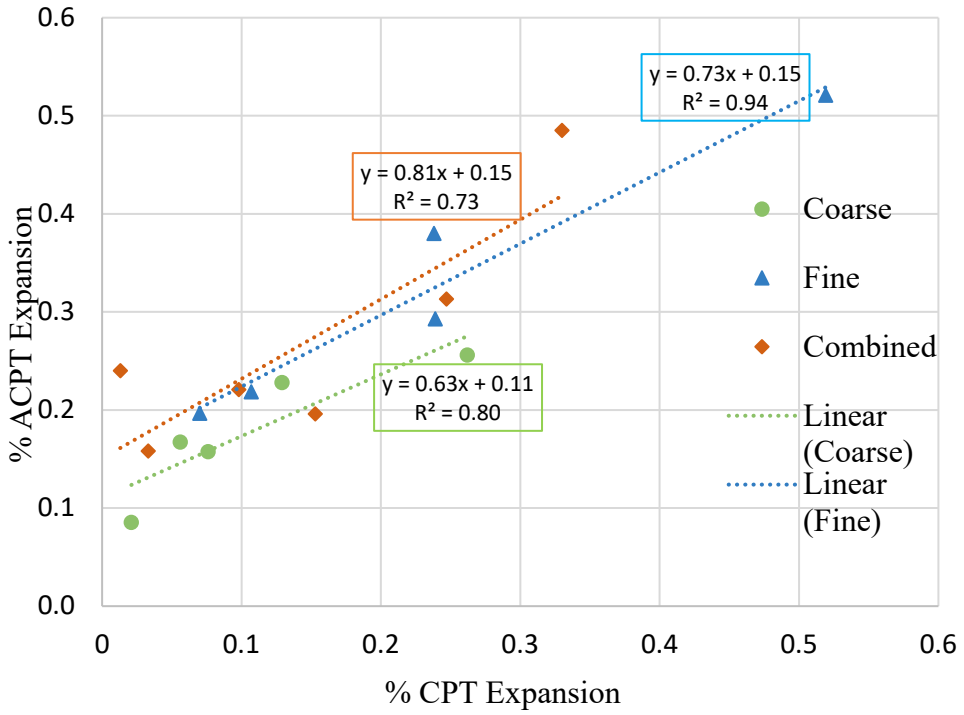

Figure 46. ACPT comparison with CPT by coarse, fine and combine aggregate combinations. Source: UW Tanner Research Group.

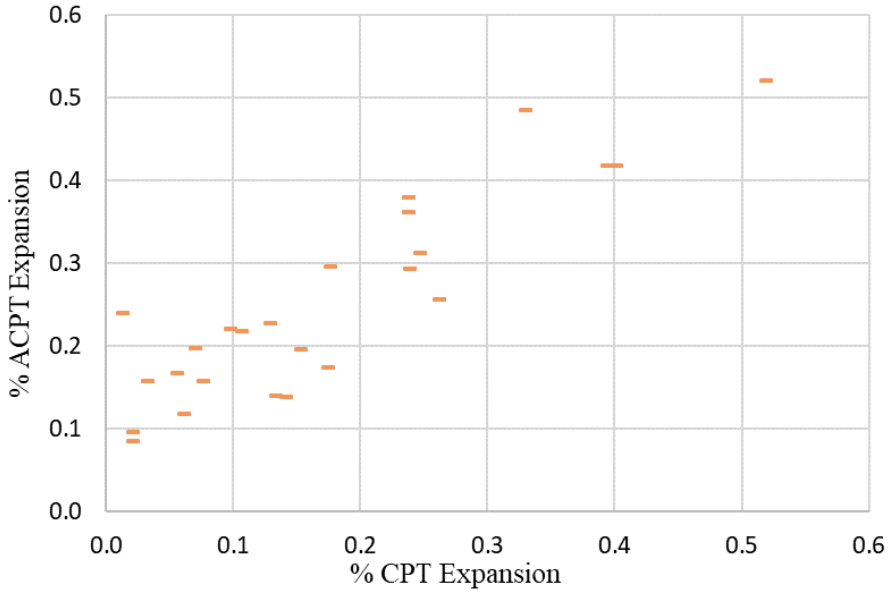

Figure 47. Compilation of ACPT results compared with one-year CPT results. Source: Fiore et al., 2018 and UW Tanner Research Group.

Figure 47 includes combining coarse and fine aggregates because that is the standard practice in the state of Wyoming. However, combining coarse and fine fractions is not permitted in the CPT standard and separated coarse and fine aggregate fractions are widely tested. For example, other investigators only report results for separated coarse or fine aggregates with the opposite non-reactive aggregate. A complete set of data for separated coarse and fine aggregates are compiled with work by other investigators (Giannini and Folliard 2013, Wood 2017, Fiore, Hossain et al. 2018) and illustrated in Figure 48. A natural break in the data occurs at an expansion of 0.09 percent. Thirty-five out of thirty-six data points confirm ACPT agrees with the CPT reactivity classifications for the proposed limit. One data point was a false positive for ACPT; that false positive has an ACPT expansion of 0.096 percent; this is close to the proposed 0.09 percent limit. Based on these 36 data points, the ACPT correctly classifies if an aggregate is reactive or not with 97.2 percent accuracy.

A linear regression ($y = 0.89x + 0.07$) of the ACPT and CPT expansion data fits this expanded scope of testing. The regression with a y-intercept has a coefficient of correlation of 0.78 ($R2=0.78$). The intercept indicates the potential for inherent expansions in the test method for a nonreactive aggregate of 0.07 percent when CPT expansions are 0 percent. This is attributed to the accelerated temperature of the exposure period.

Another indicator of the fit comes from validity conditions for the best-fit model. For the sample size of 36, the residual versus fitted plot can be seen in Figure 49. Because the residuals vary consistently (in a band) around 0, linearity is met. Because the residuals do not increase or decrease as fitted values increase and vary consistently about 0, constancy is met. The normal Q-Q plot in Figure 49 illustrates that normality is met because the majority of the standardized residuals agree with the theoretical values under normality. Finally, the Shapiro-Wilk normality test yields a p-value of 0.96 (>0.05) that confirms a normal distribution at a 5 percent significance level.

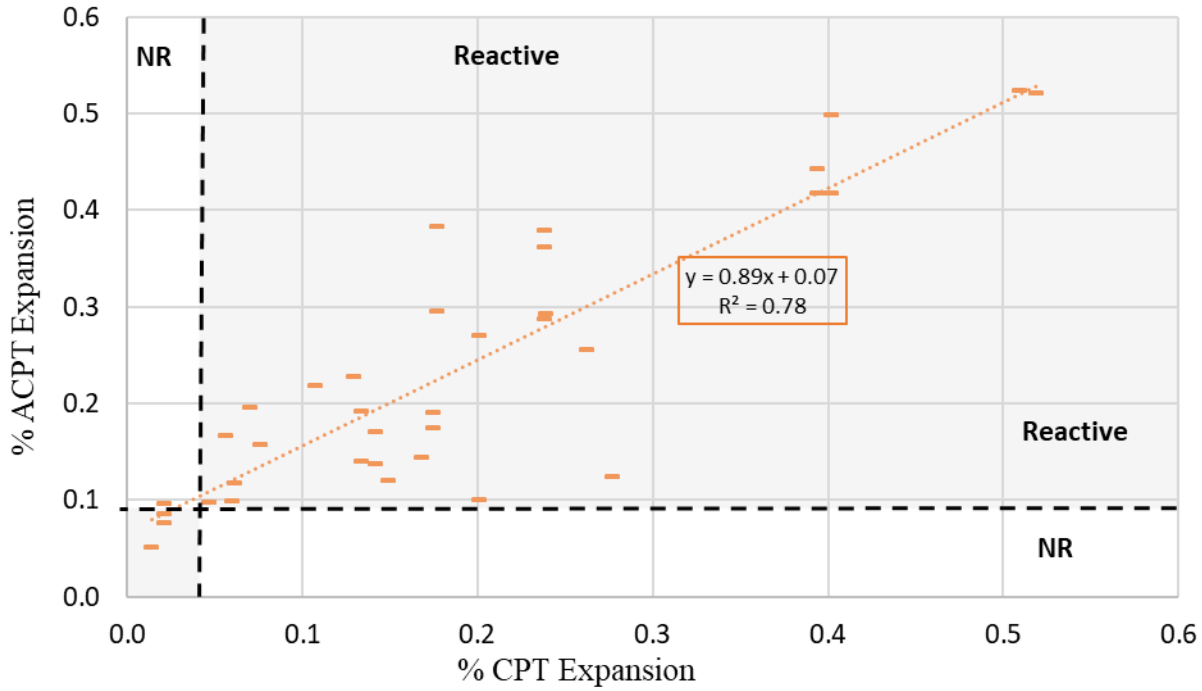

Figure 48. Summary of ACPT versus CPT data, cross and fine only, across multiple sources. Source: UW Tanner Research Group.

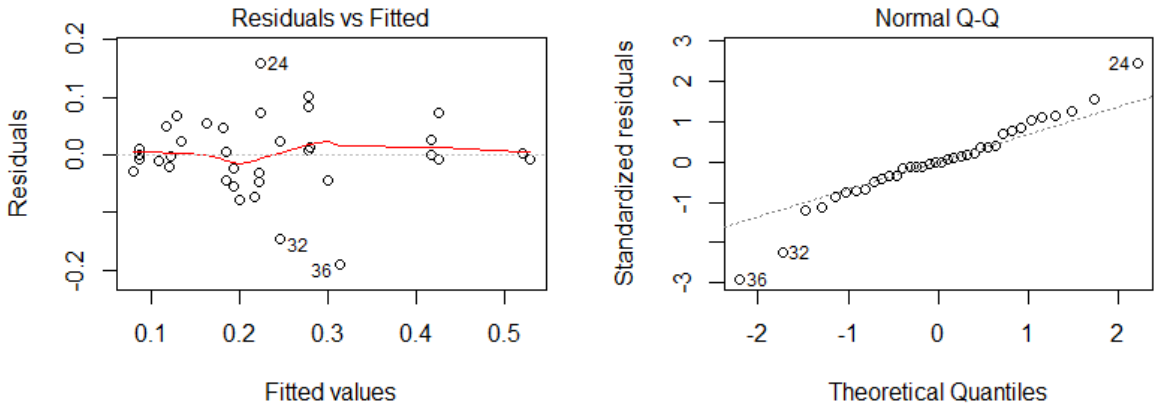

Figure 49. Regression assumptions check for the linear model. Source: UW Tanner Research Group.

5.3.2 Effect of cooling time on expansion results.

The initial autoclave testing in this project had 5 hours of the total cooling to reduce the temperature from 271.4 degrees F (133 degrees C) to 122 degrees F (50 degrees C). An additional five autoclave tests were conducted to observe the effect of the cooling period on ACPT tests. In this case, the cooling period was reduced to 2 hours which was required to cool down the temperature around 167 degrees F (75 degrees C) and to lower the autoclave pressure to zero. Out of these five tests; one nonreactive (NR1-com), two moderately reactive (JP-C and VR-F), and two highly reactive (KR-F and KR-Com) aggregates were tested. The results illustrated in Figure 50 suggest that expansions of highly reactive aggregates do not depend on the cooling temperature, but the expansion of nonreactive and moderately reactive aggregates does because it is reduced by around 28 and 20 percent, respectively. In short, smaller expansions will be more sensitive to changes in procedure.

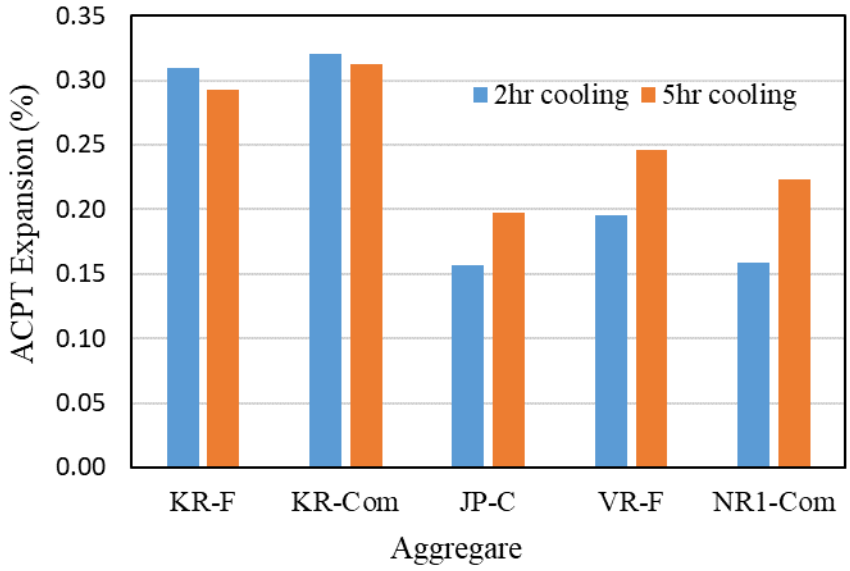

Figure 50. Graph. Effect of the cooling period for ACPT test. Source: UW Tanner Research Group.

5.4 Field exposure blocks

Outdoor exposure blocks (OEBs) are often used as benchmark ASR assessments for laboratory accelerated testing. This is because both the AMBT and CPT are stored in a controlled environment, which limits their ability to predict the true reactivity of aggregates because field conditions vary based on season and the general climate. This lack of environmental control in field specimens makes understanding all of the variables that affect ASR even more difficult. However, each of those factors affects concrete used in the real world and that is where the true value of field expansions begins to emerge. To differentiate field specimen reactivity levels, limits were fit to the values of the results to date for the boosted specimens for the original eight Wyoming aggregate sources because

they naturally fit into three groups. In this manner proposed expansion limits are a 0.02 percent increase in expansion per year separating nonreactive from moderately reactive specimens and a 0.06 percent increase in expansion per year separating moderately reactive and highly reactive aggregates. These proposed limits are halved for unboosted specimens; 0.01 percent for nonreactive to moderately reactive, and 0.03 percent for moderately reactive to highly reactive (Fertig, Kimble et al. 2017).

For the past twelve years, UW has been monitoring the ASR expansions for the original eight aggregate sources. Figure 51 and Figure 52 illustrate the expansions to date for the outdoor exposure blocks. Figure 51 represents the specimens that were cast without additional alkalis, while Figure 52 plots the results for specimens that were cast with boosted levels of alkalinity. The two dashed lines are the divisions between proposed aggregate classifications (Fertig, Kimble et al. 2017). The top line separates highly and moderately reactive aggregates while the lower line distinguishes between moderately and nonreactive aggregates.

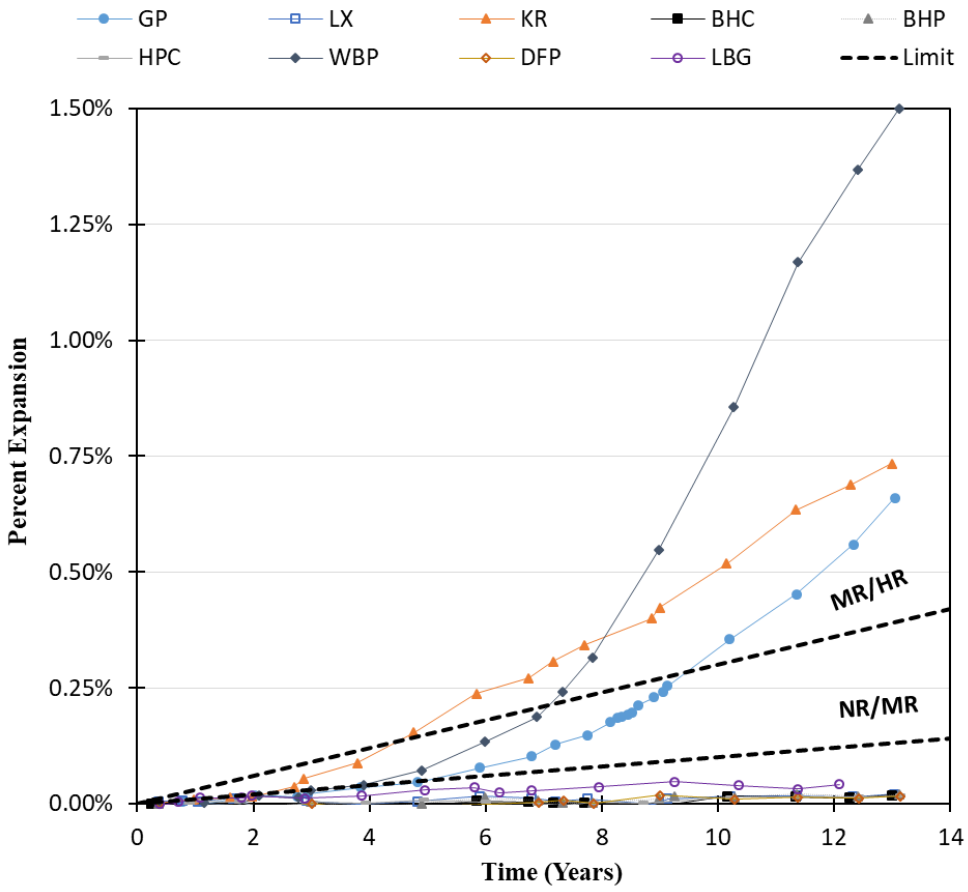

Figure 51. Graph. Exposure blocks expansion (Unboosted). Source: UW Tanner Research Group.

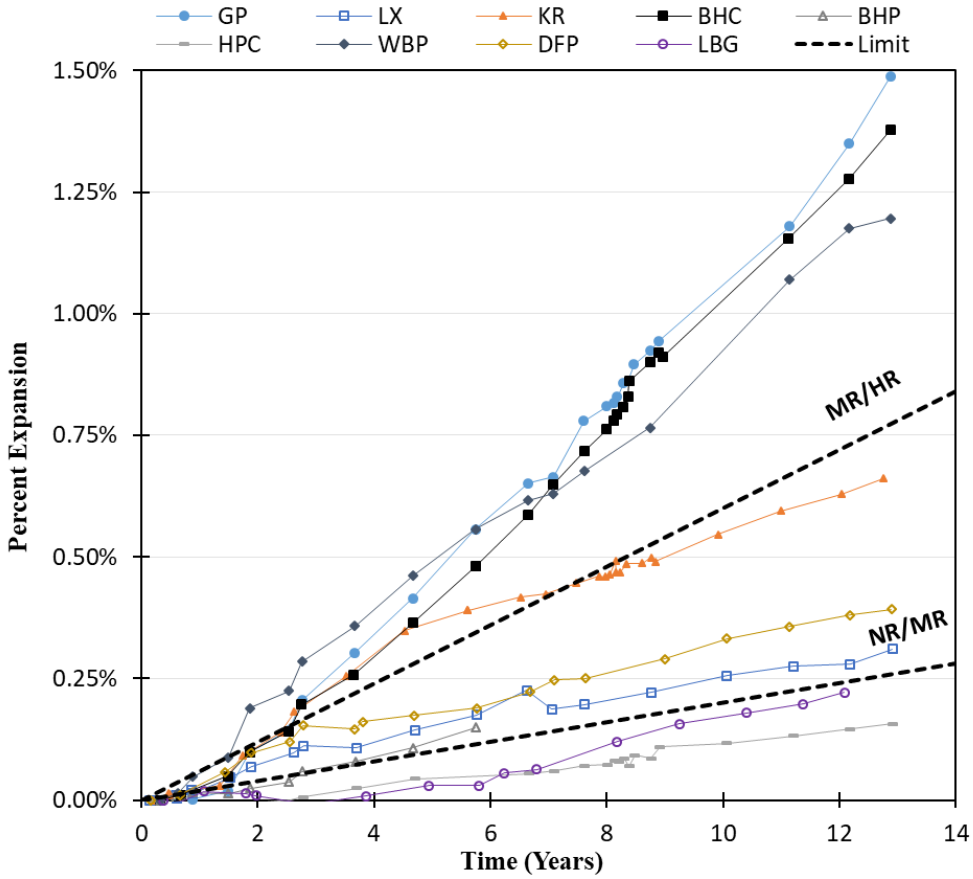

Figure 52. Graph. Exposure blocks expansion (Boosted). Source: UW Tanner Research Group.

The classification lines are a linear function of time, while the expansions will eventually approach a final limit when the reaction is complete (Multon and Toutlemonde 2010). Therefore, the final aggregate classification is the most severe classification at any point in time. A good example of this case is KR in Figure 52, where the rate of expansion has decreased relative to the classification line thereby placing KR right on the limit. If KR's trend continues, it would receive a lower classification. However, because it has already been classified as HR, it will never be demoted (Fertig, Kimble et al. 2017).

Table 15 compares the OEB classifications with the CPT classifications for each aggregate type where shaded area cells are used to show the agreements between the OEB and CPT classification of aggregate reactivity. Out of the nine field-block specimens, two agree for boosted, unboosted, and CPT data. Unboosted data agrees with CPT data for five out of nine aggregates and in a sixth type of aggregate, the boosted classification agrees with the CPT data. Out of the remaining three sources, the CPT was less reactive in two cases.

Table 15. Outdoor exposure block and CPT classification.

Aggregate Source	Unboosted OEBs	Boosted OEBs	CPT
BHP	NR	MR	NR
DFP	NR	MR	NR
BHC	NR	HR	NR
GP	HR	HR	MR
HPC	NR	NR	NR
KR	HR	HR	HR
LBG	NR	NR	HR
LX	NR	MR	MR
WBP	HR	HR	MR

Source: UW Tanner Research Group.

5.5 Accelerated Mortar Bar Tests (AMBTs) and Strength Testing

Key qualitative observations were documented and are summarized below:

- At 14 days, there was no visible ASR gel on any of the control mortar bars, whereas most of the exposed mortar bars had a thin layer of ASR gel.
- At 28 days, there was still no visible ASR gel on any of the control mortar bars and most of the exposed mortar bars had a thick layer of ASR gel.
- There were no surface cracks on any of the control mortar bars, but some of the exposed bars had numerous cracks. Most notably, the exposed DF mortar bars.
- Three of the exposed mortar bars experienced uneven expansion that led to the appearance of bending in the mortar bars. Most of the time, it was imperceptible until the mortar bar was placed against the miter saw fence.
- Most of the splitting tensile tests were similar in terms of how the specimen fractured. The critical split was usually right down the middle of the specimen.
- For the direct compressive tests, about 85 percent of the specimens fractured into an hourglass shape with vertical cracks appearing on one or both end and the other 15 percent fractured with vertical lines with no discernable hourglass shape.

5.5.1 Expansions

Aggregates are classified by using the expansion 14 days after the zero reading and by using AMBT or FHWA standards (Thomas, Fournier et al. 2012, C1260 2021). The AMBT classifies aggregates as non-reactive (NR) or potentially reactive (PR). Between these is a gray area that contains both innocuous and deleterious aggregates (C1260 2021). By conforming to the FHWA standard, the aggregates are classified as non-reactive (NR), moderately reactive (MR), highly reactive (HR), or very-highly reactive (VHR) (Thomas, Fournier et al. 2012). The AMBT and the FHWA classifications are summarized in Table 16 and Table 17, respectively.

Table 16. AMBT reactivity classifications.

Expansion	Classification
Less than or equal to 0.10%	NR
Greater than 0.10% and less than or equal to 0.20%	NR / PR
Greater than 0.20%	PR

Source: Thomas, Fournier et al. 2012.

Table 17. FHWA reactivity classifications.

Expansion	Classification
Less than or equal to 0.10%	NR
Greater than 0.10% and less than or equal to 0.30%	MR
Greater than 0.30% and less than or equal to 0.45%	HR
Greater than 0.45%	VHR

Source: Thomas, Fournier et al. 2012.

The average expansions for the different mortar bars are illustrated in Figure 53. Only the FHWA limits are shown because they cover a broader range of the measured expansions. Additionally, the average expansions at 28 days are shown in Figure 54. These expansions were not used to classify the aggregate, but the FHWA limits are still shown as points of reference.

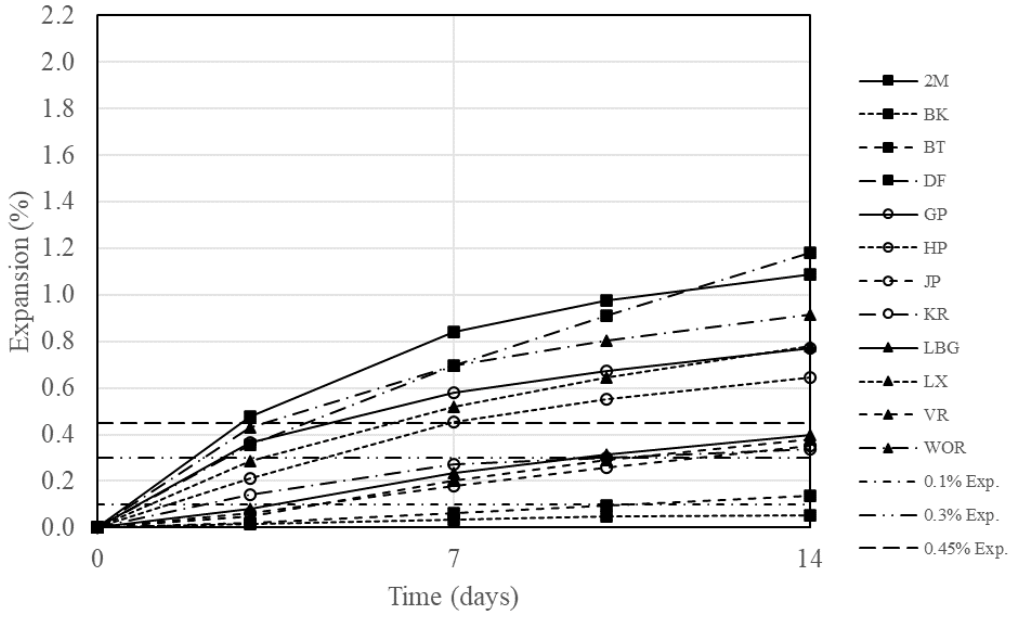

Figure 53. Fourteen-day AMBT expansions with FHWA limits. Source: UW Tanner Research Group.

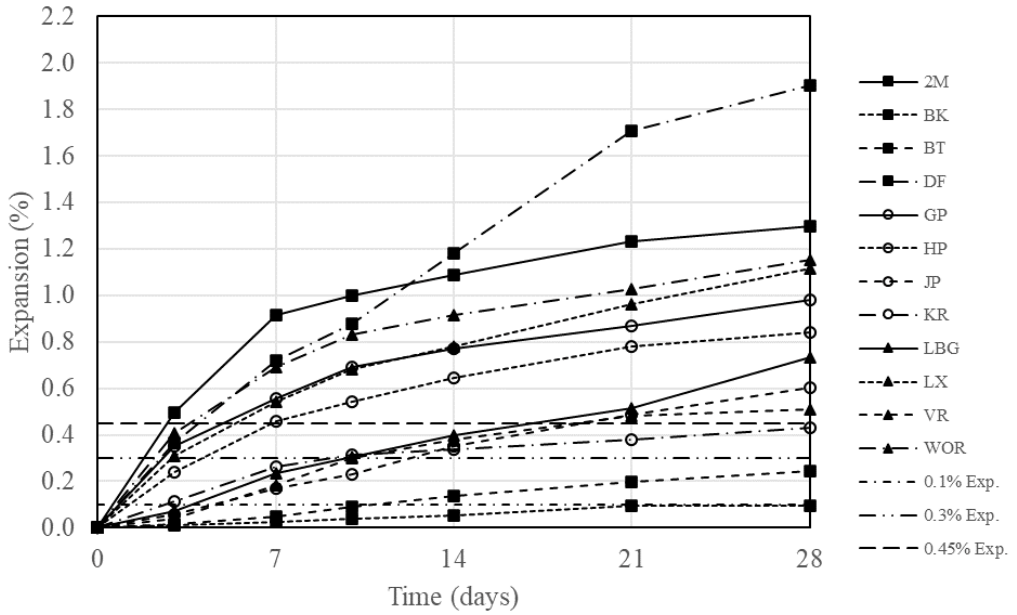

Figure 54. Twenty-eight-day expansions with FHWA limits. Source: UW Tanner Research Group.

The classifications for each aggregate are shown in Table 18.

Table 18. Aggregate classifications.

Aggregate	14-Day Expansion (%)	AMBT	FHWA
2M	1.09	PR	VHR
BK	0.06	NR	NR
BT	0.14	PR	MR
DF	1.18	PR	VHR
GP	0.77	PR	VHR
HP	0.64	PR	VHR
JP	0.35	PR	HR
KR	0.34	PR	HR
LBG	0.40	PR	HR
LX	0.78	PR	VHR
VR	0.38	PR	HR
WOR	0.92	PR	VHR

Source: UW Tanner Research Group.

In terms of the AMBT classification system, most of the aggregates can be classified as PR. For the FHWA classification system, half of the aggregates can be classified as VHR and a third can be classified as HR. These classifications indicated that most of the aggregates that were tested had significant reactivity.

5.5.2 Tensile Strength

The best way to compare the tensile strengths of the different mortar bars is with the tensile strength ratio. This is defined as the tensile strength of the exposed bars divided by the tensile strength of the respective control bars. For example, the tensile strength of the 2M exposed mortar bars was determined to be 332.4 psi (2.29 MPa) at 28 days and the tensile strength of the 2M control mortar bars was determined to be 499.5 psi (3.44 MPa). These tensile strengths yield a tensile strength ratio of 0.67 for the 2M aggregate at 28 days. The tensile strength ratios as a function of expansion for all the mortar bars is shown in Figure 55. In this figure, a logarithmic trendline was fitted to the data which results in a coefficient of determination of 77.9 percent. Additionally, Figure 56 shows the same data with a power trendline fitted to the data. The power trendline has a coefficient of determination of 78.8 percent. Based on these results, almost 80 percent of the variance in the strength ratios is explained by the expansion. Of the two, the logarithmic trendline is less complex and is preferred to the power trendline because an adjusted R^2 value will penalize additional parameters. Both trendlines, however, will be provided throughout this research. As expected, different aggregate types indicated varying rates of expansion in the mortar bars, so analyzing the cumulative data with respect to time was impractical. Therefore, the cumulative data was analyzed with respect to the expansions of the mortar bars.

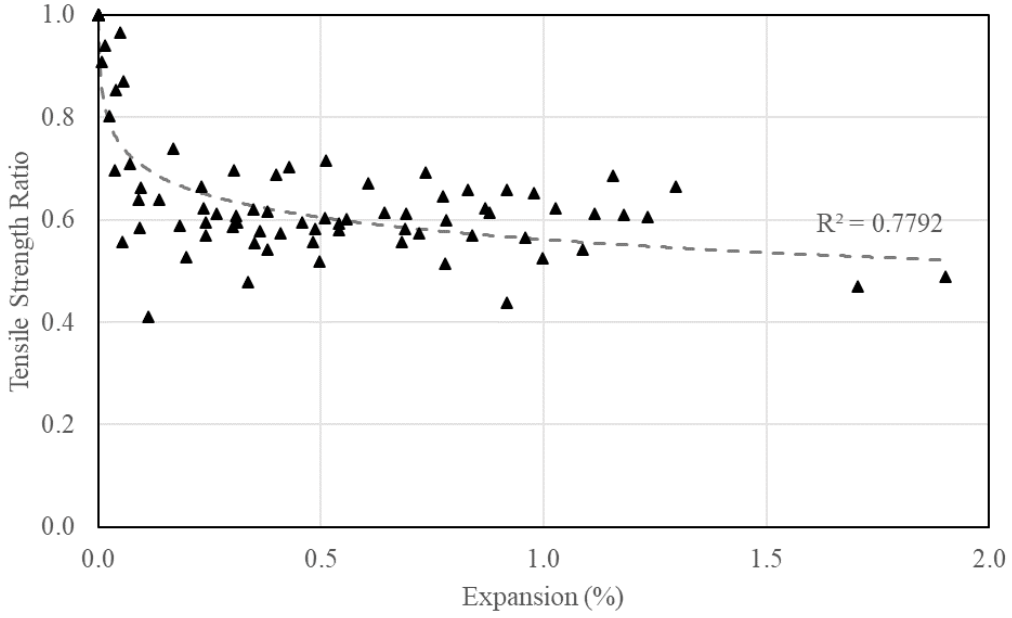

Figure 55. Tensile strength ratios versus time (logarithmic trendline). Source: UW Tanner Research Group.

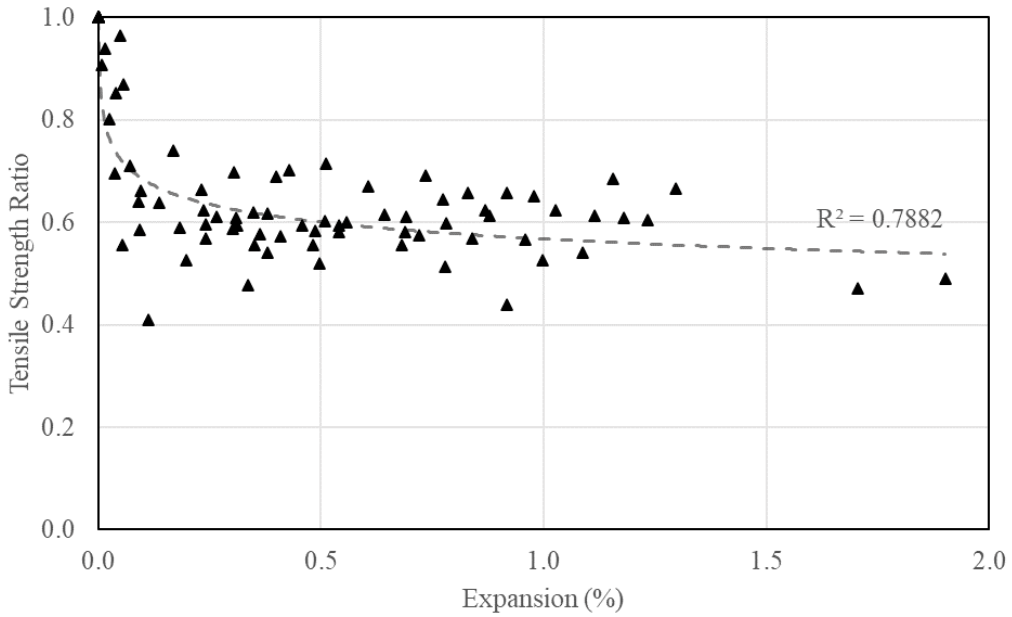

Figure 56. Tensile strength ratios versus time (power trendline). Source: UW Tanner Research Group.

5.5.3 Compressive Strength

The compressive strength of the mortar bars was analyzed in the same way as the tensile strength. The compressive strength ratios as a function of expansion are shown in Figure 57 and Figure 58 for logarithmic trendline and power trendline, respectively. The coefficient of determination for the data fitted with the logarithmic trendline is 62.1 percent. It is 62.4 percent for the data fitted with the power trendline. This suggests that a little over 60 percent of the variance in the compressive strength ratios can be explained by the expansion of the mortar bars. This relationship is not as strong as the one found for the tensile strength ratios. Similarly, the logarithmic trendline is preferred to the power trendline, but both are provided and again, the individual data was analyzed with time as the independent variable instead of expansion.

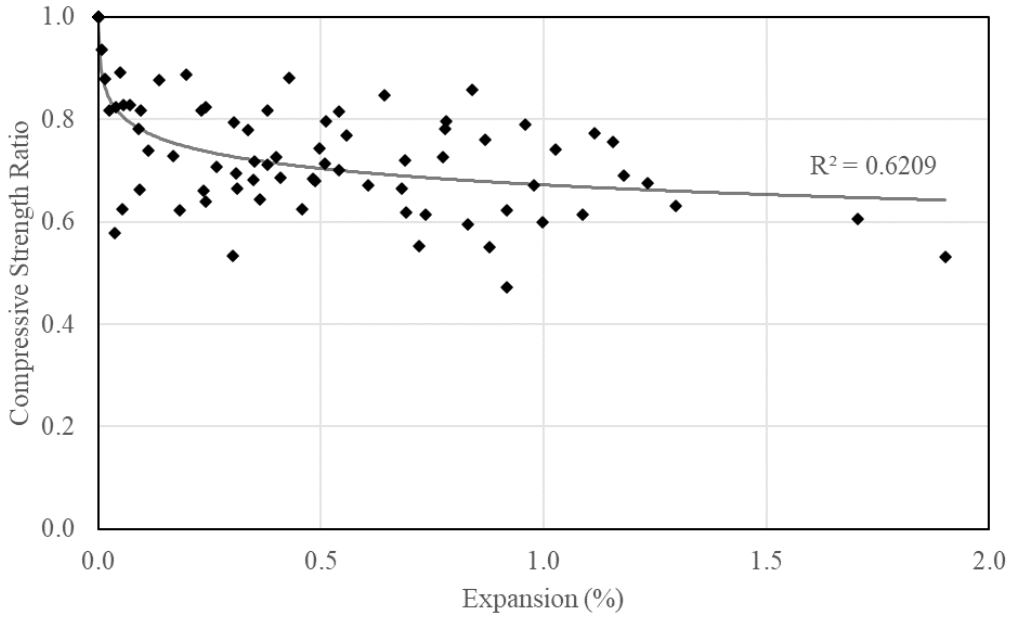

Figure 57. Compressive strength ratios versus time (logarithmic trendline). Source: UW Tanner Research Group.

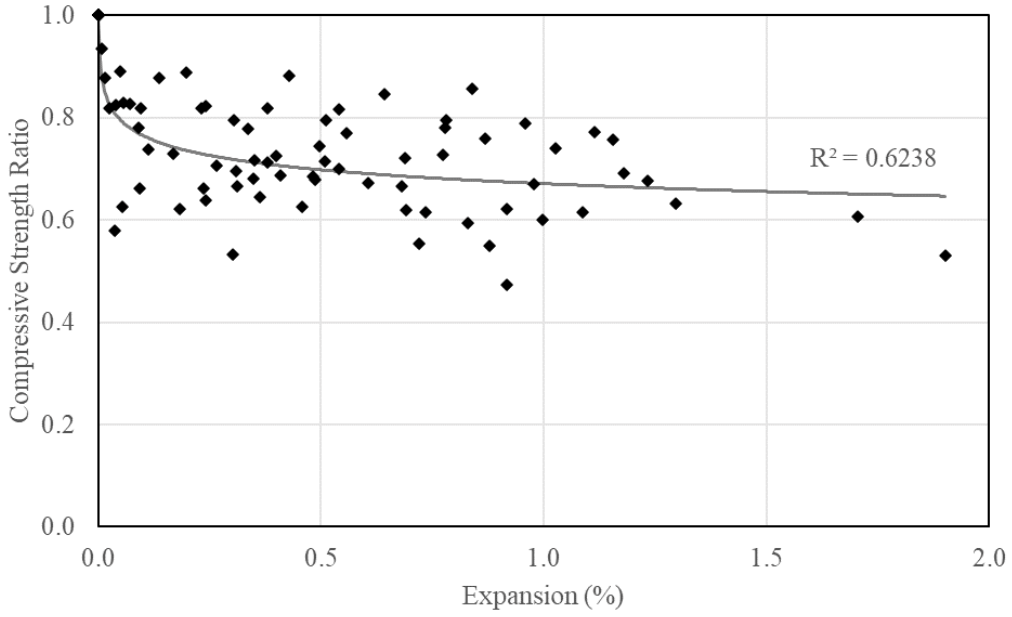

Figure 58. Compressive strength ratios versus time (power trendline). Source: UW Tanner Research Group.

5.5.4 Tension-to-Compression

The tension-to-compression (T/C) ratio is tensile strength divided by the compressive strength. ASR creates small cracks throughout the mortar bars, and it was expected to impact the tensile strength more than the compressive strength. Additionally, the

compressive strength of mortar has been documented to increase slightly after ASR (Yurtdas, Chen et al. 2013). Both phenomena would individually cause a decrease in the T/C ratio, so the total effect on the T/C ratio was expected to be significant. Initially, the percent change in the T/C ratios between exposed and control mortar bars was calculated, and there was a small decrease. However, it was uncertain if this was statistically relevant, so a multiple linear regression analysis was conducted in lieu of directly comparing the T/C ratios. A plot comparing the tensile strength to the compressive strength is shown in Figure 59. Linear trendlines are provided and the slopes of the trendlines are 0.0797 for the control and 0.0908 for exposed specimens. In general, the trendline associated with the control group is shifted up by approximately 82 psi (0.56 Mpa) compared to the trendline associated with the exposed group. More specifically, the difference between the tensile strengths according to the linear trendlines are 93, 87, 82, 76, and 71 psi (0.64, 0.60, 0.56, 0.52, and 0.49 MPa) at compressive strengths of 3500, 4000, 4500, 5000, and 5500 psi (24.1, 27.6, 31.0, 34.5, and 37.9 MPa) respectively. This means for a given compressive strength, the tensile strength of the exposed group is lower than the tensile strength of the control group. The multiple linear regression analysis, part of which is shown in Figure 60, provided additional verification. The multiple linear regression analysis is further explained in the following part of this section.

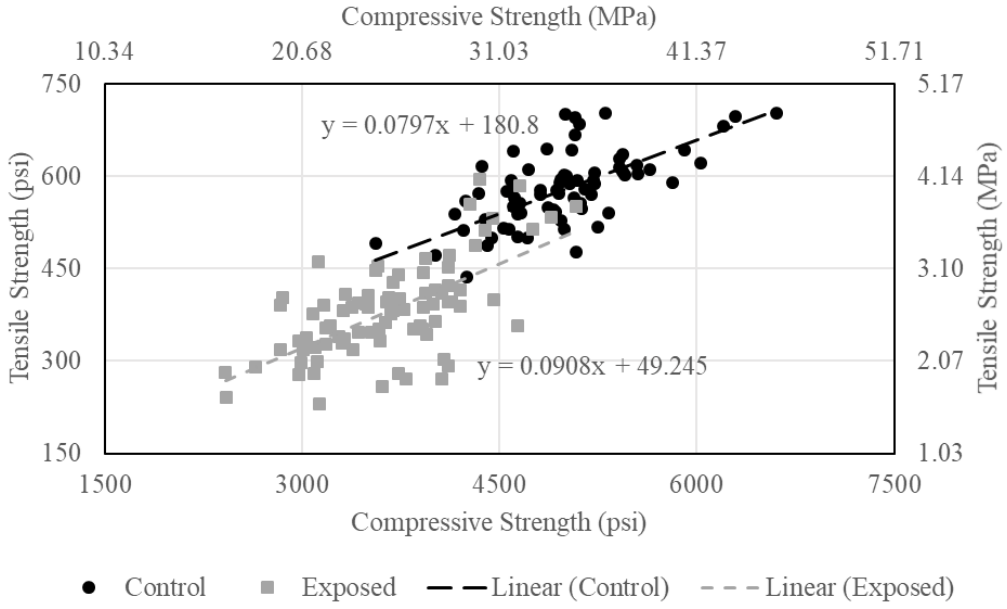

Figure 59. Tensile-to-compressive strength with linear trendlines. Source: UW Tanner Research Group.

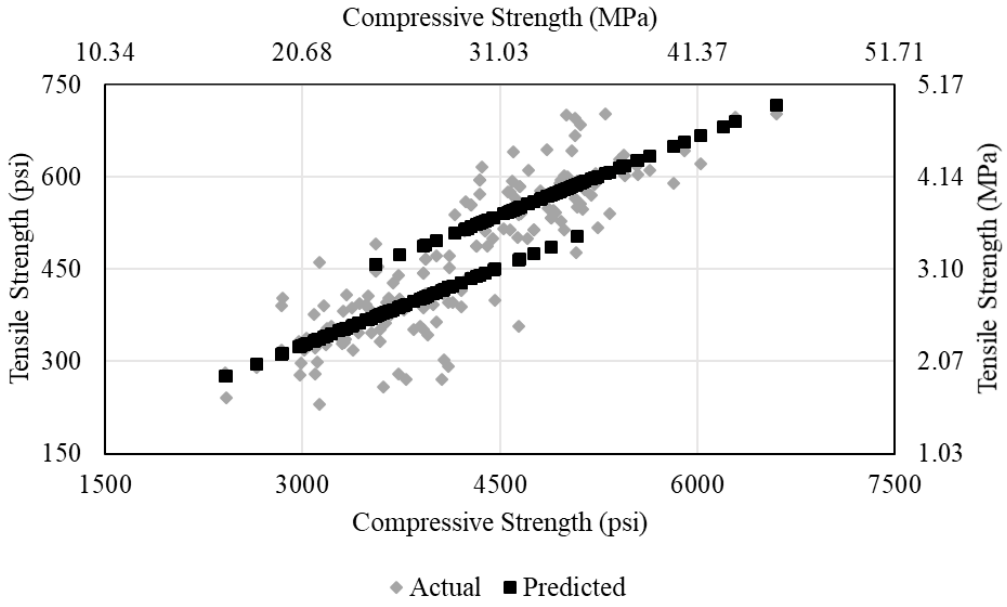

Figure 60. Multiple linear regression analysis of tensile-to-compressive strength. Source: UW Tanner Research Group.

The data for the multiple linear regression analysis was checked for normality before concluding that it is statistically meaningful. The plot of residuals is shown in Figure 61. The residuals have good scatter and are concentrated around zero indicating that they are normally distributed. This is verified in Figure 63 and Figure 64.

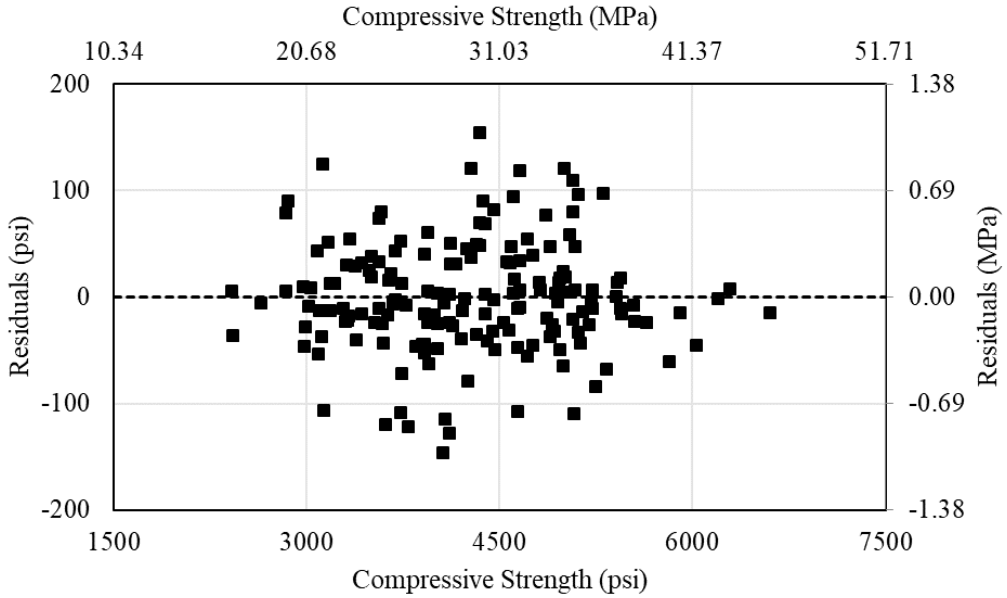

Figure 61. Residual plot. Source: UW Tanner Research Group.

The normal probability plot of the residuals is shown in Figure 62. Because the line formed by the residuals is relatively linear means the data is not skewed one way or the other.

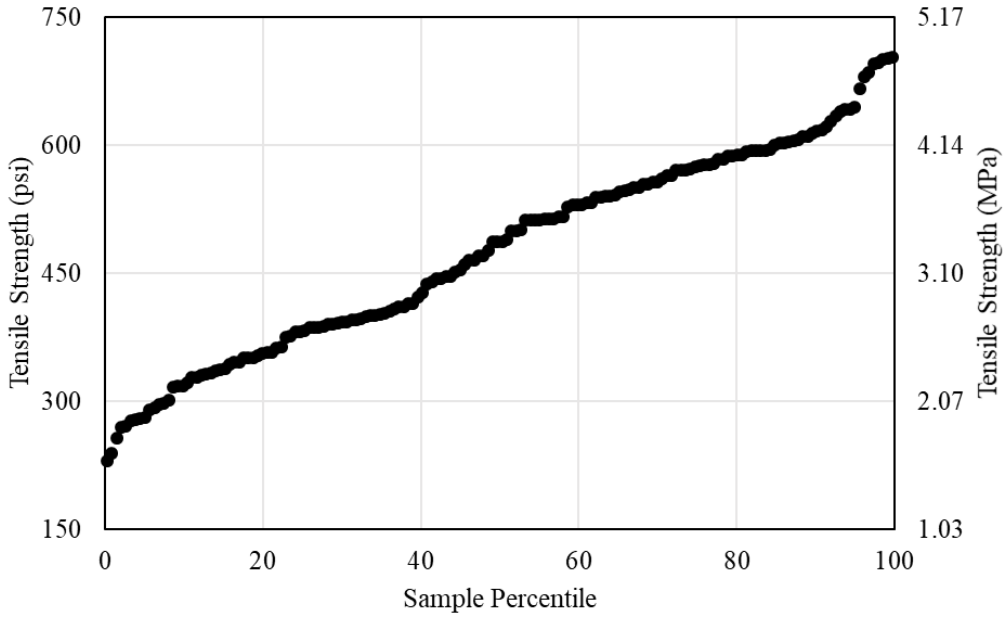

Figure 62. Normal probability plot of residuals. Source: UW Tanner Research Group.

Lastly, the histogram plots of the residuals are shown in Figure 63 and Figure 64 in imperial units and in metric units, respectively. These histograms generally follow a bell curve shape, meaning the data is normally distributed.

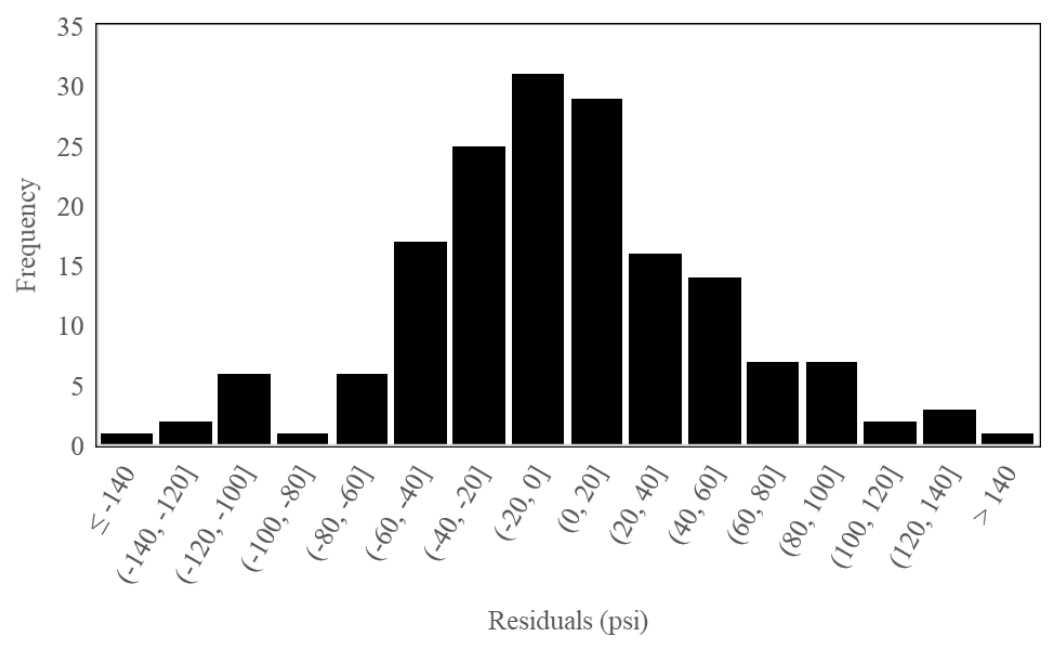

Figure 63. Residual histogram plot (in psi). Source: UW Tanner Research Group.

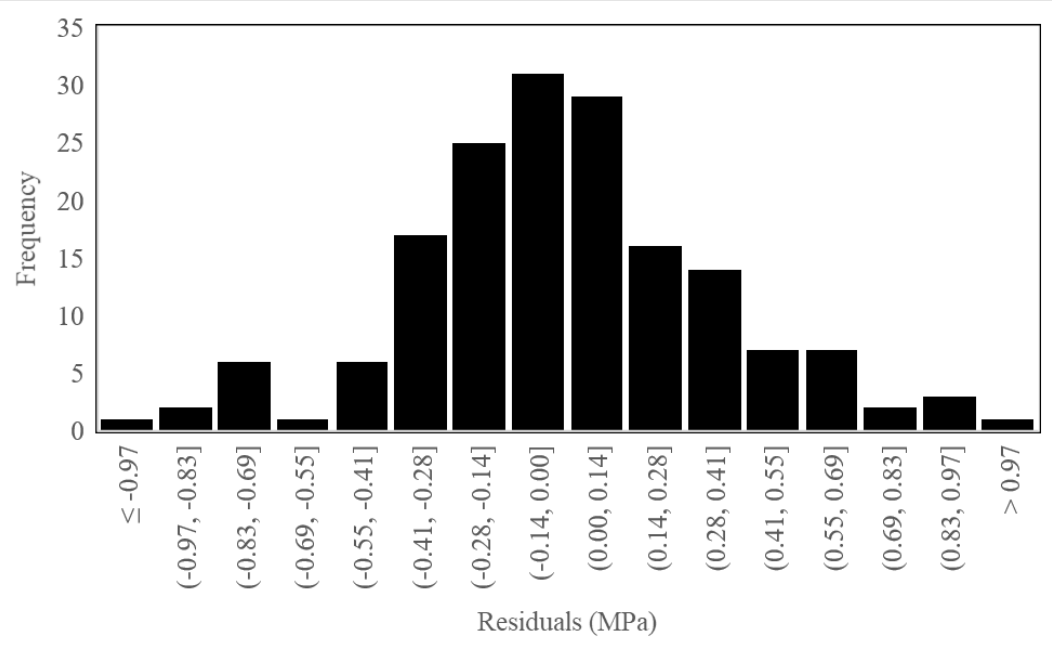

Figure 64. Residual histogram plot (in MPa). Source: UW Tanner Research Group.

When considering the multiple linear regression analysis, it was important to look at the terms used to generate the regression equation. In this case, the terms that were used to form the regression equation included the compressive strength and the condition, meaning either control or exposed. Additionally, a term for the interaction between the compressive strength and the condition was also used. The p-values for these terms were analyzed and

it was determined whether they were statistically significant. For this initial multiple linear regression analysis, the p-values were calculated to be << 0.05, 0.04, and 0.45 for the compressive strength, condition, and interaction terms, respectively. Since the compressive strength term and the condition term were less than 0.05, they are statistically significant. The interaction term, however, was greater than 0.05, so it was not statistically significant, and can be discarded. The multiple linear regression analysis was rerun without the interaction term and the p-values were calculated to be << 0.05 for both the compressive strength term and the condition term. The latter analysis was used to further investigate the relationship that the condition had on the compressive and tensile strength of the mortar bars. The associated regression equations that were used for the analysis are provided in Equation 4 and Equation 5 in terms of psi and MPa, respectively.

$$T = 154.72 + 0.0850C - 84.35X$$

Equation 4. Regression equation (in psi)

where;

T = tensile strength (psi)
C = compressive strength (psi)
X = condition (0 for control; 1 for exposed)

$$T = 1.0668 + 0.0850C - 0.5816X$$

Equation 5. Regression equation (in MPa)

where;

T = tensile strength (MPa)
C = compressive strength (MPa)
X = condition (0 for control; 1 for exposed)

As previously mentioned, there is a measurable downward shift in the tensile strengths from the control to the exposed groups of the mortar bars for a given compressive strength. Considering that the p-values for the compressive strength term and the condition term were under the threshold of 0.05 and the data was determined to be normally distributed, this shift in the tensile strengths is statistically significant.

6 CONCLUSIONS AND RECOMMENDATIONS

6.1 Conclusions

The testing methods used in this research demonstrated the ability to identify the potential ASR reactivity of aggregates, whereas Mit-CPT demonstrated the effectiveness of fly ashes to bring the ASR reactivity within allowable limits. Based on the test results the summaries of the conclusions are as follows:

CPT

- CPT expansion is higher for fine aggregates than coarse aggregates, indicating that fine aggregates are more susceptible to ASR. Because of the higher surface area of the fine aggregate compared to the corresponding coarse aggregate (Suwito, Jin et al. 2002).
- For three (JP, VR and KR) out of four aggregates, the combined CPT expansions are higher in combined versus separated coarse and fine aggregate fractions. This is attributed to the increase of reactive silica content with the addition of both fine and coarse aggregate. But when the reactive silica content exceeds the pessimum amount, for 2M aggregate, the combined CPT expansion gets lower due to the pessimum effect.
- The classification of aggregate based on ASR reactivity will help to select an aggregate with less ASR susceptibility for new concrete structures

Mit-CPT

- Twenty-five-percent replacement of cement by selected fly ashes shows a successful ASR mitigation to bring the ASR expansion below the 0.04 percent limit without compromising more than 14 percent compressive strength reduction. So, a 25 percent fly ash replacement can be used during construction to mitigate the ASR problem in concrete.
- ASR mitigation increases with the increase of dosages for both fly ashes. Whereas compressive strength decreases with the increase of dosages for both fly ashes.

Min-CPT

- The Min-CPT gives a higher reactivity classification than the CPT for eleven of the thirteen data points, which is about 85 percent. For example, one aggregate was found highly reactive in the Min-CPT test but moderately reactive in the CPT test.
- The y-intercept, of the linear regression between ACPT and CPT expansion, may indicate the potential for inherent expansions in the test method for a nonreactive aggregate of 0.049 percent when CPT expansions are 0 percent.

ACPT

- Excluding the outlier, the ACPT was able to classify the aggregates for ASR reactivity with a 97.2 percent accuracy level for the proposed limit of 0.09 percent expansion based on 36 data points when considering only fine and coarse fractions. The autoclave test with concrete prisms has the potential to be used as a tool for ASR reactivity classification.
- Additional work is required to evaluate the behavior of combined coarse and fine aggregate fractions.
- Results suggest that the expansions of highly reactive aggregates do not depend on the cooling temperature, but the expansion of nonreactive and moderately reactive aggregates does because it is reduced by around 28 and 20 percent, respectively. In short, smaller expansions will be more sensitive to changes in procedure.
- A linear regression of the ACPT and CPT expansion data was obtained in this study. The regression with a y-intercept indicates an inherent expansion in the ACPT test.

OEBs

- The Wyoming ASR research group has developed preliminary limits to provide future guidelines for field classifications. Boosted OEBs expansions gave a higher reactivity classification compared to the unboosted OEBs expansions.
- Unboosted OEBs results showed agreement with CPT, the most reliable laboratory test, to classify aggregates for ASR reactivity. Besides, unboosted OEBs represent a more realistic ASR scenario for actual concrete structures.

AMBTs and Strength Testing

- Most of the aggregates tested showed a significant amount of reactivity. This resulted in a wide range of expansion data from almost no expansion to 1.90 percent at 28 days. The FHWA classification system did a better job than the AMBT classification to deconstruct the expansion data into meaningful classifications.
- The strength ratios of the exposed mortar bar tensile strength to the control mortar bar tensile strength as a function of expansion indicate that the AMBT caused a rapid decline in strength followed by a plateau that continued to the 28-day cutoff. Based on the regression analyses of this relationship, the logarithmic (R^2 = 77.9 percent) and power (R^2 = 78.8 percent) regressions are the best fits for the data. The logarithmic trendline is preferred due to having fewer parameters and being less complex.

- Similarly, the strength ratios of the exposed mortar bar compressive strength to the control mortar bar compressive strength as a function of expansion indicate that the AMBT caused a rapid decline in strength followed by a plateau that continued to the 28-day cutoff. The relationship between expansion and compressive strength ratios, however, is not as strong as the one between expansion and tensile strength ratios. Based on the regression analyses of this relationship, the logarithmic (R^2 = 62.1 percent) and power (R^2 = 62.4 percent) regressions are the best fits for the data. Again, the logarithmic trendline is preferred.
- For a given compressive strength, the tensile strength of the exposed group was approximately 82 psi (0.56 Mpa) lower than the tensile strength of the control group. This was about a 15 percent reduction in strength. This relationship between the condition and the strength was determined to be statistically significant.

6.2 Recommendations for future works

- For a particular aggregate source, CPT with different NR aggregates can be completed to observe the influence of NR aggregates on ASR expansions.
- Changing of test parameters, such as test duration, temperature, and alkali content for ACPT can be done to finalize this ultra-accelerated test which should give better agreements with existing reliable test methods. This work was also started and investigated by Wood (Wood 2017).
- Although Min-CPT test results showed higher ASR reactivity classification with respect to CPT test results, it showed a very good promise for future study. A complete multi-laboratory study should be evaluated for future research.
- More unboosted OEBs experiments can be done which represent field performance for potentially reactive aggregates.

REFERENCES

AASHTO-TP110-14 (2014). "Standard Method of Test for Potential Alkali Reactivity of Aggregates and Effectiveness of ASR Mitigation Measures (Miniature Concrete Prism Test, MCPT)." AASHTO, Washington DC.

AASHTO, T. (2014). "110-14. Standard Method of Test for Potential Alkali Reactivity of Aggregates and Effectiveness of ASR Mitigation Measures (Miniature Concrete Prism Test, MCPT)." AASHTO, Washington DC.

ASTM-C29 (2016). Standard test method for bulk density ("Unit Weight") and voids in aggregate, West Conshohocken, PA, USA, ASTM West Conshohocken, PA, USA.

ASTM-C33 (2018). Standard Specification for Concrete Aggregates, West Conshohocken, PA, USA, ASTM West Conshohocken, PA, USA.

ASTM-C127 (2015). Relative Density (Specific Gravity) and Absorption of Coarse Aggregate, West Conshohocken, PA, USA, ASTM West Conshohocken, PA, USA.

ASTM-C128 (2015). Relative Density (Specific Gravity) and Absorption of Fine Aggregate, West Conshohocken, PA, USA, ASTM West Conshohocken, PA, USA.

ASTM-C150 (2001). Standard specification for Portland cement, Philadelphia, USA, ASTM Philadelphia^ ePA PA.

ASTM-C192 (2016). Standard Practice for Making and Curing Concrete Test Specimens in the Laboratory, Philadelphia, USA, ASTM Philadelphia^ ePA PA.

ASTM-C618 (2008). Standard specification for coal fly ash and raw or calcined natural pozzolan for use in concrete. American Society of Testing and Materials, West Conshohocken, Pennsylvania, USA, West Conshohocken Pennsylvania, USA.

ASTM-C1260 (2014). "Standard test method for potential alkali reactivity of aggregates (mortar-bar method)." American Society of Testing and Materials, West Conshohoken, Pennsylvania, USA.

ASTM-C1293 (2009). "Standard test method for determination of length change of concrete due to alkali–silica reaction." American Society of Testing and Materials, West Conshohoken, Pennsylvania, USA.

Bavasso, I., U. Costa, T. Mangialardi and A. E. Paolini (2020). "Assessment of Alkali–Silica Reactivity of Aggregates by Concrete Expansion Tests in Alkaline Solutions at 38° C." Materials 13(2): 288.

Bažant, Z. P. and A. Steffens (2000). "Mathematical model for kinetics of alkali–silica reaction in concrete." Cement and concrete research 30(3): 419-428.

Bérubé, M.-A., D. Chouinard, M. Pigeon, J. Frenette, L. Boisvert and M. Rivest (2002). "Effectiveness of sealers in counteracting alkali-silica reaction in plain and air-entrained laboratory concretes exposed to wetting and drying, freezing and thawing, and salt water." Canadian Journal of Civil Engineering 29(2): 289-300.

Bérubé, M.-A., J. Duchesne, J. Dorion and M. Rivest (2002). "Laboratory assessment of alkali contribution by aggregates to concrete and application to concrete structures affected by alkali–silica reactivity." Cement and Concrete Research 32(8): 1215-1227.

Bérubé, M.-A. and B. Fournier (1993). "Canadian experience with testing for alkali-aggregate reactivity in concrete." Cement and Concrete Composites 15(1-2): 27-47.

Bérubé, M., C. Tremblay, B. Fournier, M. Thomas and D. Stokes (2004). "Influence of lithium-based products proposed for counteracting ASR on the chemistry of pore solution and cement hydrates." Cement and Concrete Research 34(9): 1645-1660.

Bonakdar, A., B. Mobasher, S. K. Dey and D. M. Roy (2010). "Correlation of Reaction Products and Expansion Potential in Alkali-Silica Reaction for Blended Cement Materials." ACI Materials Journal 107(4).
Brantley, S. L., J. D. Kubicki and A. F. White (2008). "Kinetics of water-rock interaction."
Bulteel, D., E. Garcia-Diaz, C. Vernet and H. Zanni (2002). "Alkali–silica reaction: a method to quantify the reaction degree." Cement and concrete research 32(8): 1199-1206.
C39, A. (2021). Standard Test Method for Compressive Strength of Cylindrical Concrete Specimens. Conshohocken, PA, ASTM International.
C109, A. (2021). Standard Test Method for Compressive Strength of Hydraulic Cement Mortars (Using 2-in. or [50 mm] Cube Specimens). Conshohocken, PA, ASTM International.
C128, A. (2015). Standard Test Method for Relative Density (Specific Gravity) and Absorption of Fine Aggregate. Conshohocken, PA, ASTM International.
C305, A. (2020). Standard Practice for Mechanical Mixing of Hydraulic Cement Pastes and Mortars of Plastic Consistency. Conshohocken, PA, ASTM International.
C496, A. (2017). Standard Test Method for Splitting Tensile Strength of Cylindrical Concrete Specimens. Conshohocken, PA, ASTM International.
C1260, A. (2021). Standard Test Method for Potential Alkali Reactivity of Aggregates (Mortar-Bar Method). Conshohocken, PA, ASTM International.
Chen, X., W. Huang and J. Zhou (2012). "Effect of moisture content on compressive and split tensile strength of concrete." Indian journal of engineering and materials sciences 19(6): 427-435.
Cole, W. F., C. J. Lancucki and M. J. Sandy (1981). "Products formed in an aged concrete." Cement and Concrete Research 11(3): 443-454.
Darwin, D., C. W. Dolan and A. H. Nilson (2016). Design of concrete structures, McGraw-Hill Education, 2 Penn Plaza, New York, NY 10121.
del Viso, J. R., J. R. Carmona and G. Ruiz (2008). "Shape and size effects on the compressive strength of high-strength concrete." Cement and concrete research 38(3): 386-395.
Deschenes, R., C. Jones, E. R. Giannini and M. Hale (2019). "A Modified Chemical Index to Predict Fly Ash Dosage for Mitigating Alkali-Silica Reaction." Advances in Civil Engineering Materials 8(1): 699-722.
Fernandes, I. (2009). "Composition of alkali–silica reaction products at different locations within concrete structures." Materials Characterization 60(7): 655-668.
Fertig, R., M. Kimble, A. Jones and J. E. Tanner (2017). "ASR Potential and Mitigation Measures for Wyoming Aggregates." Journal of Materials in Civil Engineering 29(9): 04017112.
Figueira, R., R. Sousa, L. Coelho, M. Azenha, J. de Almeida, P. Jorge and C. Silva (2019). "Alkali-silica reaction in concrete: Mechanisms, mitigation and test methods." Construction and Building Materials 222: 903-931.
Fiore, B., M. T. Hossain, M. Kimble, F. AlMutawa and J. E. Tanner (2018). Evaluating the Effectiveness of Fly Ashes to Mitigate ASR and Using Recycled Concrete Aggregate in New Construction.

Fournier, B., M. Bérubé and G. Bergeron (1991). "A rapid autoclave mortar bar method to determine the potential alkali-silica reactivity of St. Lawrence lowlands carbonate aggregates (Quebec, Canada)." Cement, concrete and aggregates 13(1): 58-71.
Gautam, B. P. and D. K. Panesar (2017). "The effect of elevated conditioning temperature on the ASR expansion, cracking and properties of reactive Spratt aggregate concrete." Construction and Building Materials 140: 310-320.
Gautam, B. P., D. K. Panesar, S. A. Sheikh and F. J. Vecchio (2017). "Effect of multiaxial stresses on alkali-silica reaction damage of concrete." ACI materials journal 114(4): 595-604.
Giannini, E. R. and K. J. Folliard (2013). "A Rapid Test to Determine Alkali-Silica Reactivity of Aggregates Using Autoclaved Concrete Prisms." SN3235, Portland Cement Association, Skokie, Illinois, USA 21.
Glasser, F. (1991). Chemistry of the alkali-aggregate reaction. The alkali-silica reaction in concrete, CRC Press: 46-69.
Golmakani, F. (2017). Influence of Temperature and Storage Solution Composition on Test Methods for Alkali-silica Reactivity, University of Toronto (Canada).
Grattan-Bellew, P. (1995). "Laboratory evaluation of alkali-silica reaction in concrete from Saunders Generating Station." Materials Journal 92(2): 126-134.
Hafçı, A. (2019). Development of a new short-term concrete prism test method (SCPT) to improve predictability for potential alkali reactivity of aggregates,. PhD PhD thesis, Middle East Technical University.
Haha, M. B., E. Gallucci, A. Guidoum and K. L. Scrivener (2007). "Relation of expansion due to alkali silica reaction to the degree of reaction measured by SEM image analysis." Cement and Concrete Research 37(8): 1206-1214.
Hajighasemali, S., A. Ramezanianpour and M. Kashefizadeh (2014). "The effect of alkali-silica reaction on strength and ductility analyses of RC beams." Magazine of concrete research 66(15): 751-760.
Hayman, S., M. Thomas, N. Beaman and P. Gilks (2010). "Selection of an effective ASR-prevention strategy for use with a highly reactive aggregate for the reconstruction of concrete structures at Mactaquac generating station." Cement and Concrete Research 40(4): 605-610.
Hobbs, D. W. (1988). "Alkali-silica reaction in concrete." Telford.
Hong, S.-Y. and F. Glasser (1999). "Alkali binding in cement pastes: Part I. The CSH phase." Cement and Concrete Research 29(12): 1893-1903.
Ichikawa, T. (2009). "Alkali–silica reaction, pessimum effects and pozzolanic effect." Cement and Concrete Research 39(8): 716-726.
Ichikawa, T. and M. Miura (2007). "Modified model of alkali-silica reaction." Cement and Concrete research 37(9): 1291-1297.
Iler, R. K. and R. Iler (1979). "The chemistry of silica: solubility, polymerization, colloid and surface properties, and biochemistry."
James, A. F. and B. Kerkhoff (2007). "Diagnosis and Control of Alkali-Aggregate Reactions in Concrete." Portland Cement Association, Skokie, Illinois.
Kimble, M., R. Fertig, D. Hacker and J. E. Tanner (2015). Evaluating the Risk of Alkali-Silica Reaction in Wyoming: Continued Evaluation of Field Specimens and Proposed Mitigation Strategies, Wyoming. Dept. of Transportation.

Larive, C., A. Laplaud and O. Coussy (2000). "The role of water in alkali-silica reaction." Alkali-aggregate reaction in concrete, Québec, Canada: 61-69.
Latifee, E. R. and P. R. Rangaraju (2015). "Miniature concrete prism test: rapid test method for evaluating alkali-silica reactivity of aggregates." Journal of Materials in Civil Engineering 27(7): 04014215.
Leemann, A., G. Le Saout, F. Winnefeld, D. Rentsch and B. Lothenbach (2011). "Alkali–silica reaction: the influence of calcium on silica dissolution and the formation of reaction products." Journal of the American Ceramic Society 94(4): 1243-1249.
Leemann, A., B. Lothenbach and C. Thalmann (2011). "Influence of superplasticizers on pore solution composition and on expansion of concrete due to alkali-silica reaction." Construction and Building Materials 25(1): 344-350.
Lindgård, J., Ö. Andiç-Çakır, I. Fernandes, T. F. Rønning and M. D. Thomas (2012). "Alkali–silica reactions (ASR): Literature review on parameters influencing laboratory performance testing." Cement and Concrete research 42(2): 223-243.
Lu, D., B. Fournier and P. Grattan-Bellew (2006). "Effect of aggregate particle size on determining alkali-silica reactivity by accelerated tests." Journal of ASTM International 3(9): 1-11.
Lu, D., X. Zhou, Z. Xu, X. Lan, M. Tang and B. Fournier (2006). "Evaluation of laboratory test method for determining the potential alkali contribution from aggregate and the ASR safety of the Three-Gorges dam concrete." Cement and concrete research 36(6): 1157-1165.
Maraghechi, H., G. Fischer and F. Rajabipour (2012). "The role of residual cracks on alkali silica reactivity of recycled glass aggregates." Cement and Concrete Composites 34(1): 41-47.
Marques, A. I., J. Morais, P. Morais, M. d. R. Veiga, C. Santos, P. Candeias and J. G. Ferreira (2020). "Modulus of elasticity of mortars: Static and dynamic analyses." Construction & building materials 232: 117216.
McCoy, W. and A. Caldwell (1951). New approach to inhibiting alkali-aggregate expansion. Journal Proceedings.
Mehta, P. K. and P. J. M. Monteiro (2014). Concrete: microstructure, properties, and materials. New York, McGraw-Hill Education.
Ming-Shu, T., H. Su-Fen and Z. Shi-Hua (1983). "A rapid method for identification of alkali reactivity of aggregate." Cement and concrete research 13(3): 417-422.
Mohammadi, A., E. Ghiasvand and M. Nili (2020). "Relation between mechanical properties of concrete and alkali-silica reaction (ASR); a review." Construction & building materials 258: 119567.
Multon, S. and F. Toutlemonde (2010). "Effect of moisture conditions and transfers on alkali silica reaction damaged structures." Cement and Concrete Research 40(6): 924-934.
Nishibayashi, S., T. Kuroda, S. Inoue and Y. Okawa (1996). Expansion characteristics of AAR in concrete by autoclave method. 10th International Conference on Alkali-Aggregate Reaction in Concrete.
Nishibayashi, S., K. Yamura and H. Matsushita (1987). "A Rapid Method of Determining the Alkali-Aggregate Reaction in Concrete by Autoclave--Proceedings of the 7th international conference on concrete alkali-aggregate reactions, OTTAWA, CANADA, 1986." Publication of: NOYES PUBLICATIONS.

Oberholster, R. and G. Davies (1986). "An accelerated method for testing the potential alkali reactivity of siliceous aggregates." Cement and Concrete research 16(2): 181-189.
Ono, K. (1988). "Damaged concrete structures in Japan due to alkali silica reaction." International Journal of Cement Composites and Lightweight Concrete 10(4): 247-257.
Pandey, S. and R. Sharma (2000). "The influence of mineral additives on the strength and porosity of OPC mortar." Cement and Concrete Research 30(1): 19-23.
Parker, C. K., J. E. Tanner and J. L. Varela (2007). "Evaluation of ASTM Methods to Determine Splitting Tensile Strength in Concrete, Masonry, and Autoclaved Aerated Concrete." Journal of ASTM International 4(2): 1-12.
Pathirage, M., F. Bousikhane, M. D'Ambrosia, M. Alnaggar and G. Cusatis (2019). "Effect of alkali silica reaction on the mechanical properties of aging mortar bars: Experiments and numerical modeling." International journal of damage mechanics 28(2): 291-322.
Poyet, S., A. Sellier, B. Capra, G. Foray, J.-M. Torrenti, H. Cognon and E. Bourdarot (2007). "Chemical modelling of alkali silica reaction: influence of the reactive aggregate size distribution." Materials and structures 40(2): 229.
Rajabipour, F., E. Giannini, C. Dunant, J. Ideker and M. Thomas (2015). "Alkali-Silica reaction: Current understanding of the reaction mechanisms and the knowledge gaps." Cement and Concrete Research 76: 130-146.
Saha, A. K., M. N. N. Khan, P. K. Sarker, F. A. Shaikh and A. Pramanik (2018). The ASR mechanism of reactive aggregates in concrete and its mitigation by fly ash: A critical review. Construction and Building Materials. 171: 743+.
Saouma, V. E. and M. A. Hariri-Ardebili (2014). "A proposed aging management program for alkali silica reactions in a nuclear power plant." Nuclear Engineering and Design 277: 248-264.
Shafaatian, S. M., A. Akhavan, H. Maraghechi and F. Rajabipour (2013). "How does fly ash mitigate alkali–silica reaction (ASR) in accelerated mortar bar test (ASTM C1567)?" Cement and Concrete Composites 37: 143-153.
Shehata, M. H. and M. D. Thomas (2000). "The effect of fly ash composition on the expansion of concrete due to alkali–silica reaction." Cement and Concrete Research 30(7): 1063-1072.
Sjöberg, S. (1996). "Silica in aqueous environments." Journal of Non-Crystalline Solids 196: 51-57.
Słowik, M. and A. Akram (2022). "Length effect at testing splitting tensile strength of concrete." Materials 15(1): 250.
Stanton, T. (1950). Studies of use of pozzolans for counteracting excessive concrete expansion resulting from reaction between aggregates and the alkalies in cement. Symposium on Use of Pozzolanic Materials in Mortars and Concretes, ASTM International.
Steffens, A., K. Li and O. Coussy (2003). "Aging approach to water effect on alkali–silica reaction degradation of structures." Journal of engineering mechanics 129(1): 50-59.
Suchorzewski, J. and J. Tejchman (2018). Size effect in concrete under splitting tension. Computational Modelling of Concrete Structures. G. Meschke, B. Pichler and J. G. Rots, CRC Press: 437-445.

Sudin, M. A. S. and M. Ramli (2014). Effect of specimen shape and size on the compressive strength of foamed concrete, EDP Sciences.
Suwito, A., W. Jin, Y. Xi and C. Meyer (2002). "A mathematical model for the pessimum size effect of ASR in concrete." Concrete Science and Engineering 4(13): 23-34.
Swamy, R. N. (1990). "Alkali silica reaction in concrete: D. W. Hobbs. Thomas Telford, London, UK, 1988. 183 pp. £25.00. ISBN 0 7277 1317 5." Cement and Concrete Composites 12(1): 64.
Swamy, R. N. (1992). The alkali-silica reaction in concrete, Blackie Glasgow.
Tamura, H. (1987). "A Test Method on Rapid Identification of Alkali Reactivity Aggregate (GRBC Rapid Method)--Proceedings of the 7th international conference on concrete alkali-aggregate reactions, OTTAWA, CANADA, 1986." Publication of: NOYES PUBLICATIONS.
Thomas, M. (2007). Optimizing the use of fly ash in concrete, Portland Cement Association Skokie, IL.
Thomas, M. (2011). "The effect of supplementary cementing materials on alkali-silica reaction: A review." Cement and concrete research 41(12): 1224-1231.
Thomas, M., B. Fournier, K. Folliard, J. Ideker and M. Shehata (2006). "Test methods for evaluating preventive measures for controlling expansion due to alkali–silica reaction in concrete." Cement and concrete research 36(10): 1842-1856.
Thomas, M., B. Fournier and K. J. Folliard (2012). Selecting measures to prevent deleterious alkali-silica reaction in concrete: rationale for the AASHTO PP65 prescriptive approach (No. FHWA-HIF-13-002). United States. Federal Highway Administration, United States. Federal Highway Administration.
Thomas, M., P. Nixon and K. Pettifer (1991). "Effect of Pulverised-Fuel Ash With a High Total Alkali Content on Alkali Silica Reaction in Concrete Containing Natural UK Aggregate." Special Publication 126: 919-940.
Thomas, M. D., B. Fournier and K. J. Folliard (2013). Alkali-aggregate reactivity (AAR) facts book, United States. Federal Highway Administration. Office of Pavement Technology.
Thomas, M. D. A., B. t. Fournier, K. J. Folliard, A. United States. Federal Highway, T. United States. Federal Highway Administration. Office of Pavement and I. Transtec Group (2012). Selecting measures to prevent deleterious alkali-silica reaction in concrete: rationale for the AASHTO PP65 prescriptive approach. Washington, DC, U.S. Department of Transportation, Federal Highway Administration.
Vayghan, A. G., F. Rajabipour and J. L. Rosenberger (2016). "Composition–rheology relationships in alkali–silica reaction gels and the impact on the gel's deleterious behavior." Cement and Concrete Research 83: 45-56.
Wood, S. G. (2017). Investigation of autoclave methods for determining alkali-silica reactivity of concrete aggregates, University of Alabama Libraries.
Yurtdas, I., D. Chen, D. W. Hu and J. F. Shao (2013). "Influence of alkali silica reaction (ASR) on mechanical properties of mortar." Construction & building materials 47: 165-174.
Zhong, W., J. Pan, J. Wang and C. Zhang (2021). "Size effect in dynamic splitting tensile strength of concrete: Experimental investigation." Construction & building materials 270: 121449.

APPENDICES

Appendix A

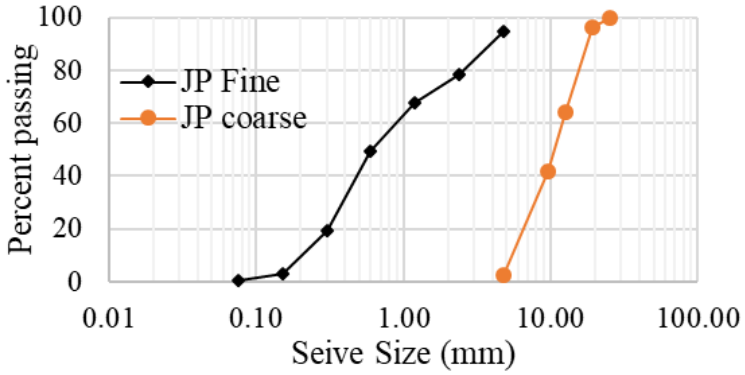

a) JP aggregate

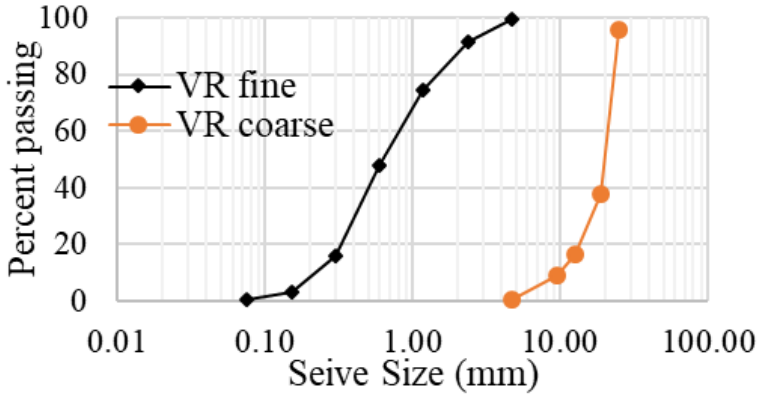

b) VR aggregate

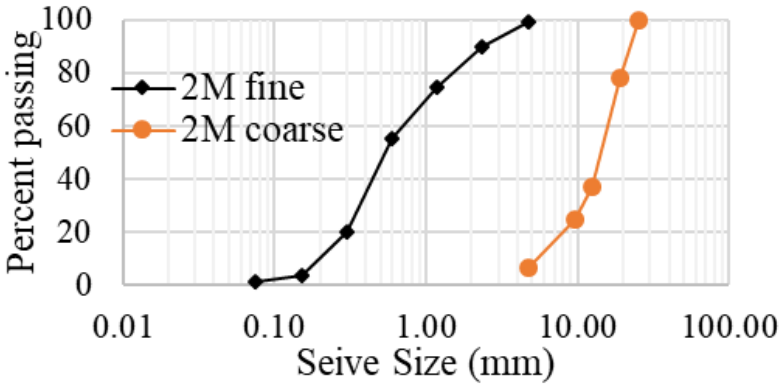

c) 2M aggregate

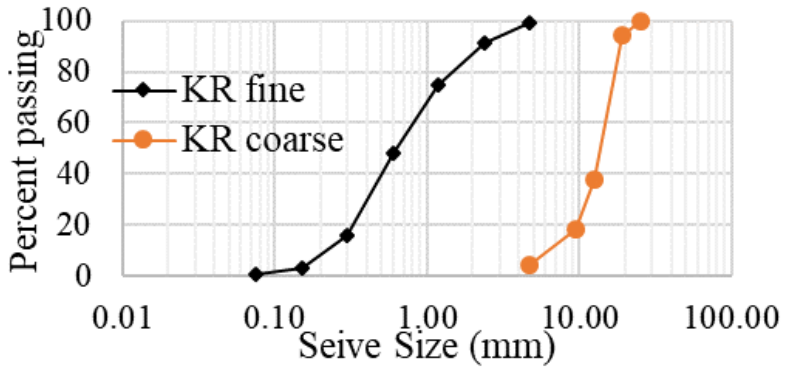

d) KR aggregate

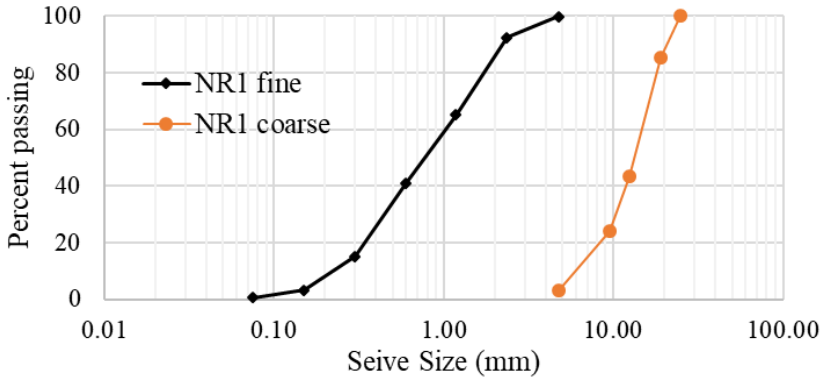

e) NR1 aggregate

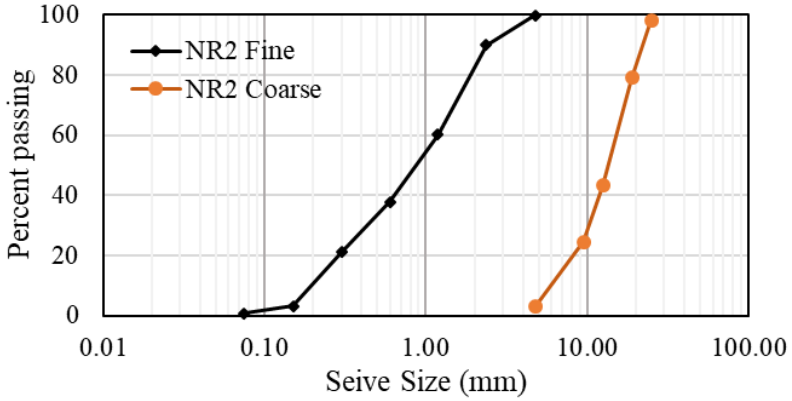

f) NR2 pit

Figure 65. Graph. As received gradation curve of natural aggregates. Source: UW Tanner Research Group.

Appendix B

Table 19. Additional materials for exposure blocks.

Specimen	Water lb (kg)	NaOH lb (kg)	Air Ent. lb (kg)	Super-plasticizer lb (kg)	Slump in. (mm.)	Air Content (%)
BHC-1	57.5 (26.1)	0 (0)	0.2 (0.09)	2.2 (1)	3 (76)	4.5
BHC-2	57.5 (26.1)	0 (0)	0.2 (0.09)	2.32 (1.05)	5.5 (140)	6
BHC-3	53.1 (24.1)	0.68 (0.3)	0.15 (0.07)	2.8 (1.27)	7.5 (191)	4.1
BHP-1	61.25 (27.8)	0 (0)	0.25 (0.11)	0 (0)	5 (126)	7
BHP-2	58 (26.3)	0 (0)	0.25 (0.11)	0 (0)	6 (152)	6
BHP-3	56.5 (25.6)	0.68 (0.3)	0.16 (0.07)	2.18 (0.99)	6.5 (165)	4.2
DF-1	57.5 (26.1)	0 (0)	0.25 (0.11)	0 (0)	3.5 (89)	5
DF-2	58 (26.3)	0 (0)	0.25 (0.11)	0 (0)	4.5 (114)	7
DF-3	57.5 (26.1)	0.68 (0.3)	0.24 (0.11)	2.74 (1.24)	4.5 (114)	5
GP-1	57.5 (26.1)	0 (0)	0.24 (0.11)	2.2 (1)	6.5 (165)	7.5
GP-2	53.4 (24.2)	0 (0)	0.2 (0.09)	2.2 (1)	4.5 (114)	4.5
GP-3	55.2 (25)	0.68 (0.3)	0.19 (0.09)	2.3 (1.04)	7 (178)	5.2
HP-1	57.5 (26.1)	0 (0)	0.25 (0.11)	0 (0)	2.5 (64)	5
HP-2	57.5 (26.1)	0 (0)	0.25 (0.11)	2.3 (1.04)	5.5 (140)	7
HP-3	57.5 (26.1)	0.68 (0.3)	0.24 (0.11)	2.44 (1.11)	3.5 (89)	5
KR-1	57.5 (26.1)	0 (0)	0.2 (0.09)	2.26 (1.03)	7.5 (191)	6.6
KR-2	49 (22.2)	0 (0)	0.2 (0.09)	2.3 (1.04)	5 (126)	4.7
KR-3	55 (24.9)	0 (0)	0.25 (0.11)	2.1 (0.95)	3.5 (89)	5
KR-4	55 (24.9)	0.68 (0.3)	0.25 (0.11)	2.3 (1.04)	4 (102)	8
LBG-1	60.4 (27.4)	0 (0)	0.25 (0.11)	0 (0)	0.5 (13)	4
LBG-2	65 (29.5)	0 (0)	0.25 (0.11)	0 (0)	2 (51)	4
LBG-3	65 (29.5)	0.68 (0.3)	0.25 (0.11)	0 (0)	6 (152)	6
LX-1	57.5 (26.1)	0 (0)	0.25 (0.11)	3 (1.36)	6 (152)	8
LX-2	53.9 (24.4)	0 (0)	0.25 (0.11)	2.4 (1.09)	8.5 (216)	9
LX-3	57.5 (26.1)	0.68 (0.3)	0.24 (0.11)	2.47 (1.12)	7.5 (191)	7.4
WOR-1	63 (28.6)	0 (0)	0.25 (0.11)	0 (0)	5.5 (140)	4.5
WOR-2	60.2 (27.3)	0 (0)	0.25 (0.11)	0 (0)	5 (126)	6
WOR-3	57.5 (26.1)	0.68 (0.3)	0.15 (0.07)	2.3 (1.04)	5.5 (140)	5.8

Source: UW Tanner Research Group.

Appendix C

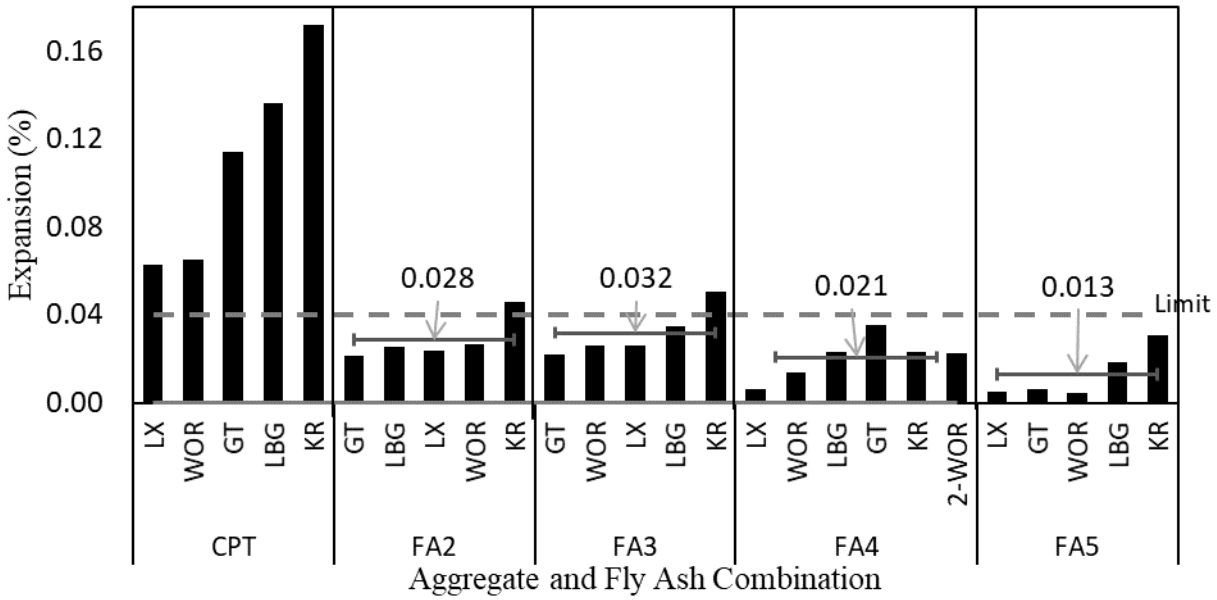

Figure 66. Graph. Effectiveness of Fly ashes (FA2 through FA5) for different aggregates.

Source: UW Tanner Research Group.

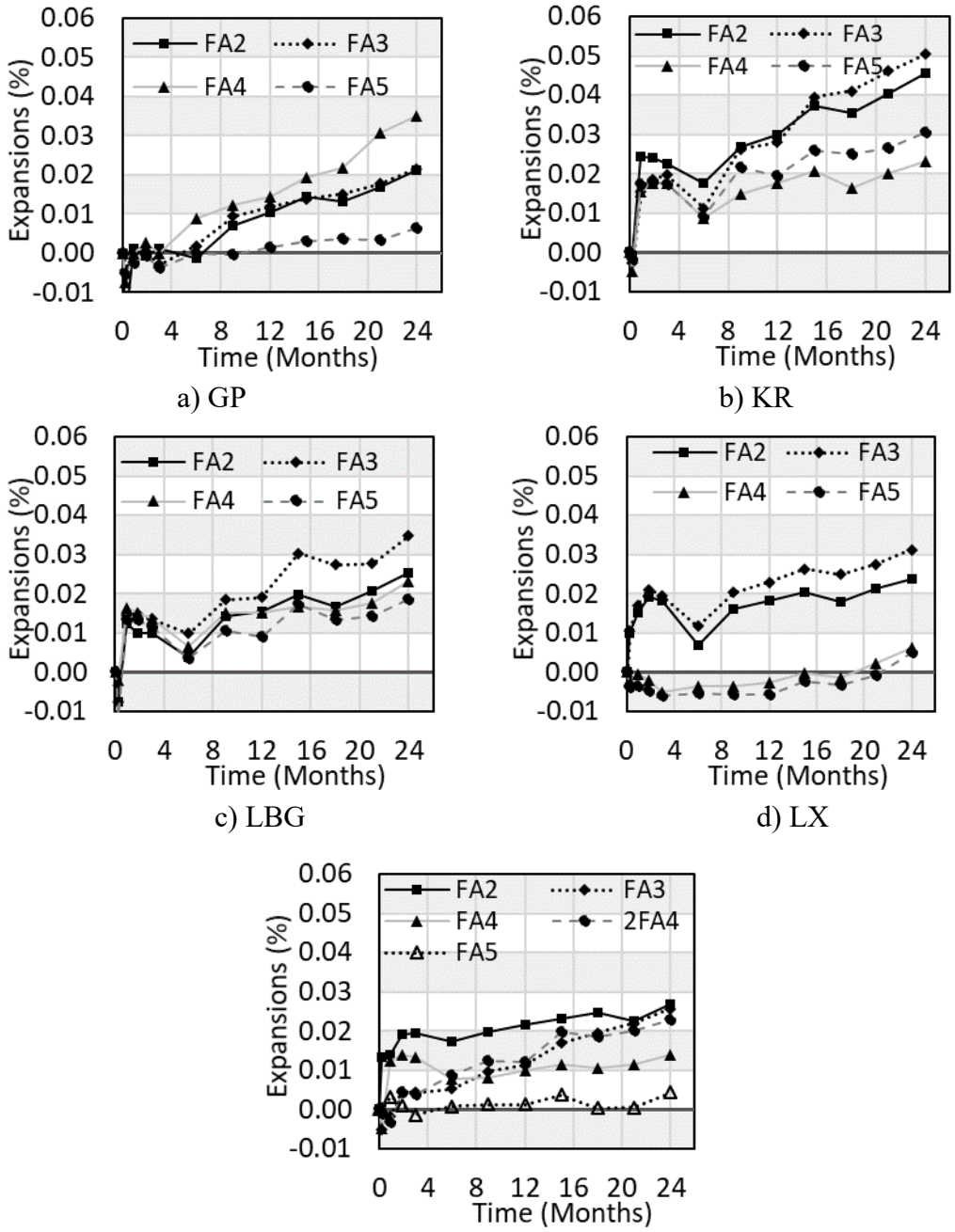

Figure 67. Graph. Mit-CPT expansions for GT, KR, LBG, LX and WOR aggregates.

Source: UW Tanner Research Group.

Appendix D

Table 20. CPT and Mit-CPT expansions data for JP aggregates.

Time		Average Expansion (%)								
Days	Months	JP-C	JP-C-FA1	JP-C-FA6	JP-F	JP-F-FA1	JP-F-FA6	JP-Com	JP-Com-FA1	JP-Com-FA6
1	0.03	0.000	0.000	0.000	0.000	0.000	0.000	0.000	0.000	0.000
7	0.23	-0.003	0.001	0.003	0.008	0.002	0.007	0.003	0.003	0.005
28	0.93	0.001	0.001	0.006	0.018	0.005	0.010	0.014	0.006	0.008
56	1.87	0.024	0.003	0.010	0.022	0.006	0.010	0.037	0.007	0.007
90	3	0.038	0.004	0.009	0.040	0.007	0.011	0.086	0.008	0.010
180	6	0.056	0.007	0.010	0.085	0.007	0.011	0.140	0.008	0.008
270	9	0.067	0.010	0.014	0.100	0.008	0.014	0.149	0.012	0.013
360	12	0.076	0.013	0.017	0.107	0.012	0.015	0.0153	0.015	0.016
450	15	-	0.017	0.018	-	0.013	0.015	-	0.021	0.020
540	18	-	0.019	0.018	-	0.016	0.019	-	0.021	0.019
630	21	-	0.020	0.019	-	0.019	0.025	-	0.023	0.025
720	24	-	0.022	0.022	-	0.019	0.026	-	0.025	0.026

Source: UW Tanner Research Group.

Table 21. CPT and Mit-CPT expansions data for VR aggregates.

Time		Average % Expansion								
Days	Months	VR-C	VR-C-FA1	VR-C-FA6	VR-F	VR-F-FA1	VR-F-FA6	VR-Com	VR-Com-FA1	VR-Com-FA6
1	0.03	0.000	0.000	0.000	0.000	0.000	0.000	0.000	0.000	0.000
7	0.23	0.003	0.002	0.001	0.007	-0.002	0.004	0.003	-0.002	0.002
28	0.93	0.012	0.003	0.001	0.017	0.001	0.009	0.004	0.002	0.002
56	1.87	0.019	0.004	-0.001	0.024	0.004	0.011	0.013	0.004	0.003
90	3	0.024	0.004	0.002	0.027	0.005	0.011	0.028	0.006	0.003
180	6	0.036	0.005	0.003	0.048	0.007	0.011	0.068	0.008	0.004
270	9	0.047	0.006	0.004	0.066	0.007	0.012	0.087	0.009	0.004
360	12	0.056	0.009	0.004	0.070	0.011	0.012	0.098	0.010	0.005
450	15	-	0.010	0.004	-	0.013	0.013	-	0.010	0.007
540	18	-	0.009	0.005	-	0.012	0.015	-	0.012	0.008
630	21	-	0.009	0.008	-	0.014	0.017	-	0.014	0.012
720	24	-	0.012	0.009	-	0.016	0.017	-	0.014	0.012

Source: UW Tanner Research Group.

Table 22. Average expansions for CPT and Mit-CPT expansions data for 2M aggregates.

Days	Months	2M-C	2M-C-FA1	2M-C-FA6	2M-F	2M-F-FA1	2M-F-FA6	2M-Com	2M-Com-FA1-25	2M-Com-FA1-30	2M-Com-FA1-40	2M-Com-FA6-25	2M-Com-FA6-30	2M-Com-FA6-40
0	0	0.000	0.000	0.000	0.000	0.000	0.000	0.000	0.000	0.000	0.000	0.000	0.000	0.000
7	0.23	0.028	0.003	0.003	0.019	0.012	0.011	0.023	0.005	-0.001	-0.002	0.010	0.001	0.003
28	0.93	0.087	0.004	0.007	0.182	0.018	0.014	0.143	0.013	0.003	0.001	0.013	0.003	0.003
56	1.87	0.140	0.007	0.008	0.352	0.018	0.015	0.214	0.014	0.004	0.003	0.015	0.007	0.003
90	3	0.178	0.008	0.010	0.469	0.023	0.022	0.271	0.013	0.006	0.006	0.019	0.009	0.005
180	6	0.228	0.011	0.013	0.498	0.027	0.022	0.305	0.015	0.009	0.006	0.017	0.008	0.002
270	9	0.252	0.010	0.015	0.516	0.028	0.025	0.326	0.017	0.008	0.008	0.018	0.010	0.005
360	12	0.262	0.013	0.016	0.519	0.032	0.028	0.330	0.017	0.012	0.012	0.019	0.010	0.003
450	15	-	0.015	0.017	-	0.036	0.029	-	0.017	0.012	0.012	0.021	0.013	0.004
540	18	-	0.015	0.016	-	0.035	0.029	-	0.019	0.011	0.011	0.022	0.012	0.005
630	21	-	0.018	0.019	-	0.037	0.032	-	0.021	0.015	0.015	0.026	0.014	0.009
720	24	-	0.019	0.020	-	0.039	0.032	-	0.021	0.016	0.016	0.026	0.015	0.009

Source: UW Tanner Research Group.

Table 23. CPT and Mit-CPT expansions data for KR aggregates.

Days	Months	KR-C	KR-C-FA1	KR-C-FA6	KR-F	KR-F-FA1	KR-F-FA6	KR-Com	KR-Com-FA1-25	KR-Com-FA1-30	KR-Com-FA1-40	KR-Com-FA6-25	KR-Com-FA6-30	KR-Com-FA6-40
0	0	0.000	0.000	0.000	0.000	0.000	0.000	0.000	0.000	0.000	0.000	0.000	0.000	0.000
7	0.23	0.004	-0.002	-0.002	0.006	0.001	0.003	0.003	-0.003	-0.003	-0.003	-0.003	0.001	0.000
28	0.93	0.018	-0.002	0.001	0.020	0.007	0.005	0.050	0.002	-0.001	-0.003	-0.003	0.000	-0.004
56	1.87	0.044	-0.001	0.003	0.032	0.009	0.006	0.121	0.003	0.000	-0.002	-0.001	0.000	-0.002
90	3	0.072	0.004	0.003	0.097	0.010	0.007	0.171	0.004	0.003	-0.002	-0.001	0.001	-0.003
180	6	0.101	0.004	0.004	0.188	0.011	0.008	0.217	0.007	0.003	-0.002	0.003	0.004	-0.002
270	9	0.120	0.008	0.009	0.223	0.014	0.010	0.237	0.011	0.010	0.004	0.008	0.007	0.001
360	12	0.129	0.011	0.013	0.0239	0.016	0.012	0.247	0.015	0.012	0.004	0.012	0.011	0.005
450	15	-	0.013	0.012	-	0.016	0.014	-	0.018	0.013	0.005	0.016	0.012	0.006
540	18	-	0.013	0.014	-	0.017	0.014	-	0.018	0.014	0.005	0.019	0.015	0.007
630	21	-	0.016	0.015	-	0.017	0.014	-	0.019	0.015	0.007	0.021	0.016	0.008
720	24	-	0.016	0.016	-	0.017	0.016	-	0.023	0.017	0.008	0.022	0.018	0.008

Source: UW Tanner Research Group.